
Doctoral Dissertations


Student Theses and Dissertations

Summer 2020

An integrated wellbore stability study to mitigate expensive wellbore instability problems while drilling into Zubair shale/sand sequence, southern Iraq

Ahmed Khudhair Abbas

Follow this and additional works at: https://scholarsmine.mst.edu/doctoral_dissertations

 Part of the [Geological Engineering Commons](#), [Geology Commons](#), and the [Petroleum Engineering Commons](#)

Department: Geosciences and Geological and Petroleum Engineering

Recommended Citation

Abbas, Ahmed Khudhair, "An integrated wellbore stability study to mitigate expensive wellbore instability problems while drilling into Zubair shale/sand sequence, southern Iraq" (2020). *Doctoral Dissertations*. 2904.

https://scholarsmine.mst.edu/doctoral_dissertations/2904

This thesis is brought to you by Scholars' Mine, a service of the Missouri S&T Library and Learning Resources. This work is protected by U. S. Copyright Law. Unauthorized use including reproduction for redistribution requires the permission of the copyright holder. For more information, please contact scholarsmine@mst.edu.

AN INTEGRATED WELLBORE STABILITY STUDY TO MITIGATE EXPENSIVE
WELLBORE INSTABILITY PROBLEMS WHILE DRILLING INTO ZUBAIR
SHALES/SAND SEQUENCE, SOUTHERN IRAQ

by

AHMED KHUDHAIR ABBAS

A DISSERTATION

Presented to the Faculty of the Graduate School of the
MISSOURI UNIVERSITY OF SCIENCE AND TECHNOLOGY

In Partial Fulfillment of the Requirements for the Degree

DOCTOR OF PHILOSOPHY

in

PETROLEUM ENGINEERING

2020

Approved by:

Ralph Flori, Advisor
David Rogers
Mingzhen Wei
Shari Dunn-Norman
Mortadha Al Saba

© 2020

AHMED KHUDHAIR ABBAS

All Rights Reserved

PUBLICATION DISSERTATION OPTION

This dissertation consists of the following four articles, formatted in the style used by the Missouri University of Science and Technology:

Paper I: Pages 5-39 have been published in Journal of Petroleum Science and Engineering

Paper II: Pages 40-70 have been published in Journal of Natural Gas Science and Engineering.

Paper III: Pages 71-109 have been published in Journal of Energy Resources Technology.

Paper IV: Pages 110-142 have been published in Journal of Natural Gas Science and Engineering.

ABSTRACT

The Zubair Formation is the most prolific reservoir in Iraq, which is comprised of sandstones interbedded with shale sequences. Due to the weak nature of the shale sequence, the instability of a wellbore is one of the most critical challenges that continuously appears during drilling across this formation. Historically, over 90% of wellbore problems in the Zubair Formation were due to wellbore instability. Problems associated with wellbore instability, such as tight hole, shale caving, stuck logging tools along with subsequent fishing, stuck pipe, and sidetracking result in increasing the non-productive time. This non-productive time has cost an enormous amount of money.

The main objective of this research is to reduce the drilling time and cost for 8 ½” phase of wells in Zubair Formation by minimizing wellbore stability problems. This will be achieved by different laboratory tests on core samples from the targeted formation to obtain the rock mechanical properties and by applying a geomechanical model based on offset well data coupled with suitable rock failure criteria to obtain a safe mud weight and an appropriate well trajectory. Furthermore, this project presents some of the primary laboratory and wellsite testing techniques that are often used by mud engineers to characterize and remediate drilling fluids and shale interactions to improve the selection of chemical additives for clay inhibit.

The present research work can be applied as a cost-effective tool to assess and address existing wellbore instability problems and to guide future neighboring wells for better drilling efficiency by reducing the non-productive time and well costs.

ACKNOWLEDGMENTS

First, I would like to thank Allah (God) for giving me many blessings, opportunities, and the strength to complete this long research journey. Second, I would like to express my sincere gratitude to my PhD advisor, Dr. Ralph Flori, for his invaluable support throughout my research. He has always been an excellent mentor, contributor, supporter, and friend during my whole study.

I would also like to thank my committee members, Dr. David Rogers, Dr. Mingzhen Wei, Dr. Shari Dunn-Norman, and Dr. Mortadha Al Saba for their valuable advice and recommendations. I am very grateful to the Higher Committee for Education Development (HCED) in Iraq for granting me a PhD scholarship and financial support.

A special thanks to my family, especially my parents, for their love, support, encouragement, and prayers throughout my study.

Ultimately, I would like to thank my wife and my kids for their love, support, encouragement, and prayers throughout my study. Without my wife's support, I would not be able to get this study done.

TABLE OF CONTENTS

	Page
PUBLICATION DISSERTATION OPTION	iii
ABSTRACT	iv
ACKNOWLEDGMENTS	v
LIST OF ILLUSTRATIONS	xiii
LIST OF TABLES	xvii
 SECTION	
1. INTRODUCTION	1
1.1. GEOLOGICAL SETTING OF THE STUDIED AREA	1
1.2. PROBLEM AND OBJECTIVE	2
 PAPER	
I. INTEGRATED APPROACH USING CORE ANALYSIS AND WIRELINE MEASUREMENT TO ESTIMATE ROCK MECHANICAL PROPERTIES OF THE ZUBAIR RESERVOIR, SOUTHERN IRAQ	5
ABSTRACT	5
1. INTRODUCTION	6
2. PREVIOUS LITERATURE'S RELATIONS REVIEW	9
3. METHODOLOGY	10
3.1. CT SCANNING TECHNIQUE	10
3.2. SCANNING ELECTRON MICROSCOPE	11
3.3. THIN SECTION ANALYSIS	12
3.4. X-RAY DIFFRACTION (XRD)	13

3.5. SAMPLE PREPARATION	13
3.6. POROSITY, GRAIN DENSITY, AND BULK DENSITY	14
3.7. MULTISTAGE TRIAXIAL TEST	14
3.8. TRIAXIAL TESTS.....	15
4. RESULTS AND DISCUSSION	16
4.1. STRUCTURE AND COMPOSITION OF ZUBAIR SANDSTONE	16
4.2. ROCK STRENGTH PARAMETERS	19
4.3. STATIC ELASTIC PARAMETERS.....	20
4.4. CORRELATIONS	21
4.5. STATISTICAL ANALYSIS	22
4.6. DERIVATION OF ROCK MECHANICAL PROPERTIES	27
4.6.1. Calibration of Wireline Log Porosity with the Laboratory-Measured Porosity.....	27
4.6.2. Implementation of the Correlations to Derive Rock Mechanical Properties.....	28
5. FIELD APPLICATIONS OF THE FINDINGS OF THIS STUDY	31
5.1. SAND PRODUCTION PREDICTION	31
5.1.1. Shear and Bulk Modulus Method.....	31
5.1.2. Unconfined Compressive Strength Method.	31
5.2. DESIGNING ACID FRACTURING TREATMENT	32
6. CONCLUSIONS.....	34
ACKNOWLEDGMENTS.....	35
REFERENCES.....	35

II. ESTIMATING ROCK MECHANICAL PROPERTIES OF THE ZUBAIR SHALE FORMATION USING A SONIC WIRELINE LOG AND CORE ANALYSIS	40
ABSTRACT	40
1. INTRODUCTION	41
2. LITERATURE REVIEW OF RELEVANT CORRELATIONS	43
3. METHODOLOGY	45
3.1. CHARACTERIZATION OF THE SHALE FORMATION	45
3.1.1. CT Scanning Technique.	46
3.1.2. Scanning Electron Microscope.....	46
3.1.3. Thin Section Analysis.	47
3.1.4. X-Ray Diffraction (XRD).	47
3.1.5. Porosity.....	48
3.2. ROCK MECHANICAL PROPERTIES	48
3.2.1. Sample Preparation.....	49
3.2.2. Triaxial Tests.....	49
3.2.3. Compressional Wave Velocity.....	51
4. RESULTS AND DISCUSSION	51
4.1. STRUCTURE AND POROSITY.....	51
4.2. MINERAL COMPOSITION AND TEXTURE ANALYSIS	53
4.3. ROCK STRENGTH PROPERTIES	55
4.4. ELASTIC PROPERTIES	56
4.5. CORRELATIONS	57
4.5.1. Rock Strength Parameters.	57

4.5.2. Static Young's Modulus	58
4.5.3. Static Poisson's Ratio	58
4.6. STATISTICAL ANALYSIS	59
4.7. DERIVATION OF ROCK MECHANICAL PROPERTIES	61
4.7.1. Calibration of Wireline Sonic Log (P-Wave Velocity) with the Laboratory-Measured P-Wave Velocity.	61
4.7.2. Implementation of the Correlations to Derive Rock Mechanical Properties.....	63
5. SUMMARY AND CONCLUSIONS.....	64
ACKNOWLEDGMENTS.....	66
REFERENCES.....	66
III. STABILITY ANALYSIS OF HIGHLY DEVIATED BOREHOLES TO MINIMIZE DRILLING RISKS AND NONPRODUCTIVE TIME	71
ABSTRACT.....	71
1. INTRODUCTION.....	72
2. MECHANICAL EARTH MODEL.....	74
2.1. MECHANICAL STRATIGRAPHY	76
2.2. ROCK MECHANICAL PARAMETERS	76
2.2.1. Rock Strength Parameters.	77
2.2.2. Tensile Strength.....	78
2.2.3. Rock Elastic Parameters.	78
2.3. FORMATION PORE PRESSURE.....	79
2.4. IN-SITU STRESS MAGNITUDE	80
2.4.1. Vertical Stress.....	80
2.4.2. Horizontal Stresses (Minimum and Maximum).....	80

2.5. ORIENTATION OF IN-SITU STRESSES.....	82
3. STRESS DISTRIBUTION AROUND THE DEVIATED BOREHOLE	82
4. ROCK FAILURE CRITERIA.....	85
4.1. MOHR-COULOMB FAILURE CRITERION.....	86
4.2. MOGI-COULOMB FAILURE CRITERION	86
5. FIELD CASE STUDY	88
5.1. MEM CONSTRUCTED FOR THE ZUBAIR FORMATION.....	88
5.2. TRAJECTORY SENSITIVITY ANALYSIS.....	93
5.3. MUD WEIGHT VERSUS WELLBORE INCLINATION AND AZIMUTH	96
5.4. MODEL VALIDATION	98
5.5. WELLBORE STABILITY FORECAST.....	100
6. CONCLUSIONS.....	102
ACKNOWLEDGMENTS.....	103
REFERENCES.....	103
IV. LABORATORY ANALYSIS TO ASSESS SHALE STABILITY FOR THE ZUBAIR FORMATION, SOUTHERN IRAQ	110
ABSTRACT	110
1. INTRODUCTION.....	111
2. METHODOLOGY.....	114
2.1. SHALE SAMPLES.....	114
2.2. SHALE CHARACTERIZATIONS METHODS.....	115
2.2.1. CT Scanning Technique.....	115
2.2.2. Scanning Electron Microscope (SEM).....	116

2.2.3. Thin-Section Analysis.....	116
2.2.4. X-Ray Diffraction (XRD).....	117
2.2.5. Cation Exchange Capacity (CEC).....	117
2.3. FLUIDS AND SHALE INTERACTIONS.....	118
2.3.1. Preparation Of Test Fluids.....	118
2.3.2. Capillary Suction Time (CST) Test.....	119
2.3.3. Hot Rolling Dispersion Test.....	120
2.3.4. Bulk Hardness Test.....	121
2.3.5. Linear Swell Meter (LSM) Tests.....	122
2.3.6. Fracture Development Test.....	123
3. RESULTS AND DISCUSSION.....	114
3.1. SHALE CHARACTERIZATIONS METHODS.....	124
3.1.1. Structure.....	124
3.1.2. Mineralogical Composition and CEC.....	127
3.2. FLUIDS AND SHALE INTERACTION EVALUATION.....	129
3.2.1. Capillary Suction Time Test (CST).....	129
3.2.2. Hot Rolling Dispersion Test.....	131
3.2.3. Bulk Hardness Test.....	132
3.2.4. Swelling Test.....	133
3.2.5. Fracture Development Test.....	134
4. CONCLUSIONS.....	135
ACKNOWLEDGMENTS.....	137
REFERENCES.....	137

SECTION	
2. CONCLUSIONS AND RECOMMENDATIONS.....	143
2.1. CONCLUSIONS	143
2.2. RECOMMENDATIONS.....	144
VITA.....	146

LIST OF ILLUSTRATIONS

SECTION	Page
Figure 1.1. Generalised stratigraphic column for the study area in southern Iraq, with major oil pays of the Lower Cretaceous Zubair Reservoir.	2
Figure 1.2. Total time analysis for 12 deviated wells.	4
 PAPER I	
Figure 1. CT scan images of one section of the core show 11 axial scan slices along the longitudinal view for one full diameter core section.	17
Figure 2. CT scan images of the three axial scan slices along the longitudinal view of the plug samples.	17
Figure 3. Scanning electron image of a sample of Zubair sandstone.	18
Figure 4. Thin-section plate of the Zubair sandstone formation.	18
Figure 5. Failure envelope derived from multistage triaxial tests.	19
Figure 6. Static elastic parameters derived from triaxial tests.	20
Figure 7. Calibration plots of rock mechanical properties versus lab-measured porosity.	23
Figure 8. Histograms showing the frequency versus the difference in the estimated (E) and measured (M) mechanical properties.	26
Figure 9. Empirical correction between the neutron log porosity and core-measured porosity.	28
Figure 10. Wireline neutron porosity and calibrated neutron porosity logs.	28
Figure 11. Predicted unconfined compressive strength and internal friction angle logs from Eqs. 15 and 16, respectively.	29
Figure 12. Predicted Young's modulus and Poisson's ratio logs using Eqs. 17 and 20, respectively.	30
Figure 13. Predicted bulk and shear modulus logs using Eqs. 18 and 19, respectively. ...	30

Figure 14. Sanding potential plot showing the yellow zones as likely zones to produce sand.	32
Figure 15. Predicted Young's modulus and Poisson's ratio from the current empirical relationships, using a commercial hydrofracturing simulator.....	33
PAPER II	
Figure 1. CT scan images for one section of the shale core preserved in a metal casing.	52
Figure 2. CT scan images showing the three axial scan slices along the longitudinal view of the plug samples.....	52
Figure 3. Scanning electron image of Zubair shale specimens.....	53
Figure 4. Thin section plate of the Zubair shale formation.....	54
Figure 5. Failure envelope derived from the CU triaxial test on plug samples of Zubair shale taken from the same depth.	55
Figure 6. Static elastic parameters derived from plotting the axial stress against the axial and radial strain using the triaxial test conducted on plug samples for Zubair shale.....	56
Figure 7. Timeline of the CU triaxial test for Zubair shale.	57
Figure 8. Calibration plots of rock mechanical properties versus lab-measured P-wave velocity.....	58
Figure 9. Histograms showing the frequency versus the difference in the estimated (E) and measured (M) of the rock mechanical properties for Zubair shale using the empirical equations shown in Table 1 and the suggested empirical relationships (Eqs. 8–11).	60
Figure 10. Empirical correlation between the sonic log P-wave velocity and lab-measured P-wave velocity.	62
Figure 11. Wireline sonic log and lab-measured P-wave velocity.	62
Figure 12. Predicted unconfined compressive strength and internal friction angle logs using Eqs. 8 and 9, respectively.....	63
Figure 13. Predicted Young's modulus and Poisson's ratio logs using Eqs. 10 and 11, respectively.	64

PAPER III

Figure 1. General workflow for the geomechanical model.	76
Figure 2. Stress transformation in polar systems for a deviated borehole.	83
Figure 3. Predicted rock mechanical properties logs and laboratory measurements.	90
Figure 4. Pore pressure profile calibrated against the available measured pressure points.....	91
Figure 5. Estimation of the in-situ principal stress magnitudes at a single well location.	92
Figure 6. Orientation of the identified borehole breakouts (direction of minimum horizontal stress).	93
Figure 7. Minimum mud weight plots using the Mohr-Coulomb failure criterion.	95
Figure 8. Minimum mud weight plots using the Mogi-Coulomb failure criterion.	95
Figure 9. Minimum mud weight plots using the Mohr-Coulomb failure criterion.	97
Figure 10. Minimum mud weight plots using the Mogi-Coulomb failure criterion.	97
Figure 11. Evaluation of the accuracy of 1D-MEM using Mohr-Coulomb criteria.	99
Figure 12. Evaluation of the accuracy of 1D-MEM using Mogi-Coulomb criteria.	99
Figure 13. Wellbore stability forecast for the planned highly deviated well.....	101

PAPER IV

Figure 1. CT scan images for one section of the shale core.	126
Figure 2. SEM image of Zubair shale specimens.	126
Figure 3. Fragments of the Zubair shale core samples	127
Figure 4. Thin-section plate of the Zubair shale formation.	129
Figure 5. CST test results of the base fluid with and without different inhibitors, using Zubair shale.	130
Figure 6. Hot rolling dispersion test of the base fluid with and without different inhibitors, using Zubair shale.....	131

Figure 7. Bulk hardness test results for different test fluids, using Zubair shale..... 132

Figure 8. Swelling test results of the Zubair shale samples treated with different additives throughout the testing time..... 133

Figure 9. Change in Zubair shale after exposure to different test fluids for 48 hours at ambient conditions 135

LIST OF TABLES

PAPER I	Page
Table 1. Empirical relationships between rock mechanical properties and porosity in sandstone.	10
Table 2. Mineral composition by X-ray diffraction of Zubair sandstone.	18
Table 3. Suggested correlations for predicting static rock mechanical properties of Zubair sandstone.	21
Table 4. The RMSE and ARAD of equations in Table 1 and Table 3 in the estimation of rock mechanical parameters.	24
PAPER II	
Table 1. Empirical relationships between rock mechanical properties and the P-wave velocity for shale.	45
Table 2. Porosity measured by determination of the free water content.	53
Table 3. X-ray diffraction results for Zubair shale.	54
Table 4. RMSE of Eqs. 8–11 in estimating rock mechanical parameters.	59
PAPER IV	
Table 1. X-ray diffraction results for the entire sample analysis.	128
Table 2. X-ray diffraction results for the entire sample analysis.	128
Table 3. Cation exchange capacity (CEC) results for Zubair shale.	129

SECTION

1. INTRODUCTION

1.1. GEOLOGICAL SETTING OF THE STUDIED AREA

The Lower Cretaceous Zubair Formation is a regionally extended oil-producing sandstone sequence in Iraq, Kuwait, Syria, Iran, and Saudi Arabia. Zubair Formation is the most important sandstone reservoir in Southern Iraq. It is recorded as oil-bearing in 30 structures which contain about 30% of Iraq's hydrocarbon reserves (Jassim and Goff, 2006). This formation measures approximately 400–500 m in average gross vertical thickness. It is composed mainly of alternating shale and sandstone, with minor streaks of limestone and siltstone. The formation is overlain by the Shuaiba Formation (limestone and dolomite) and is underlain by the Ratawi Formation (shale and limestone interbeds). This multilayered reservoir has been subdivided based on its sand/shale ratio into five members: upper shale, upper sand, middle shale, lower sand, and lower shale. Upper and lower sand members are considered as reservoirs targeted for development, where it is known as the Third and Fourth Pays, respectively (Figure 1.1). The most important occurrences of oil in the Zubair Formation are in the South Iraq oil fields of Zubair, Rumaila, Ratawi, Tuba, and Luhais. Oil has also been discovered in the Zubair Formation further east in the Majnoon, Halfaya and Huwaiza fields. Zubair Formation has shown to have a significant geomechanical problems for several wells in these fields, based on the issues experienced during drilling stages such as lost circulation, wellbore collapse, shale caving, stuck logging tools, stuck pipe, and loss of some borehole sections. It seems that

these issues manifest at the interfaces of the weak and non-depleted shale and depleted sandstone sections.

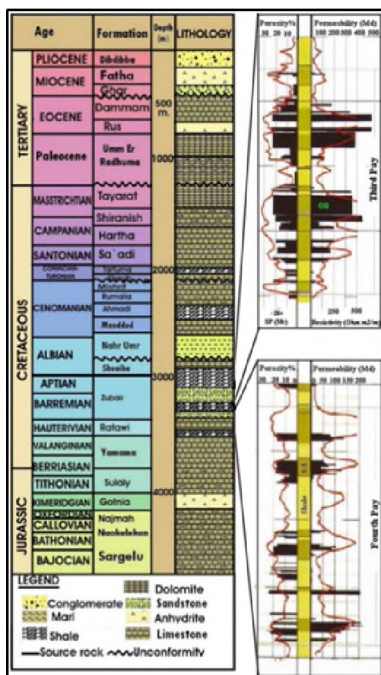


Figure 1.1. Generalised stratigraphic column for the study area in southern Iraq, with major oil pays of the Lower Cretaceous Zubair Reservoir.

1.2. PROBLEM AND OBJECTIVE

In order to study the impact of wellbore instability in Zubair Formation (8 ½" section) on drilling performance, daily drilling reports, daily mud reports, final well reports and mud logs (master logs) of twelve deviated wells were extensively investigated. On average, the total thickness drilled through the Zubair Formation starting from the top of the upper shale (previous casing shoe of a 12¼" section) to the bottom of the lower shale (well total depth) varied between 350 m (+/-30 m), which accounted for about 12% of the total well meterage.

The total time analysis for the 12 deviated wells is represented in Figure 1.2a. The time distribution clearly indicates that the Zubair section constituted of about 30% of the total days spent to drill the 12 deviated wells. Moreover, the total time breakdown for the 8½” section was then analyzed separately to determine the impact of the nonproductive time on the drilling progress for this section. The non-productive time (due to the wellbore instability incidents) constituted more than 44% of the total time spent on the 8½” section (Figure 1.2b). The majority of instability problems that have taken place in the Zubair Formation were tight hole, shale caving, and stuck logging tools, along with subsequent fishing, stuck pipe, and sidetracking in the worse cases. Out of the 20 deviated wells that were studied, four had to be sidetracked due to a stuck pipe and unsuccessful fishing operations. As shown in Figure 1.3c, the major loss of productivity was due to the tight hole problems. These problems contributed to the nonproductive time by increasing the time of circulation and reaming. The tight hole problems, sidetracked wells, and stuck pipe took more than 31%, 27%, and 22% of the nonproductive time, respectively.

In addition to the time analysis for these 12 deviated wells, drilling operation reports for these wells were analyzed to assist in identifying the main reasons behind the issues related to wellbore instability. Examining the drilling data revealed that these wellbore problems were mostly related to the shear failure of the wellbore. The majority of the most severe wellbore instability-related problems were experienced at wellbore inclinations higher than 20 degrees and did not depend on the drilling direction. Sidetrack incidents were encountered more often at wellbore deviations higher than 30 degrees. Overall, wellbore instability in the Zubair Formation increased the total well drilling time by an additional 14.5 days on average per well. An economic evaluation was also

performed, showing a substantial cost due this an additional nonproductive time. The extra cost for an average well is close 1.25 million USD. With these 20 deviated wells have been drilled in the field, the total cost would have been in excess of 25 million USD (without considering the additional cost of two directional bottom hole assemble (BHA) which were lost due to sidetracking); therefore, the potential for cost-saving is huge. Excessive increases in well costs also affect the field development activity plan.

Therefore, the motivation for this research was to tackle this issue efficiently. The main objective of this research is to reduce the drilling time and cost for 8 1/2” section in Zubair Formation by minimizing wellbore stability problems.

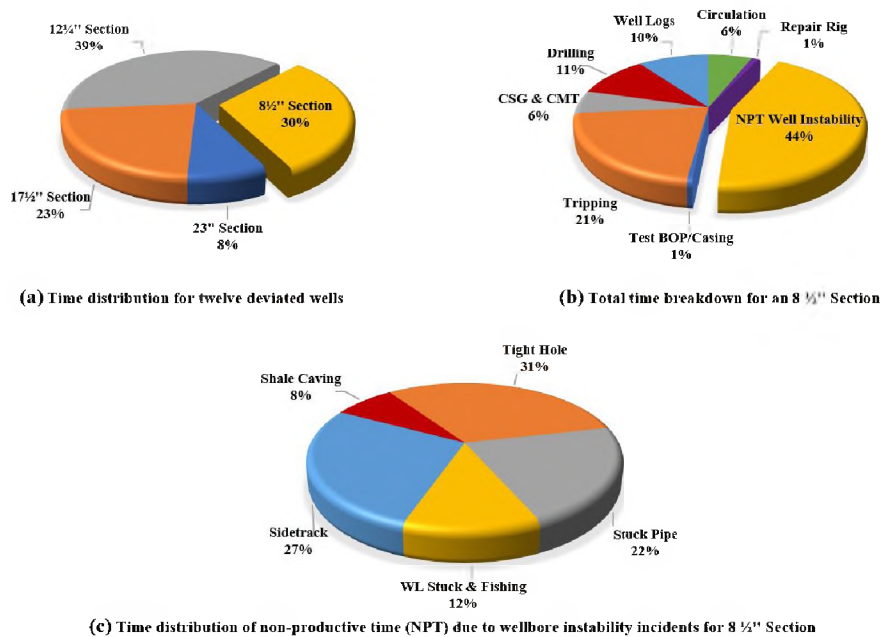


Figure 1.2. Total time analysis for 12 deviated wells.

PAPER

I. INTEGRATED APPROACH USING CORE ANALYSIS AND WIRELINE MEASUREMENT TO ESTIMATE ROCK MECHANICAL PROPERTIES OF THE ZUBAIR RESERVOIR, SOUTHERN IRAQ

Ahmed K. Abbas, Ralph Flori, Mortadha Alsaba, Haider Dahmd, and Ethar Alkamil

Department of Petroleum Engineering Engineering, Missouri University of Science and Technology, Rolla, MO 65409

ABSTRACT

The Zubair Reservoir is a regionally extensive oil-producing sandstone sequence which is part of the petroleum system in Iraq, Kuwait, Syria, Iran, and Saudi Arabia. Rock mechanical properties are extremely useful in optimizing drilling, production, and reservoir compaction. Hence, an accurate technique for estimating rock mechanical properties may significantly improve the economic revenues derivable from the reservoir. However, information about rock mechanical properties along the depth is often discontinuous and limited to core samples taken within the reservoir interval. The present study aims to predict a continuous profile of rock mechanical properties throughout the depth of the Zubair Reservoir directly from wireline porosity logs. Special characteristics of Zubair sandstone were evaluated and described using thin-section photographs, X-ray diffraction analysis, and scanning electron microscope imaging to identify and characterize the mineralogy, texture, and structure of the sandstone unit. Thereafter, both triaxial and triaxial multistage testing techniques were carried out on 130 plug samples from the Zubair

sandstone formation to measure the rock's mechanical properties. Valid local empirical correlations were established between the porosity and these mechanical parameters. The obtained results revealed that the rock mechanical properties are primarily functions of porosity and the direct linear expression is more reliable than power functions and exponential functions. The best relationship obtained between UCS, internal friction angle, Young's modulus, bulk modulus, shear modulus, and Poisson's ratio with porosity had a correlation coefficient (R^2) of 0.84, 0.75, 0.80, 0.59, 0.83 and 0.70, respectively. The accuracy of the newly suggested empirical correlations was subjected to statistical analysis. Moreover, these relationships were compared with the existing commonly used correlations reported in the literature on real field data from Zubair sandstone. The results showed that the suggested empirical correlations have a high accuracy and reliability, while the previous correlations could not adequately cover the Zubair sandstone data. This emphasizes the importance of using local correlations to estimate rock mechanical properties. The predicted continuous rock mechanical profile provides a good indication of the strength and stability of the formation around the wellbore. Consequently, it can be used in solving wellbore instability problems; preventing sand production; optimizing drilling processes, which includes the selection of the bit type and drilling parameters; and fracturing operations across the Zubair sandstone reservoir.

1. INTRODUCTION

Rock mechanical properties mainly consist of the elastic modulus, Poisson's ratio, and rock strength parameters (Peng and Zhang, 2007). Understanding these parameters is

essential for estimating in situ stresses in subsurface formations (Zoback et al., 2003), fracturing operations (Wang and Sharma, 2017), wellbore stability analysis (Zeynali, 2012), prevention of sand production (Santarelli et al., 1989), optimization of drilling operations, and development of geomechanical models to address the minimum required mud weight to drill a stable well (Kidambi and Kumar, 2016). Typically, rock mechanical properties (static properties) can be obtained by gently applying uniaxial or triaxial stresses on cylindrical plug samples until failure occurs. Laboratory tests are the most direct and reliable way of determining rock mechanical properties (Fjær et al., 2008). However, laboratory techniques are extremely expensive. Furthermore, the core samples of overburdened formations are almost never available for testing. Even if core samples are taken from depths of interest, the cores may be further damaged by the action of the drill bit during coring operations and by subsequent improper sample preparation and conditioning. This may be critically significant to the outcome of the rock mechanical analysis. In addition, laboratory tests can only cover a small part (several feet) of the reservoir interval. There are two main reasons that geophysical well logs are considered to be a useful method for predicting rock mechanical properties in continuous profiles through the entire interval of the reservoir. First, wireline logs give direct measurements of the petrophysical properties of the rock. Secondly, the wireline log is one of the few downhole measurements available throughout the entire reservoir. However, the mechanical properties cannot be inferred directly from wireline logs. A number of correlations have been introduced as a practical solution to bridge this gap (Sharma et al., 2010; Yagiz, 2010; Najibi et al., 2015; Dewhurst et al., 2015). Most of these correlations are based on empirical correlations of laboratory-derived rock mechanical properties with geophysical well logs,

such as porosities or acoustic velocities (Yagiz, 2011). The basis for these relationships is the fact that many of the same factors that affect rock mechanical properties also affect other physical properties, such as porosity, velocity, and elastic moduli (Chang et al., 2006). In general, rock mechanical and physical property relationships are developed for a specific formation based on the calibration of laboratory tests on rock samples from a given field. There are many choices of rock mechanical relationships available for the various rock formations in different geographical areas. Therefore, it is important to recognize the nature of the formation and the applicability range of the relationships before using them.

In this study, retrieved core samples from the Zubair sandstone reservoir in Southern Iraq were run through extensive testing, including a number of petrophysical and rock mechanical characterization tests. The mineralogy, texture, and structure of Zubair sandstone were described using thin-section photographs, X-ray diffraction analysis, and a scanning electron microscope. The values of porosity, grain density, and bulk density were measured for each plug sample. The rock strength parameters (i.e., unconfined compressive strength, cohesive strength, and internal friction angle) were measured using consolidated drained (CD) multistage triaxial tests. The static elastic parameters (i.e., Young's modulus, bulk modulus, shear modulus, and Poisson's ratio) were determined using consolidated drained (CD) triaxial tests. The measured rock mechanical properties were plotted against their corresponding porosity to predict local empirical correlation formulas. These empirical relationships were directly applied to wireline log-derived porosity to establish continuous rock mechanical property logs. This continuous profile of rock mechanical properties through the logged section of the reservoir can be applied in many approaches to the operational exploration and development processes across the Zubair Reservoir.

2. PREVIOUS LITERATURE'S RELATIONS REVIEW

Since the 1950s, a number of empirical correlations have been introduced to estimate rock mechanical properties from geophysical logging data (e.g., Ryskhewitch, 1953). These relationships were derived from case studies performed in different geological structures worldwide. Correlations of porosity with many rock mechanical properties have been successfully applied as an accurate and efficient method of obtaining a rock mechanical profile. Hoshino (1974) classified porosity as a major factor affecting rock strength and elasticity. Kowalski (1975) and Sethi (1981) introduced the use of porosity wireline logs to determine rock strength parameters.

Eqs 1 to 11 in Table 1 present a number of correlations in common use for estimating the rock mechanical properties of sandstones from porosity log data. Vernik et al. (1993) established Eq. 1 to calculate the unconfined compressive strength from porosity for sedimentary basins worldwide, which is particularly applicable to very clean, well-consolidated sandstones with porosity < 0.3 . Sarda et al. (1993) derived a simple empirical correlation (Eq. 2) between rock porosity and unconfined compressive strength. The relation was developed using data obtained from laboratory tests on sandstone core samples of the Germigny-sous-Coulombs structure in France. Weingarten and Perkins (1995) suggested that the internal friction angle can be predicted using the porosity for sandstone reservoirs in the Texas/Louisiana region of the Gulf of Mexico, as presented in Eq. 3. Edlmann et al. (1998) used core-measured porosity and rock mechanical properties for North Sea sandstone samples to derive direct linear correlations between the porosity and the rock mechanical properties (Eqs. 4-7) and to estimate the continuous rock mechanical

profile. Khair et al. (2015) reported nonlinear relationships between the elastic modulus and porosity (Eqs. 8-10) and derived linear correlations of Poisson's ratio with porosity (Eq. 11). These relationships were presented for the sandstone reservoir in the Fulla oilfield in Southern Sudan using field data and core measurements.

Table 1. Empirical relationships between rock mechanical properties and porosity in sandstone.

Eq. no.	Equation	R ²	Reference
1	$UCS = 254(1 - 2.7\phi)^2$	-	Vernik et al. (1993)
2	$UCS = 258 \exp^{-9\phi}$	-	Sarda et al. (1993)
3	$UCS = 57.8 - 105\phi$	-	Weingarten and Perkins (1995)
4	$UCS = -3.225\phi + 129.54$	0.68	Edlmann et al. (1998)
5	$\phi = -0.7779\phi + 41.929$	0.71	Edlmann et al. (1998)
6	$E_s = -0.7831\phi + 38.878$	0.68	Edlmann et al. (1998)
7	$\nu_s = 0.0052\phi + 0.0508$	0.64	Edlmann et al. (1998)
8	$E_s = 0.0173\phi^{-3.1389}$	0.93	Khair et al. (2015)
9	$K_s = 0.0803\phi^{-1.2734}$	0.71	Khair et al. (2015)
10	$G_s = 0.0047\phi^{-3.5034}$	0.92	Khair et al. (2015)
11	$\nu_s = 1.1148\phi + 0.1356$	0.77	Khair et al. (2015)

3. METHODOLOGY

3.1. CT SCANNING TECHNIQUE

X-ray computed tomography (CT) is a technique that allows visualization of the internal structure of a scanned object without cutting. The CT operates by using an X-ray generator that rotates around the central axis of scanned sample. Each of the specimens was scanned at 1-degree increments about the vertical axis for a full 360 degrees. The X-ray detectors are positioned on the opposite side of the circle from the X-ray source. CT

images record differences in the degree of attenuation of the X-rays, which is material and energy-dependent (Choo et al., 2014). CT produces data that can be manipulated in order to demonstrate various bodily structures based on their ability to absorb the X-ray beam. The CT images generated were in the axial or transverse plane, perpendicular to the long axis of the body sample. The degree of digital image resolution depends mainly on the distance the camera is positioned within the scanning device from the scanned object. In this study, one recovered full diameter core section (~1 m) was scanned by 2-D computed tomography (CT) scanner to examine the initial sample conditions and evaluate the presence of any preexisting (natural) fractures and/or mechanical damage caused by drilling and the coring processes. The CT scan was performed in two orientations: longitudinal (vertical) and axial. Eleven axial images (slices) were selected (at 10-cm intervals) to cover the internal features.

3.2. SCANNING ELECTRON MICROSCOPE

A sandstone sample from the Zubair Formation was imaged using a scanning electron microscope (SEM) to determine the integrity of the rock and measure the degree of cementing and compaction. SEM photographs allow for better three-dimensional observations of micro-cracks and micro-laminations in the specimen that are not easily seen using transmitted light or transmitted electron microscope techniques. The texture and orientation of the sandstone, its degree of compaction, and the presence of embedded minerals and pores can be observed (Mike et al., 2009). SEM images of a specimen were produced by scanning the surface with a focused beam of electrons. These electrons interact with atoms in the specimen, producing various signals that contain data about the

specimen's surface topography and composition. For SEM, a specimen needs to be completely dry and large enough to withstand the vacuum conditions and high energy beam of electrons. Sample preparation was performed to clean sample being mounted on the specimen stage and placed into the instrument. Magnification in a scanning electron microscope can be controlled over a range of about 6 orders of magnitude from about 10 to 1,000,000 times. The magnification ranges that were used for sandstone analyses ranged from 100 to 500x.

3.3. THIN SECTION ANALYSIS

A petrographic analysis was carried out to provide a detailed description of the texture (grain size, sorting, and grain contacts), sedimentary structures (laminations, bioturbation), framework grain composition, authigenic minerals, and types and distribution of macroporosity seen in a thin section. Thin sectioning and impregnation procedures are critical to the successful petrographic analysis. Thin section preparation involved vacuum impregnation with low-viscosity blue dyed resin to facilitate the recognition of porosity and staining with a mixed Alizarin Red-S and potassium ferricyanide solution to allow the observation of the carbonate minerals (Kassab et al., 2015). In addition, samples were stained with a sodium cobaltinitrite solution to aid the identification of alkali feldspars. Thin sections were carefully ground to 30-micron thick sections of rock mounted on a glass slide to avoid fracturing and plucking. Basic petrographic analysis is performed in transmitted light using a petrographic polarizing microscope. Petrographic analysis of thin sections involves either qualitative description or quantitative estimation of the texture, mineralogy and porosity. Rock types were

petrographically classified according to established rock classification scheme of Dott (1964).

3.4. X-RAY DIFFRACTION (XRD)

X-ray Diffraction (XRD) analysis were performed on Zubair sandstone sample. The specimen was placed into the X-ray diffractometer and rotated through a series of angles to help homogenize the intensity of the measured X-ray beam. As the specimen is rotated in the X-ray diffractometer, it was being illuminated with a very intense X-ray beam. The crystalline structures of the individual minerals present diffract the X-ray beam. This results in an X-ray diffraction pattern that is unique for each mineral in the sample (Mike et al., 2009). The computer automates the data collection and data reduction steps of the analysis. In order to obtain a semi-quantitative measurement of the mineral components of a given sample, the maximum intensity of each identified mineral has been measured and compared to a standard intensity obtained from a pure mineral sample.

3.5. SAMPLE PREPARATION

The core samples used in this study were obtained from three wells, covering a wide range of the Zubair sandstone formation interval. The core samples were well stored in cushion boxes at the point of recovery and after plugging in attempts to reduce the core damage during transport and during storage. Cylindrical plugs were cut from the entire core with a length to diameter ratio of 2:1 according to the International Society for Rock Mechanics standards (ISRM) (Kovari et al., 1983) (generally 1.5 in. diameter and 3 in. length). The plug samples were scanned by CT (2-D) to investigate and evaluate the

induced microcracks created during plug preparation. Only three axial images were selected to cover the internal features of the plug from the top, middle, and bottom sections. The selected plugs were cleaned of hydrocarbon and salt using a hot solvent extraction Soxhlet apparatus. The cleaned plug samples were allowed to dry and cool to room temperature, and their weight and dimensions were measured. After the porosity was measured, the plugs were 100% saturated in a light mineral oil in preparation for the triaxial and triaxial multistage tests. Seventy-five plug samples were prepared for static strength parameters using multistage triaxial tests, and 55 plug samples were tested for static elastic parameters using triaxial tests.

3.6. POROSITY, GRAIN DENSITY, AND BULK DENSITY

The porosity of each plug was determined using Boyle's law and a helium porosimeter. The plug samples were weighed and the weight recorded prior to the grain volume measurement. The grain volume of the plug was measured using a calibrated helium gas volume expansion meter. The bulk volume was measured by mercury displacement using Archimedes' principle. The obtained results were used in combination with the weights of the samples to calculate the porosity, grain density, and bulk density values.

3.7. MULTISTAGE TRIAXIAL TEST

Rock strength parameters can be measured using laboratory tests on broken or intact rock samples due to the natural heterogeneity of the rock and the strong limitations on the amount of the core sample available for the rock mechanical test. The multistage

triaxial test is an adequate technique for measuring an entire failure envelope with just one core sample (Kovari et al., 1983). However, this test is not recommended for evaluating elastic parameters because these parameters are influenced by damage caused in the previous load steps (Holt and Fjær, 1991). The plug was placed in a standard Hoek cell and loaded axially by a hydraulic load frame and radially by a servo pump. The multistage test started from 5 MPa as the initial confining pressure. When failure was reached (a significant change in the slope of the stress-strain curve), the confining pressure was increased to 10 MPa. The same procedure was replicated by increasing the confining pressure in 5 MPa intervals for each stage until the confining pressure reached 25 MPa. The axial stress was then increased further until failure occurred. During the tests, a computer control and data acquisition system was used to operate the triaxial test equipment, monitor and record the axial stress, confining pressure, and strains.

3.8. TRIAXIAL TESTS

Static elastic parameters were determined using the consolidated drained (CD) triaxial tests. In the current work, samples were loaded hydrostatically to confining pressure of 25 MPa, which represents the estimated formation pressure experienced in situ by the reservoir (Ameen et al., 2009). During each test, radial and axial deformation were monitored by a computerized digital data acquisition system. Radial deformation of the plug was measured by four strain gauges glued directly to the sample. On the other hand, axial deformation was measured using a linear voltage displacement transducer (LVDT) mounted on the top of the piston assembly (the axial movement of the piston is related to the axial deformation of the test plug).

4. RESULTS AND DISCUSSION

4.1. STRUCTURE AND COMPOSITION OF ZUBAIR SANDSTONE

The results of (CT) scanner for full diameter core section (~1 m) and the plug samples showed that both types of fractures were observed on some of the samples. As shown in Figure 1 and Figure 2, the green arrow refers to induced fractures, and the yellow arrow refers to natural open fractures (fracture porosity). The SEM image shows that the rock sample has a well-consolidated texture of sandstone, with grains moderately-to-strongly cemented and moderately compacted as well as a lamination-free structure (Figure 3). Thin-section analysis, as shown in Figure 4, revealed that the majority of the plug samples are well-sorted, fine-grained quartz arenite. The sample grains are moderately cemented, and moderately compacted, with relatively high porosity and good pore interconnectivity (indicated by blue space). In terms of mineral composition, the Zubair Formation sandstone is generally composed of dominant amounts of monocrystalline quartz, with minor quartz overgrowths, kaolinite booklets, rare detrital clays, K-feldspars, heavy minerals, ferroan calcite, black pyrite crystals, chlorite, and residual hydrocarbons as well as traces of polycrystalline quartz, lithics, plagioclase feldspars, opaques, illite, and barite. These results strongly agree with the results of the X-ray diffraction test, as summarized in Table 2.

The rock mechanical properties are a function of the rock internal and external characteristics, such as the mineral composition, grain size and shape, porosity, and degree of cementing and compaction. Those characteristics play significant roles that govern the rocks' behavior under applied stresses (Ribeiro et al., 2009; Alikarami et al., 2013; Pan et

al., 2016). Therefore, the primary purpose for including these tests in this study is to characterize the mineralogy, texture, structure, grain distribution, and consolidation of Zubair sandstone. This is very helpful to understanding the fundamental mechanical behavior of Zubair sandstone.

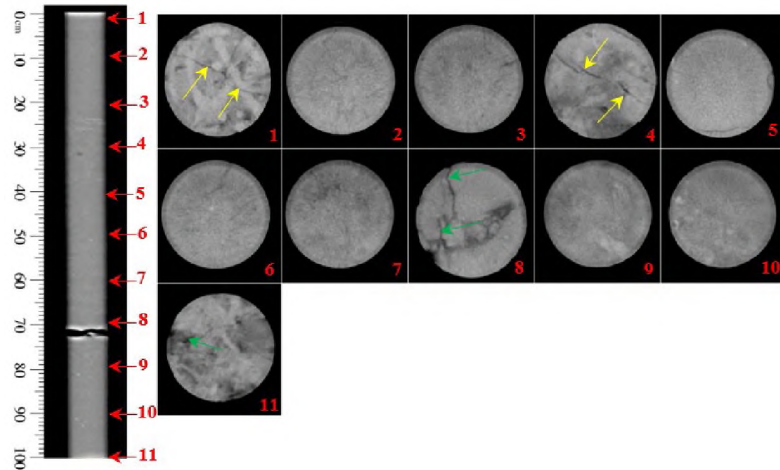


Figure 1. CT scan images of one section of the core show 11 axial scan slices along the longitudinal view for one full diameter core section.

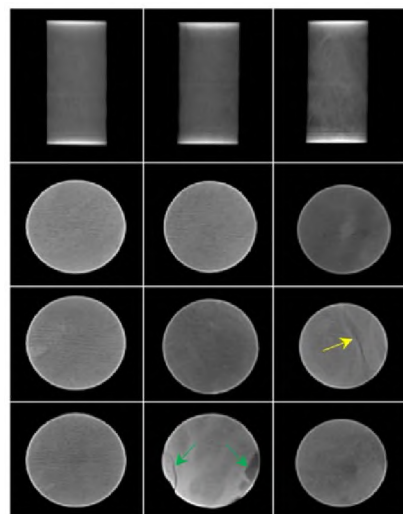


Figure 2. CT scan images of the three axial scan slices along the longitudinal view of the plug samples.

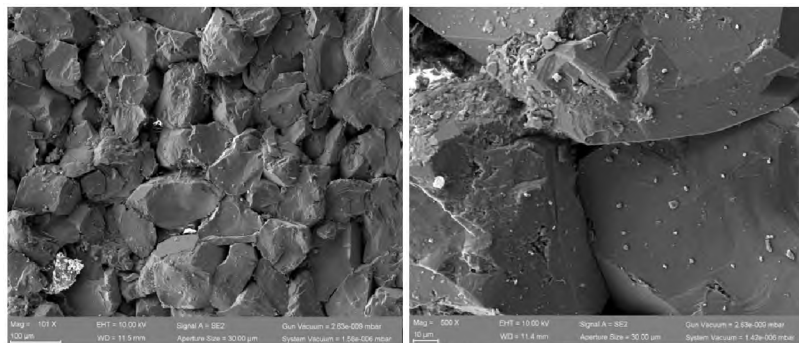


Figure 3. Scanning electron image of a sample of Zubair sandstone.

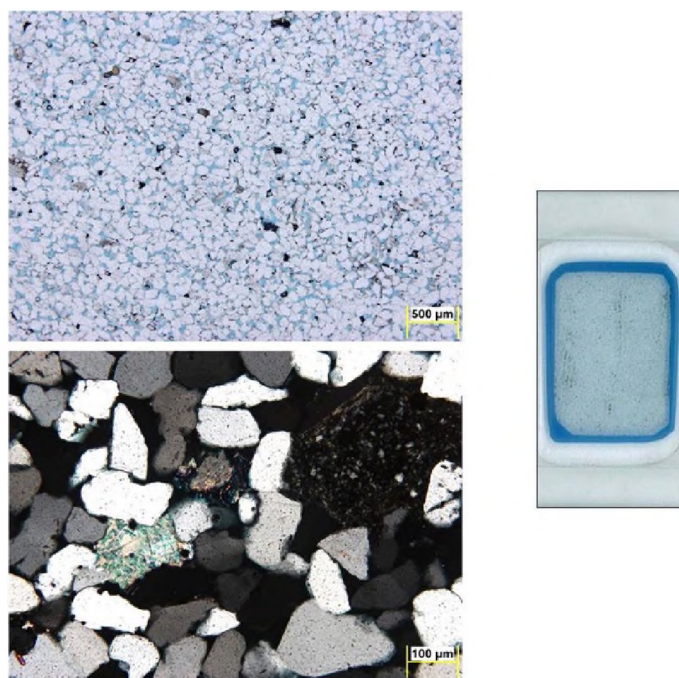


Figure 4. Thin-section plate of the Zubair sandstone formation.

Table 2. Mineral composition by X-ray diffraction of Zubair sandstone.

Sample	Mineral composition (%)							
	Quartz	Calcite	Pyrite	Plagioclase Feldspars	Siderite	Dolomite	K- Feldspar	Clay
1	76.71	8.34	-	6.74	1.20	3.62	-	3.39
2	82.25	-	1.12	-	-	-	9.04	7.59
3	89.54	3.67	-	-	3.13	2.11	-	1.55
4	75.43	-	-	9.65	10.35	-	4.23	0.34
5	77.10	11.53	1.87	-	-	8.48	-	1.02

4.2. ROCK STRENGTH PARAMETERS

Rock strength parameters primarily include the unconfined compressive strength, cohesive strength, and internal friction angle. Mohr circle construction is a very useful technique to graphically determine rock strength parameters. The Mohr circle was plotted for the maximum stress (peak axial stress at brittle failure) and minimum stress (confining pressure) for all tests in a test series (at different confining pressures) conducted on the same plug sample. On a graph with shear stress plotted along the y-axis and normal stress along the x-axis, a circle centered on $x = (\sigma_1 + \sigma_3)/2$ of radius $(\sigma_1 - \sigma_3)/2$ was drawn for each test in the test series. An analytical method was applied to calculate the best-fit linear failure envelope by drawing a straight-line tangent to each Mohr circle (Stafford et al., 1986). The intercept of the failure envelope on the shear stress axis when normal stress equals zero provides the cohesive strength (C), and $\tan^{-1}m$ is the internal friction angle (ϕ), as shown in Figure 5. The unconfined compressive strength (UCS) was calculated using Eq. 12:

$$UCS = \frac{2C \cos \phi}{1 - \sin \phi} \quad (12)$$

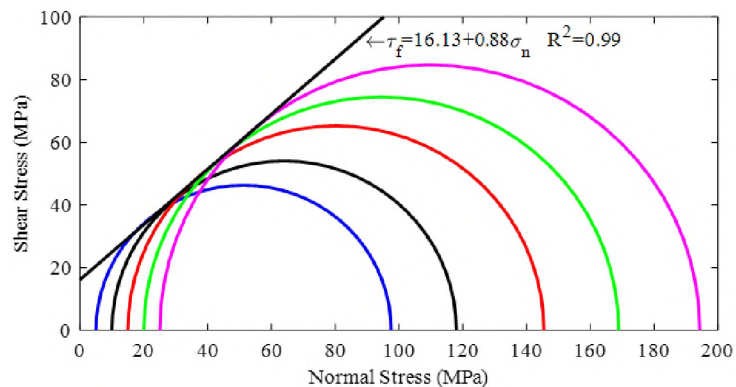


Figure 5. Failure envelope derived from multistage triaxial tests.

4.3. STATIC ELASTIC PARAMETERS

The static Young's modulus and static Poisson's ratio were calculated by plotting the axial and radial strains against the axial stress, which was determined by dividing the measured axial load by the initial cross-sectional area of the plug. The static Young's modulus was determined from slope of the tangent (at 50% of the peak stress) to the axial stress-strain curve in the drained triaxial phase, while the static Poisson's ratio was determined by calculating the ratio between the slopes of both the radial and the axial stress-strain curves in the drained triaxial phase (Asef and Farrokhrouz, 2017), as shown in Figure 6. The static bulk modulus and shear modulus were derived using Eqs. 13 and 14, respectively (Aadnoy and Looyeh, 2011):

$$K_s = E_s / (3(1 - 2\nu_s)) \quad (13)$$

$$G_s = E_s / (2(1 + \nu_s)) \quad (14)$$

where E_s is the static Young's modulus (GPa), ν_s is the static Poisson's ratio, K_s is the static bulk modulus (GPa), and G_s is the static shear modulus (GPa).

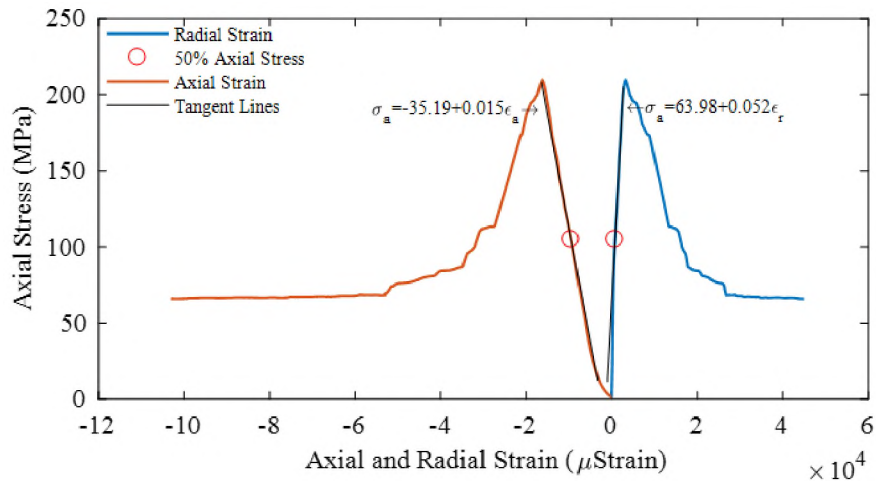


Figure 6. Static elastic parameters derived from triaxial tests.

4.4. CORRELATIONS

It is well understood that empirical correlations are not universally applicable (Chang et al., 2006). In this regard, local correlations were established to provide more confidence for estimating rock mechanical properties. Figures 7a-7f illustrate the results of the single-variable correlation technique employed to evaluate correlations for the rock strength parameters, elastic modulus, and Poisson's ratio of the Zubair Reservoir. In these Figures, the fitting model is plotted as a thick line between rock mechanical properties determined from the tests and laboratory-measured porosity. The correlation formulae and the magnitude of the correlation coefficient R^2 were summarized in Table 3.

Table 3. Suggested correlations for predicting static rock mechanical properties of Zubair sandstone.

Eq. no.	Equation	R^2
15	$UCS = 133.2 - 370.82\phi$	0.84
16	$\phi = 64.369 - 99.238\phi$	0.75
17	$E_s = 40.476 - 136.79\phi$	0.80
18	$K_s = 20.24 - 54.006\phi$	0.59
19	$G_s = 17.217 - 60.058\phi$	0.83
20	$\nu_s = 0.1203 - 0.766\phi$	0.70

The outlined results correlate well to core-measured rock mechanical properties with laboratory-measured porosity. A simple linear least squares regression was applied to all instances. The scatter in the data can be attributed to sample heterogeneities and limited laboratory errors. The resulting correlation equations indicate that:

- Both UCS and ϕ decrease as the porosity increases, with the best-fit curves as simple linear least square regressions (Figures 7a and 7b).

- The static elastic moduli (Young's modulus, bulk modulus, and shear modulus) decrease with increasing porosity, as presented in Figures 7c, 7d, and 7e.
- Poisson's ratio increases as porosity increases, with the best-fit curve as a simple linear least squares regression, as illustrated in Figure. 7f.

This was reflected in the anticipated trend: as porosity increased, the magnitude of the open pore space increased, while both the rock strength and the elastic modulus decreased. In contrast, Poisson's ratio rose with increasing porosity. These findings agree with those in previous studies in other geographical regions.

Finally, it should be noted that the correlations in Table 3 are limited to sandstone; therefore, a lithology check should be performed. The brittle mineral (quartz and calcite) content should be larger than approximately 75% to ensure a brittle mineral-bearing structure. The newly suggested empirical correlations are based on data from the Zubair sandstone formation in Southern Iraq, where they appear to apply with reasonable confidence to other geographical areas. It is highly recommended to compare some standard types of characterizations (i.e., porosity, mineralogy, texture, structure, etc.) for the specific zones of interest with Zubair sandstone characterizations.

4.5. STATISTICAL ANALYSIS

The accuracy of the predicted rock mechanical properties based on the mentioned empirical relationships was examined by statistical analysis. The following table shows the root mean square error (RMSE) and absolute relative average difference (ARAD) of the compared estimated values (based on equations in Table 1 and Table 3) with the

corresponding measured data. The ARAD and RMSE were calculated using Eq. 21 and Eq. 22, respectively.

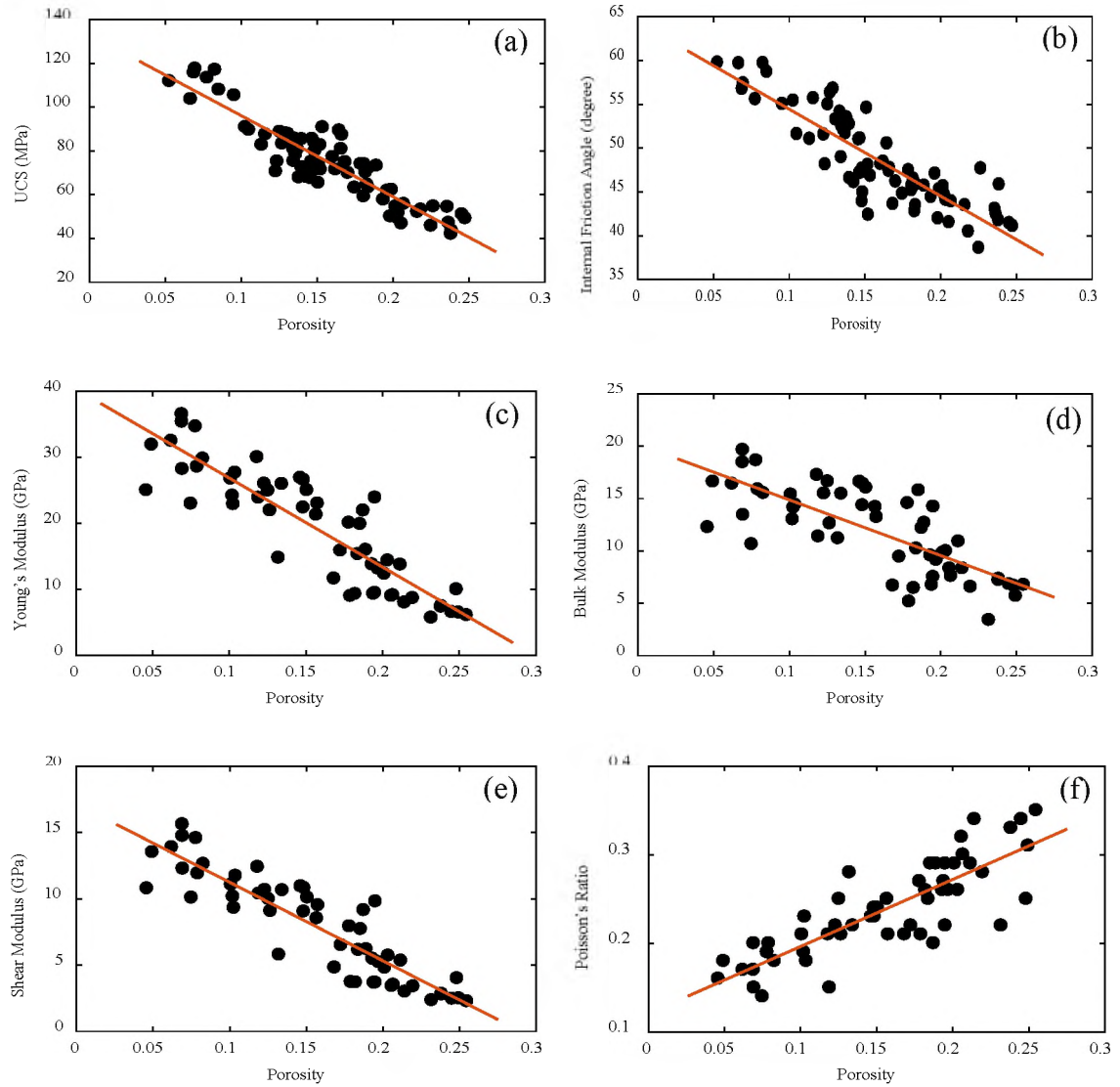


Figure 7. Calibration plots of rock mechanical properties versus lab-measured porosity.

$$ARAD = \frac{\sum |(x_i - y_i)| * \frac{100}{x_i}}{n} \quad (21)$$

$$RMSE = \sqrt{\frac{\sum (x_i - y_i)^2}{n}} \quad (22)$$

where x_i is the core-measured value, y_i is estimated value, and n is the number of core-measured values.

Table 4. The RMSE and ARAD of equations in Table 1 and Table 3 in the estimation of rock mechanical parameters.

Empirical Relationship	RMSE	ARAD
UCS predicted from ϕ		
Eq.1	24.25 MPa	23.20%
Eq.2	16.06 MPa	19%
Eq.4	10.73 MPa	12.73%
Eq.15	7.42 MPa	8.56%
ϕ predicted from ϕ		
Eq.3	7.93 degree	15.37%
Eq.5	19.22 degree	39.16%
Eq.16	2.61 degree	4.30%
E_s predicted from ϕ		
Eq.6	11.08 GPa	61.36%
Eq.8	45.26 GPa	89.08%
Eq.17	4.08 GPa	19.77%
K_s predicted from ϕ		
Eq.9	11.31 GPa	80.56%
Eq.18	2.67 GPa	17.69%
G_s predicted from ϕ		
Eq.10	29.08 GPa	96.42%
Eq.19	1.67 GPa	15.97%
ν_s predicted from ϕ		
Eq.7	0.11	44.38%
Eq.11	0.08	30.93%
Eq.20	0.03	9.78%

As shown in Table 4, the newly suggested correlations give lowest root mean square error (RMSE) and lowest absolute relative average difference (ARAD). Furthermore, the suggested empirical correlations were compared with correlations in the literature (Table 1) using a histogram of misfits between the estimated rock mechanical properties and the core-measured values. The results are summarized in Figures 8a-8f for the aforementioned correlations (Eqs. 15 - 20), respectively. The histogram of misfits (Figure 8a) shows that Eq. 15 predicted the unconfined compressive strength very well, fitting 70% of the data within ± 5 MPa. However, Eqs. 1, 2, and 4 fit 32%, 35%, and 41% of the data, respectively, within ± 5 MPa. Eq 4 tended to considerably overestimate the unconfined compressive strength. Figure 8b shows that Eq. 16 determined the internal friction angle extremely well, fitting 97% of the data within ± 5 degrees, whereas Eqs. 3 and 5 fit 84% and 0% of the data, respectively, within ± 5 degrees. Eqs. 3 and 5 tended to underestimate the internal friction angle. Figure 8c indicates that Eq. 17 calculated the Young's modulus very well, fitting 87% of the data within ± 5 GPa, while Eqs. 6 and 8 fit 40% and 39% of the data, respectively, within ± 5 GPa. Eq. 6 seemed to generally overestimate the Young's modulus, while Eq. 8 tended mainly to underestimate the Young's modulus. Figure 8d illustrates that Eq. 18 calculated the bulk modulus very well, fitting 95% of the given data within ± 5 GPa, while Eq. 9 tended to underestimate the bulk modulus, fitting only 44% of the data within ± 5 GPa. Figure 8e displays that Eq. 19 estimated the shear modulus excellently, fitting 100% of the data within ± 5 GPa, whereas Eq. 10 fits 82% of the data within ± 5 GPa. Figure 8f illustrates that Eq. 20 predicted Poisson's ratio very well, fitting 93% of the given data within ± 0.05 , while Eqs. 7 and 11

fit 38% and 25% of the data, respectively, within ± 0.05 . Eq. 7 appeared to underestimate Poisson's ratio, while Eq. 11 extremely overestimated Poisson's ratio.

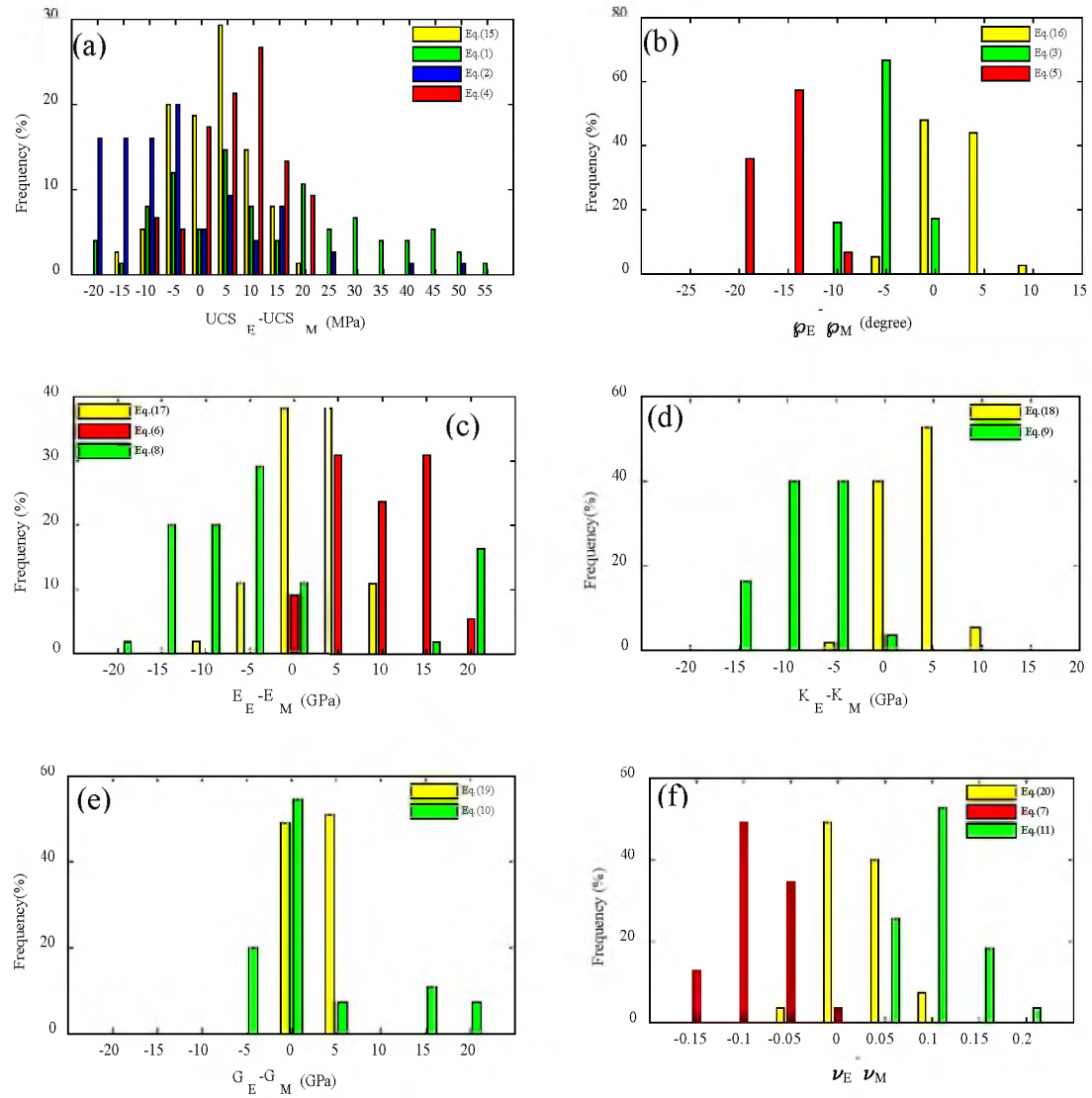


Figure 8. Histograms showing the frequency versus the difference in the estimated (E) and measured (M) mechanical properties.

4.6. DERIVATION OF ROCK MECHANICAL PROPERTIES

The suggested empirical correlations (Table 3) were implemented to derive a continuous profile of the rock mechanical properties from wireline log porosity. This is done in two steps:

4.6.1. Calibration of Wireline Log Porosity with the Laboratory-Measured Porosity. Porosity can be directly estimated from density, sonic, and neutron logs, or a combination of these. Borehole conditions, such as pressure, temperature, mud weight, and washout in a shale interval, have considerable influence on the wireline log quality readings. A high-quality porosity log provides an estimate of the rock mechanical properties with a high degree of confidence. Therefore, it is necessary to calibrate the wireline log porosity against the laboratory-measured porosity prior to the derivation of the rock mechanics from the porosity log. An empirical correction was implemented between the wireline-calculated porosity from the density, sonic, and neutron logs for one of the cored wells and the core-measured porosity. The results show that the neutron porosity is the best-fitting porosity for the different depths, with a correlation coefficient of $R^2 = 0.84$, as shown in Figure. 9. Then, Eq. 23, which expresses the best-fit line, was applied to derive the calibrated neutron porosity log:

$$\phi_{NC} = 0.0322 + 0.8165\phi_N \quad (23)$$

where ϕ_{NC} is the calibrated neutron porosity, and ϕ_N is the neutron porosity. The laboratory- measured porosities were added to the plot of the calibrated neutron porosity log. As shown in fig. 10, there is good agreement between the calibrated neutron porosity log and the individual laboratory-measured porosities, with 7.39% ARAD.

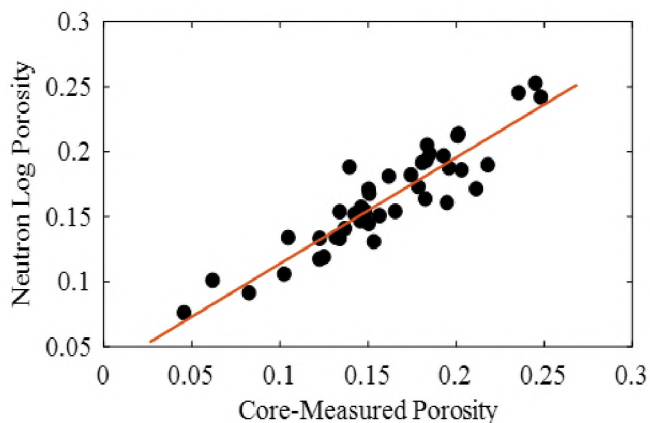


Figure 9. Empirical correction between the neutron log porosity and core-measured porosity.

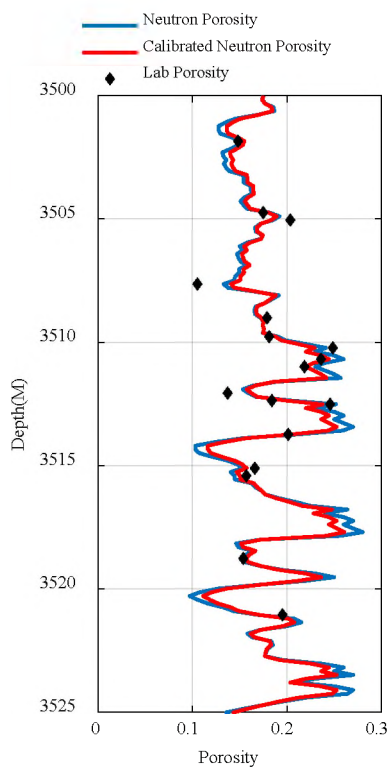


Figure 10. Wireline neutron porosity and calibrated neutron porosity logs.

4.6.2. Implementation of the Correlations to Derive Rock Mechanical Properties. The empirical correlations described previously were used to derive rock

mechanical properties from the calibrated neutron wireline porosity log. The derived rock mechanical logs were plotted against depth. The laboratory-measured rock mechanical properties were added to the plot to assess the level of agreement between the experimentally measured rock mechanical properties and the derived rock mechanical logs. Figures 11, 12, and 13 present examples of the rock mechanical property logs for one of the cored wells in the Zubair sandstone reservoir. As can be seen, there is a high degree of positive correlation between the calculated rock mechanical property logs (i.e., UCS, internal friction angle, Young's modulus, Poisson's ratio, bulk modulus, and shear modulus) and those derived from the laboratory, with 8.71%, 7.99%, 9.36%, 11.90%, 11.70%, and 11.48% ARAD, respectively.

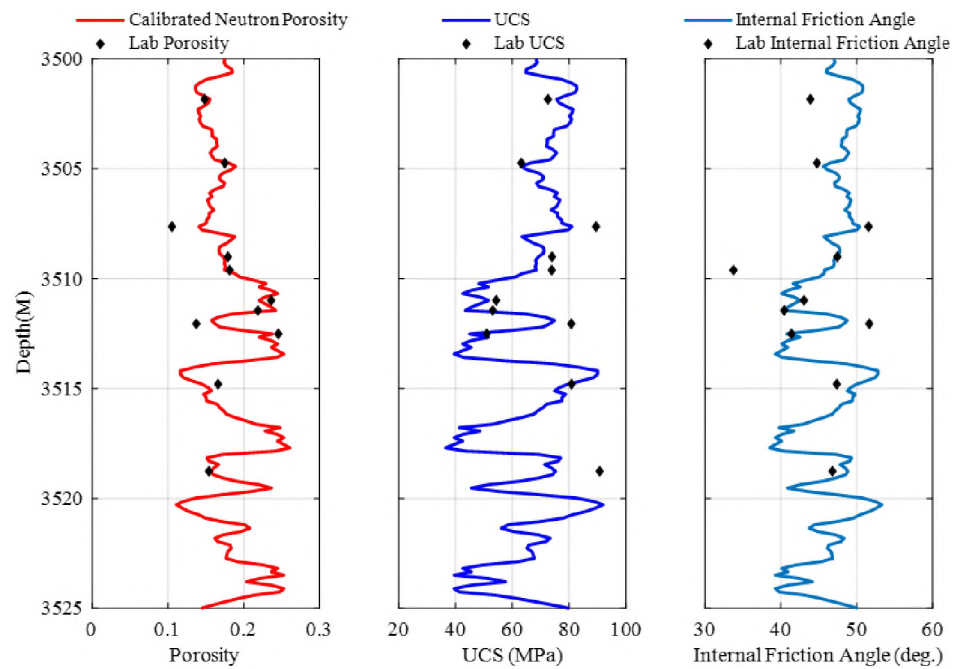


Figure 11. Predicted unconfined compressive strength and internal friction angle logs from Eqs. 15 and 16, respectively.

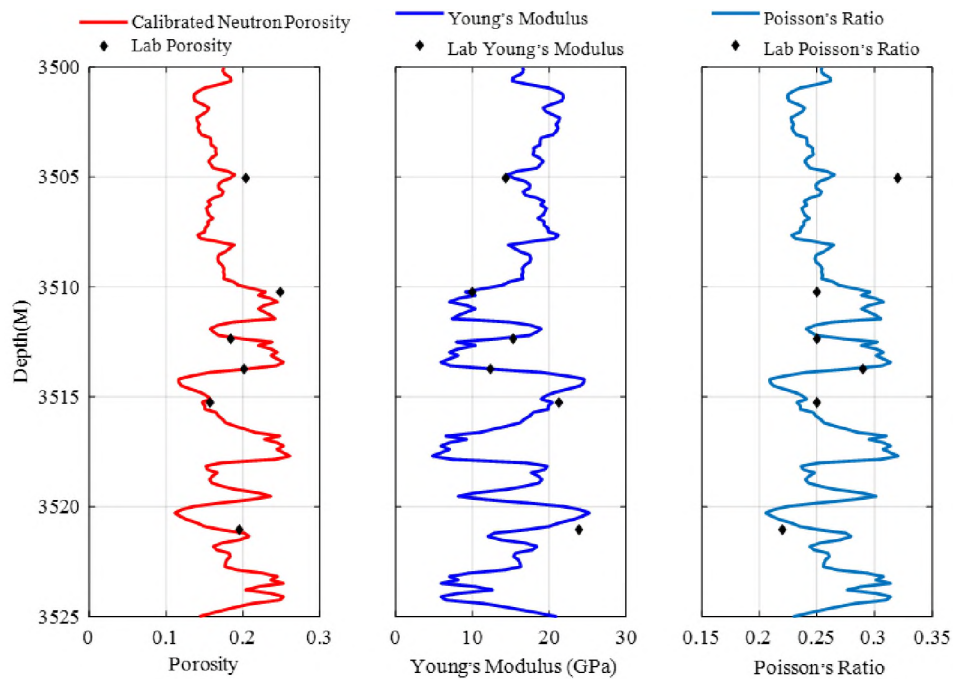


Figure 12. Predicted Young's modulus and Poisson's ratio logs using Eqs. 17 and 20, respectively.

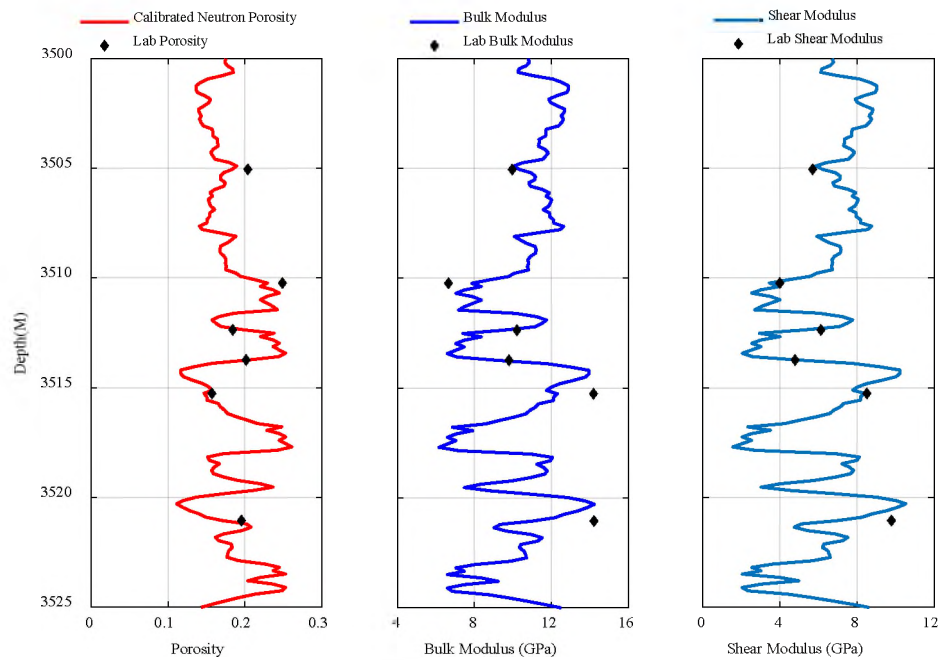


Figure 13. Predicted bulk and shear modulus logs using Eqs. 18 and 19, respectively.

5. FIELD APPLICATIONS OF THE FINDINGS OF THIS STUDY

The results of this work can be used in the design and implementation of production and drilling processes throughout the Zubair Reservoir. Some applications are illustrated below.

5.1. SAND PRODUCTION PREDICTION

Sand production becomes a serious problem during the life of a well in the Zubair Reservoir. The most dominant remedy is the gravel-pack completion, which blocks the influx of sand with specially selected gravel held in place by screens (Rodrigues et al., 2016). This method is expensive but not nearly as costly as losing a producer. Thus, it is quite important to know if a well will produce sand before it is placed in production. The sand production through the Zubair Reservoir can be assessed by the following methods:

5.1.1. Shear and Bulk Modulus Method. The mathematical product of the shear and bulk modulus has been related empirically to the sand influx. This mechanical property log method is 81% effective (Khomehchi and Reisi, 2015). Tixier et al. (1975) found that sand production could be expected if the product $G_s K_s$ of two elastic parameters was below 38 GPa². The shear and bulk moduli were calculated from the suggested empirical correlation of the experimental measurements of the shear and bulk moduli with the porosity.

5.1.2. Unconfined Compressive Strength Method. A hydrocarbon production operation is associated with reservoir depletion. The drawdown in a reservoir relates directly to the unconfined compressive strength. Sandstone collapse is most likely if the

drawdown in the reservoir exceeds the unconfined compressive strength (Bratli and Risnes, 1981). If the predicted UCS is below 50 MPa, sanding is likely to occur.

A plot for the prediction of sand production is presented in Figure 14, where the UCS and $G_s K_s$ logs are shaded below their sanding thresholds to show the intervals that are likely to produce sand.

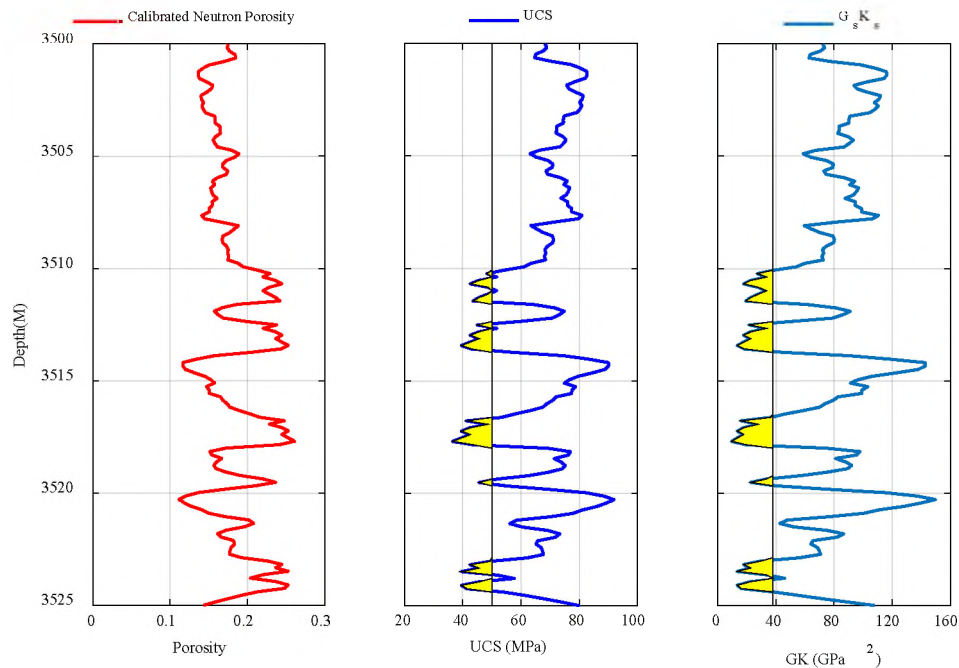


Figure 14. Sanding potential plot showing the yellow zones as likely zones to produce sand.

5.2. DESIGNING ACID FRACTURING TREATMENT

Acid fracturing is performed to improve the natural permeability of the reservoir around the wellbore by the injection of acids at a pressure above the fracturing pressure of the formation (Hassani and Kamali, 2017). Hydraulic fracturing acid is used to create an etched, non-smooth fracture, with sufficient roughness to keep the fracture open during the

life of a well. The empirical correlations established in the current study were implemented to derive a static Young's modulus and Poisson's ratio for the design of acid fracturing in the Zubair Reservoir. As shown in Figure 15, the predicted Young's modulus and Poisson's ratio from the current relationships show reasonably good agreement with those derived from the mini-fracturing and the main hydrofracturing stimulation, with 12.59% and 14.89% ARAD, respectively.

This example indicates that the predicted Young's modulus and Poisson's ratio from the mentioned empirical correlations can be a valuable tool in an acid fracturing operation

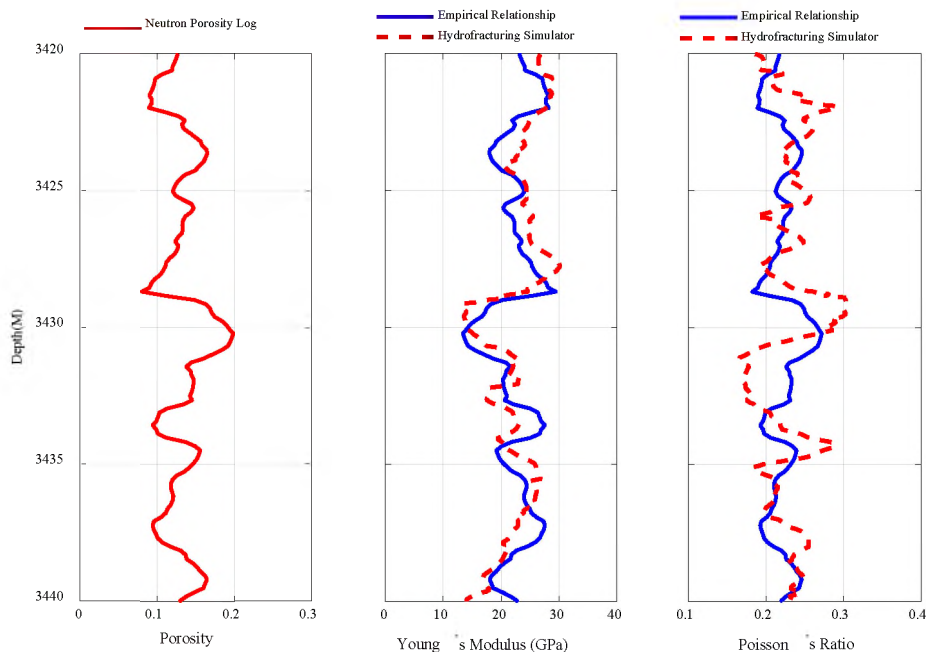


Figure 15. Predicted Young's modulus and Poisson's ratio from the current empirical relationships, using a commercial hydrofracturing simulator.

6. CONCLUSIONS

Knowledge of rock characterization is necessary in order to identify the nature of lithology. The Zubair sandstone was extensively characterized in terms of mineralogy, texture, structure, grain distribution, and consolidation. Triaxial and multistage triaxial tests were performed on Zubair sandstone core specimens, and the values of the rock mechanical properties were measured. The results illustrate that the rock mechanical properties are mainly functions of porosity. The empirical expressions described herein were formulated to relate the rock mechanical properties with laboratory-measured porosity. Throughout the Zubair sandstone oilfield, the linear expression correlations were more reliable than the exponential functions and power functions for the rock mechanical properties. The porosity is a primary input parameter in all the correlations; thus, various sources for determining the porosity, such as density, sonic, and neutron wireline logs, can be used to obtain continuous estimates of the Zubair sandstone mechanical properties. The obtained results from statistical analysis provide further evidence that empirically based correlations are not universally applicable. The correlations are based on one type of lithology for the specific geographical area; these correlations may not be applicable to other geographical regions. Consequently, it is highly recommended to check the validity of the correlations before using them in rock mechanical prediction for another geographical area. It can therefore be concluded that the specific empirical correlations for a specific formation are more reliable than general ones. Due to the importance of rock mechanical properties in studies for the petroleum industry, it is always worth predicting these parameters for a specific formation from empirical correlations that have been

developed for the same formation in the same geographical area. The derived relationships have been applied as cost-effective tools in reservoir management and development.

ACKNOWLEDGMENTS

The first author would like to thank the Higher Committee for Education Development (HCED) in Iraq for awarding him a fully funded Ph.D. scholarship. The authors would like to thank Basrah Oil Company in Iraq for support in core samples and for their permission to publish the results. We also want to thank Missouri University of Science and Technology for providing the facilities to do this work.

REFERENCES

- Aadnoy, B. and Looyeh, M. R., 2011. *Petroleum Rock Mechanics Drilling Operations and Well Design*. Burlington, VT: Elsevier Science.
- Abeed, Q., Alkhafaji, A., and Littke, R., 2011. Source Rock Potential of the Upper Jurassic - Lower Cretaceous Succession in the Southern Mesopotamian Basin, Southern Iraq. *Journal of Petroleum Geology* 34 (2): 117-134. <https://doi.org/10.1111/j.1747-5457.2011.00497.x>.
- Alikarami, R., Torabi, A., Kolyukhin, D. and Skurtveit, E., 2013. Geostatistical Relationships between Mechanical and Petrophysical Properties of Deformed Sandstone. *Int J Rock Mech Min Sci* 63: 27-38. <http://dx.doi.org/10.1016/j.ijrmms.2013.06.002>.
- Ameen, M. S., Smart, B. G., Somerville, J., Hammilton, S., and Naji, N. A. 2009. Predicting rock mechanical properties of carbonates from wireline logs (A case study: Arab-D reservoir, Ghawar field, Saudi Arabia). *Mar. Pet. Geol.* 26 (4): 430-444. <https://doi.org/10.1016/j.marpetgeo.2009.01.017>.

- Asef, M. R. and Farrokhrouz, M., 2017. A Semi-Empirical Relation between Static and Dynamic Elastic Modulus. *J Petrol Sci Eng* 157: 359–363. <http://dx.doi.org/10.1016/j.petrol.2017.06.055>.
- Bratli, R. K. and Risnes, R., 1981. Stability and Failure of Sand Arches. *SPE J.* 21 (02): 236–248. <http://dx.doi.org/10.2118/8427-pa>.
- Chang, C., Zoback, M. D. and Khaksar, A., 2006. Empirical Relations between Rock Strength and Physical Properties in Sedimentary Rocks. *J Petrol Sci Eng* 51 (3–4): 223–237. <http://dx.doi.org/10.1016/j.petrol.2006.01.003>.
- Choo, C., Takahashi, M., and Jeong, G., 2014. Identification and Three-Dimensional Characterization of Micropore Networks Developed in Granite using Micro-Focus X-ray CT. *Journal of Engineering Geology*, 24(2), 179-189. <https://doi.org/10.9720/kseg.2014.2.179>.
- Dewhurst, D. N., Sarout, J., Delle Piane, C., Siggins, A. F., & Raven, M. D., 2015. Empirical strength prediction for preserved shales. *Mar. Pet. Geol.* 67, 512-525. <http://dx.doi.org/10.1016/j.marpetgeo.2015.06.004>.
- Dott, R.H., 1964. Wacke, Graywacke and Matrix-What Approach to Immature Sandstone Classification? *SEPM Journal of Sedimentary Research*, Vol. 34. <https://doi.org/10.1306/74d71109-2b21-11d7-8648000102c1865d>.
- Edlmann, K., Somerville, J., Smart, B., Hamilton, S. and Crawford, B., 1998. Predicting Rock Mechanical Properties from Wireline Porosities. Presented at SPE/ISRM Rock Mechanics in Petroleum Engineering, Trondheim, Norway. 8–10 July. SPE-47344-MS. <http://dx.doi.org/10.2118/47344-ms>.
- Fjær, E., Holt, R. M., Horsrud, P., Raaen, A. M. and Risnes, R., 2008. *Petroleum Related Rock Mechanics*, 2nd ed. Amsterdam: Elsevier Science.
- Hassani, A. and Kamali, M. R., 2017. Optimization of Acid Injection Rate in High Rate Acidizing to Enhance the Production Rate: An Experimental Study in Abteymour Oil Field, Iran. *J Petrol Sci Eng* 156: 553–562. <http://dx.doi.org/10.1016/j.petrol.2017.06.049>.
- Holt, A. M. and Fjær, E., 1991. Validity of Multiple Failure State Triaxial Tests in Sandstones. *International Society for Rock Mechanics*.
- Hoshino, K., 1974. Effect of Porosity on the Strength of the Clastic Sedimentary Rocks. In *Reports of Current Research Vol. III, Part A, Themes 1–2, Proc. 3rd Cong. Int. Soc. Rock Mech.*, Denver, Colorado, 511–516.

- Jassim, S. Z. and Goff, J. C., 2006. *Geology of Iraq*, first edition. Brno and Prague, Czech Republic: Dolin and Moravian Museum.
- Kassab, M. A., Teama, M. A., Cheadle, B. A., El-Din, E. S., Mohamed, I. F., and Mesbah, M. A., 2015. Reservoir characterization of the Lower Abu Madi Formation using core analysis data: El-Wastani gas field, Egypt. *Journal of African Earth Sciences*, 110, 116-130. <https://doi.org/10.1016/j.jafrearsci.2015.06.008>.
- Khair, E. M., Zhang, S. and Abdelrahman, I. M., 2015. Correlation of Rock Mechanic Properties with Wireline Log Porosities through Fulla Oilfield - Mugllad Basin - Sudan. Presented at the SPE North Africa Technical Conference and Exhibition, Cairo, Egypt, 14–16 September. <http://dx.doi.org/10.2118/175823-ms>.
- Khamehchi, E., and Reisi, E., 2015. Sand Production Prediction Using Ratio of Shear Modulus to Bulk Compressibility (Case Study). *Egypt J Pet* 24 (2): 113–118. <http://dx.doi.org/10.1016/j.ejpe.2015.05.002>.
- Kidambi, T. and Kumar, G. S., 2016. Mechanical Earth Modeling for a Vertical Well Drilled in a Naturally Fractured Tight Carbonate Gas Reservoir in the Persian Gulf. *J Petrol Sci Eng* 141: 38–51. <http://dx.doi.org/10.1016/j.petrol.2016.01.003>.
- Kovari, K., Tisa, A., Einstein, H. H. and Franklin, J. A., 1983. Suggested Methods for Determining the Strength of Rock Materials in Triaxial Compression: *Rev. Int J Rock Mech Min Sci*. 20: 283–290.
- Kowalski, J., 1975. Formation Strength Parameters from Well Logs. Society of Petrophysicists and Well-Log Analysts. Presented at the PWLA 16th Annual Logging Symposium, New Orleans, Louisiana, 4–7 June.
- Mike, S., Sandra, G., and Marc, C., 2009. Laboratory Methods to Assess Shale Reactivity with Drilling Fluids. AADE National Technical Conference & Exhibition, New Orleans, Louisiana.
- Najibi, A. R., Ghafoori, M., Lashkaripour, G. R., & Asef, M. R., 2015. Empirical relations between strength and static and dynamic elastic properties of Asmari and Sarvak limestones, two main oil reservoirs in Iran. *J Petrol Sci Eng* 126: 78-82. <http://dx.doi.org/10.1016/j.petrol.2014.12.010>.
- Pan, R., Zhang, G., Li, S., An, F., Xing, Y., Xu, D. and Xie, R., 2016. Influence of Mineral Compositions of Rocks on Mechanical Properties. Presented at the 50th U.S. Rock Mechanics/Geomechanics Symposium, American Rock Mechanics Association, Houston, Texas, 26–29 June.
- Peng, S. and Zhang, J., 2007. *Engineering Geology for Underground Rocks*. Berlin: Springer-Verlag. <http://dx.doi.org/10.1007/978-3-540-73295-2>.

- Ribeiro, R. C., Correia, J. C. and Seidl, P. R., 2009. The Influence of Different Minerals on the Mechanical Resistance of Asphalt Mixtures. *J Petrol Sci Eng* 65 (3–4): 171–174. <http://dx.doi.org/10.1016/j.petrol.2008.12.025>.
- Rodrigues, R. K., Folsta, M. G., Martins, A. L. and Sabadini, E., 2016. Tailoring of Wormlike Micelles as Hydrodynamic Drag Reducers for Gravel-Pack in Oil Field Operations. *J Petrol Sci Eng* 146: 142–148. <http://dx.doi.org/10.1016/j.petrol.2016.04.021>.
- Ryshkewitch, E., 1953. Compression Strength of Porous Sintered Alumina and Zirconia. *J Am Ceram Soc* 36 (2): 65–68. <http://dx.doi.org/10.1111/j.11512916.1953.tb12837.x>.
- Santarelli, F. J., Detienne, J. L. and Zundel, J. P., 1989. Determination of the Mechanical Properties of Deep Reservoir Sandstones to Assess the Likelihood of Sand Production. International Society for Rock Mechanics.
- Sarda, J., Kessler, N., Wicquart, E., Hannaford, K. and Deflandre, J., 1993. Use of Porosity as a Strength Indicator for Sand Production Evaluation. Presented at the SPE Annual Technical Conference and Exhibition, Houston, Texas, 3–6 October. SPE-26454-MS. <http://dx.doi.org/10.2118/26454-ms>.
- Sethi, D. K., 1981. Well Log Applications in Rock Mechanics. Presented at the SPE/DOE Low Permeability Gas Reservoirs Symposium, Denver, Colorado, 27–29 May. SPE-9833-MS. <http://dx.doi.org/10.2118/9833-MS>.
- Sharma, M. R., O'Regan, M., Baxter, C., Moran, K., Vaziri, H., & Narayanasamy, R., 2010. Empirical relationship between strength and geophysical properties for weakly cemented formations. *J Petrol Sci Eng* 72 (1-2), 134-142. <http://dx.doi.org/10.1016/j.petrol.2010.03.011>.
- Sissakian, V. K., 2013. Geological Evolution of The Iraqi Mesopotamia Foredeep, Inner Platform and Near Surroundings of the Arabian Plate. *Journal of Asian Earth Sciences* 72: 152-163. <https://doi.org/10.1016/j.jseaes.2012.09.032>.
- Stafford, J., Audsley, E. and Sharp, J., 1986. The Determination of Best Fit Linear Failure Envelopes to Mohr Circles. *J Agr Eng Res* 33 (1): 33–38. [http://dx.doi.org/10.1016/s0021-8634\(86\)80027-0](http://dx.doi.org/10.1016/s0021-8634(86)80027-0).
- Tixier, M., Loveless, G. and Anderson, R., 1975. Estimation of Formation Strength from the Mechanical-Properties Log (includes associated paper 6400). *J Pet Technol* 27 (3): 283–293. <http://dx.doi.org/10.2118/4532-pa>.

- Vernik, L., Bruno, M. and Bovberg, C., 1993. Empirical Relations between Compressive Strength and Porosity of Siliciclastic Rocks. *Int J Rock Mech Min Sci* 30 (7): 677–680. [http://dx.doi.org/10.1016/0148-9062\(93\)90004-w](http://dx.doi.org/10.1016/0148-9062(93)90004-w).
- Wang, H. and Sharma, M. M., 2017. A Non-Local Model for Fracture Closure on Rough Fracture Faces and Asperities. *J Petrol Sci Eng* 154: 425–437. <http://dx.doi.org/10.1016/j.petrol.2017.04.024>.
- Weingarten, J. and Perkins, T., 1995. Prediction of Sand Production in Gas Wells: Methods and Gulf of Mexico Case Studies. *J Pet Technol* 47 (7): 596–600. <http://dx.doi.org/10.2118/24797-pa>.
- Yagiz, S., 2010. Correlation between Slake Durability and Rock Properties for Some Carbonate Rocks. *Bulletin of Engineering Geology and the Environment* 70 (3): 377-383. <https://doi.org/10.1007/s10064-010-0317-8>.
- Yagiz, S., 2011. P-Wave Velocity Test for Assessment of Geotechnical Properties of Some Rock Materials. *Bulletin of Materials Science* 34 (4): 947-953. <https://doi.org/10.1007/s12034-011-0220-3>.
- Zeynali, M. E., 2012. Mechanical and Physico-chemical Aspects of Wellbore Stability during Drilling Operations. *J Petrol Sci Eng* 82–83: 120–124. <http://dx.doi.org/10.1016/j.petrol.2012.01.006>.
- Zoback, M., Barton, C., Brudy, M., Castillo, D., Finkbeiner, T., Grollmund, B., Moos, D., Peska, P., Ward, C. and Wiprut, D., 2003. Determination of Stress Orientation and Magnitude in Deep Wells. *Int J Rock Mech Min Sci* 40 (7–8): 1049–1076. <http://dx.doi.org/10.1016/j.ijrmms.2003.07.001>.

II. ESTIMATING ROCK MECHANICAL PROPERTIES OF THE ZUBAIR SHALE FORMATION USING A SONIC WIRELINE LOG AND CORE ANALYSIS

Ahmed K. Abbas, Ralph Flori, and Mortadha Alsaba

Department of Petroleum Engineering Engineering, Missouri University of Science and Technology, Rolla, MO 65409

ABSTRACT

The Zubair Formation is the most prolific reservoir in Iraq, which is comprised of sandstones interbedded with shale sequences. Drilling boreholes in this formation has always been a challenge due to the weak nature of the shale sequence. Historically, over 90% of wellbore problems in the Zubair Formation are due to shale instability. To solve this problem, it is necessary to understand the rock mechanical properties and the response of shale. The main objective of this study is to develop local empirical correlations of rock mechanical properties that can be used to estimate a continuous profile of these properties throughout the depth of the Zubair shale formation directly from a wireline sonic log.

Well-preserved core samples of Zubair shale were run through extensive testing, including a number of shale characterization and rock mechanical tests. Special characteristics of shale were measured and described, including the porosity, structure, texture, and mineralogy, using the free water content method, a scanning electron microscope image, a thin section photograph, and X-ray diffraction analysis. Consolidated undrained triaxial tests were conducted to determine the static rock mechanical properties. Local empirical correlations were established, with the acoustic compressional velocity as

a primary input parameter. Thus, sonic wireline logs can be used directly to obtain a continuous profile of the rock mechanical properties through the entire interval of the Zubair shale formation. The accuracy of the newly developed empirical correlations was examined using statistical analysis. Moreover, these correlations were compared with previous correlations from the literature. The results showed that the suggested empirical correlations are highly accurate and reliable, in contrast to those in the literature, which did not adequately fit the Zubair shale data. This highlights the importance of using local correlations to estimate rock mechanical properties.

The predicted continuous rock mechanical profile gives a good indication of the strength and stability of the shale around the wellbore. Consequently, it can be used to solve shale instability problems, optimize drilling processes (i.e., the selection of bit type and drilling parameters), seal integrity evaluation, and otherwise improve fracturing operations across the Zubair shale formation.

1. INTRODUCTION

Shale instability is frequently reported as one of the most serious obstructions during drilling in the Zubair shale formation in several oil fields in Southern Iraq (Abbas et al., 2018). Shale instability problems, such as borehole collapse, tight hole, stuck pipe and logging tools, poor log quality, borehole enlargement, and poor primary cement jobs result in excessive operational costs and delays in drilling time. For an economical and successful development of these fields, knowledge of the mechanical properties of Zubair shale is of crucial importance for drilling process optimization, wellbore stability analysis,

well trajectory optimization, and hydraulic fracturing design (Onyia 1988; Yuan et al. 2012; Rasouli and Sutherland 2013; Guo et al. 2015; Li and Tang 2016). Stjern et al. (2003) reported an average cost reduction close to 2.5 million USD for an average well through the knowledge of shale mechanical properties; given that the field had 50 more wells to be drilled, the total savings would have been in excess of 100 million USD. However, shale formations are not the main target of hydrocarbon exploration; consequently, shale samples from deep boreholes are almost never available for testing due to the extra cost related to coring operations in deep wellbores. Even if the core samples are taken from depths of interest, the shale cores may be further damaged by the action of the drill bit during coring operations and by subsequent improper preservation and sample preparation. This may affect shale properties significantly and make core samples useless for rock mechanical analysis. In addition, laboratory tests can only cover a small part (several feet) of the section interval. Thus, it is imperative to find methods that can provide mechanical properties in continuous profile through the entire interval of the shale formation. Such methods can be based on wireline measurements that are available throughout the entire section of the shale (e.g., porosity logs and acoustic velocity logs). Since the mechanical properties cannot be inferred directly from wireline logs, a number of empirical correlations have been introduced as a practical solution to this issue (Edlmann et al. 1998; Ameen et al. 2009; Ranjbar-Karami et al. 2014). Most of these correlations are based on the empirical correlation of laboratory-derived rock mechanical parameters with geophysical well logs, providing estimations of porosities or acoustic velocities. The basis for these relationships is the fact that many of the same factors that affect rock mechanical properties also affect other physical properties, such as porosity, velocity, and elastic moduli (Chang et al. 2006).

In this study, consolidated undrained (CU) triaxial tests were performed on preserved core samples from the Zubair shale formation in Southern Iraq, to determine the strength parameters (i.e., unconfined compressive strength, cohesive strength, and internal friction angle) and static elastic parameters (i.e., Young's modulus and Poisson's ratio). In addition, Zubair shale was fully characterized in terms of porosity, structure, texture, and mineralogy using the free water content method, a scanning electron microscope, a thin section photograph, and X-ray diffraction analysis. Forty-five plug samples were tested for compressional acoustic wave velocity and mechanical properties at increasing triaxial stress levels. The shale samples used in this study were well-preserved from the moment of retrieval until testing. The measured rock mechanical properties were plotted against their corresponding compressional wave velocities to predict the local empirical correlations formulae. These empirical relationships were directly applied to a sonic wireline log to establish continuous rock mechanical property logs. This continuous profile of rock mechanical properties through the section of the shale can be used in the design and implementation of drilling and production processes throughout the Zubair shale formation.

2. LITERATURE REVIEW OF RELEVANT CORRELATIONS

Because shale formations are not the primary targets in hydrocarbon exploration, shale samples are very rare. This is the main reason for the lack of published data on these overburdened formations and the reason that many investigators have used outcrop shales instead.

To derive correlations between porosity and the unconfined compressive strength, Lashkaripour and Dusseault (1993) used a large set of shale data that were collected from published literature and in-house studies. Most of the shale samples had porosities below 20%. Horsrud (2001) established a relationship between the unconfined compressive strength and porosity, which was based on data obtained from laboratory tests on shale core samples with high porosity (30–55%). These correlations differ from those found for lower porosity shales by Lashkaripour and Dusseault (1993). Both investigations verified that compressional wave velocity measurements showed a good correlation to shale strength, making it a valuable tool for estimating shale mechanical properties from sonic measurements on drill cuttings or from the log and seismic data.

The empirical correlations for the mechanical properties of shale listed in Table 1 are based on the acoustic compressional velocity as a primary input parameter. Lal (1999) derived empirical correlations between rock strength parameters and compressional wave velocity (Eqs. 1 and 2). The relations were developed using core-measured compressional wave velocity and rock strength for North Sea Tertiary shales. Lal (1999) found that the shale strength properties were affected by three factors: clay content, clay mineralogy, and the degree of compaction (characterized by water content, sonic velocity, porosity, etc.), which is the dominant factor.

Horsrud (2001) developed a number of empirical correlations (Eqs. 3 and 4) that can be used to estimate the continuous profile of shale mechanical properties from various sources of acoustic compressional velocity, such as sonic wireline logs, sonic logging while drilling (MWD), and ultrasonic measurements on core plugs or cuttings. These correlations use data obtained from laboratory tests of a variety of deeply cored shales from the North

Sea, including some outcrop clays/mudstones. Horsrud (2001) observed that the friction coefficient does not generally correlate with the more easily measured properties and also shows some dependence on kaolinite content.

To determine empirical strength correlations for a global and a local shale population (Eqs. 5 and 6), Dewhurst et al. (2010) presented the relationship between static mechanical properties and compressional wave velocity. This relationship was obtained using the measurements made on a selection of well-characterized shales from the Norwegian Sea and the Australian margin, combining them with the few tests recorded in the literature on well-preserved, fully saturated shales.

Table 1. Empirical relationships between rock mechanical properties and the P-wave velocity for shale.

Eq. no.	Equation	R ²	Reference
1	$UCS = 10(v_p - 1)$	-	Lal (1999)
2	$\varphi = \sin^{-1}((v_p - 1) / (v_p + 1))$	-	Lal (1999)
3	$UCS = 0.77v_p^{2.93}$	0.99	Horsrud (2001)
4	$E = 0.076v_p^{3.23}$	0.99	Horsrud (2001)
5	$UCS = 0.03e^{2v_p}$	0.98	Dewhurst et al. (2010)
6	$E = 5v_p - 10.26$	0.87	Dewhurst et al. (2010)

3. METHODOLOGY

3.1. CHARACTERIZATION OF THE SHALE FORMATION

Shales are fine-grained sedimentary rocks that contain a substantial amount of clay minerals. In practice, this means that shales have a clay content higher than about 40% (Fjær et al. 2008). A shale's property characterization (e.g., porosity, mineralogy, texture,

and structure) has a profound influence on its mechanical behavior (Josh et al. 2012; Labani and Rezaee 2014; Fang et al. 2016; Wang et al. 2016). To understand shale behavior under applied stresses, these characteristics must be investigated.

3.1.1. CT Scanning Technique. The mathematical product of the shear and bulk modulus has been related empirically to the sand influx. This mechanical property log method is 81% effective (Khamehchi and Reisi, 2015). Tixier et al. (1975) found that sand production could be expected if the product $G_s K_s$ of two elastic parameters was below 38 GPa². The shear and bulk moduli were calculated from the suggested empirical correlation of the experimental measurements of the shear and bulk moduli with the porosity.

3.1.2. Scanning Electron Microscope. A shale sample from the Zubair Formation was imaged using a scanning electron microscope (SEM) to determine the integrity of the rock and measure the degree of cementing and compaction. SEM photographs allow for better three-dimensional observations of micro-cracks and micro-laminations in the specimen that are not easily seen using transmitted light or transmitted electron microscope techniques. The texture and orientation of the shale, its degree of compaction, and the presence of embedded minerals and pores can be observed (Mike et al., 2009). SEM images of a specimen were produced by scanning the surface with a focused beam of electrons. These electrons interact with atoms in the specimen, producing various signals that contain data about the specimen's surface topography and composition. For SEM, a specimen needs to be completely dry and large enough to withstand the vacuum conditions and high energy beam of electrons. Sample preparation was performed to clean sample being mounted on the specimen stage and placed into the instrument. Magnification in a scanning electron microscope can be controlled over a range of about 6 orders of magnitude from about 10

to 1,000,000 times. The magnification ranges that were used for shale analyses ranged from 100 to 500x.

3.1.3. Thin Section Analysis. A petrographic analysis was carried out to provide a detailed description of the texture (grain size, sorting, and grain contacts), sedimentary structures (laminations, bioturbation), framework grain composition, authigenic minerals, and types and distribution of macro-porosity seen in a thin section. Thin sectioning and impregnation procedures are critical to the successful petrographic analysis. Thin section preparation involved vacuum impregnation with low-viscosity blue dyed resin to facilitate the recognition of porosity and staining with a mixed Alizarin Red-S and potassium ferricyanide solution to allow the observation of the carbonate minerals (Kassab et al., 2015). In addition, samples were stained with a sodium cobaltinitrite solution to aid the identification of alkali feldspars. Thin sections were carefully ground to 30 microns thick sections of rock mounted on a glass slide to avoid fracturing and plucking. Basic petrographic analysis is performed in transmitted light using a petrographic polarizing microscope. Petrographic analysis of thin sections involves either qualitative description or quantitative estimation of the texture, mineralogy and porosity.

3.1.4. X-Ray Diffraction (XRD). X-ray diffraction (XRD) analysis were performed on Zubair shale sample. The shale samples were initially milled in methanol to a particle size of less than 10 microns, then filtered and air-dried. Thereafter, the specimen was placed into the X-ray diffractometer and rotated through a series of angles to help homogenize the intensity of the measured X-ray beam. As the specimen is rotated in the X-ray diffractometer, it was being illuminated with a very intense X-ray beam. The crystalline structures of the individual minerals present diffract the X-ray beam. This

results in an X-ray diffraction pattern that is unique for each mineral in the sample (Mike et al., 2009). The computer automates the data collection and data reduction steps of the analysis. In order to obtain a semi-quantitative measurement of the mineral components of a given sample, the maximum intensity of each identified mineral has been measured and compared to a standard intensity obtained from a pure mineral sample.

3.1.5. Porosity. The offcuts from plug samples in the saturated state (i.e., pore fluid preserved as recovered) were used to measure shale porosity. Horsrud et al. (1998) reported that shale porosity estimated from the free water content gives a better estimate compared to using helium porosity. Also with this method for porosity determination, shale porosity is completely independent of any structural changes in the shale (e.g., creation of micro-cracks) during coring processes, laboratory handling, etc. Therefore, porosity was measured using the free water content by drying 50 gm of each sample in an oven at 221°F until a constant sample weight was reached. The bulk volume was measured by mercury displacement. These were used in combination with the pore water density to calculate the porosity.

3.2. ROCK MECHANICAL PROPERTIES

Shale's extremely low permeability, clay content, and sensitivity to fluids make it a very special rock material to study (Chenevert and Sharma 1993; Zhang et al. 2015). Due to the low permeability of shale, mechanical rock tests become extremely time-consuming and consequently expensive (Mokhtari et al., 2017). For these reasons, it has been recommended that the consolidated undrained (CU) triaxial technique be performed for shale mechanical tests (Steiger and Leung 1992). Shale is very sensitive to wetting fluids,

such as water, or to loss of fluid from its pores (Lyu et al. 2015). Van Oort et al. (2016) further clarified these concerns, describing that the pore natural fluid of a poorly preserved shale evaporates from the pore space, which then fills with air. As the shale sample is no longer 100% saturated when it is exposed to atmospheric conditions, special procedures should be applied to prevent the loss of pore natural fluid. Otherwise, the laboratory testing will not give an accurate reflection of the actual shale mechanical properties (Santarelli and Carminati 1995). Strength correlations derived from the mechanical testing of unpreserved shales (dry shales) tend to over-predict shale strength (Dewhurst et al. 2015). Therefore, the shale samples that were used in this study were all well-preserved at the point of recovery in a metal casing, and the two ends were sealed with rubber caps to prevent the native pore fluid from being lost after the coring operations. The preserved cores were obtained from three wells, covering a wide range of the Zubair shale formation interval.

3.2.1. Sample Preparation. Right cylindrical plugs were drilled (using mineral oil as coolant) from whole preserved cores, with a length-to-diameter ratio of 2:1 (generally 1.5 in. diameter and 3 in. length), in accordance with ISRM (International Society for Rock Mechanics) standards (Kovari et al. 1983). All the plugs were cut with their axis perpendicular to the apparent bedding plane. Then, plug samples were scanned by CT (computer tomography) (2-D) to investigate and evaluate the mechanically induced micro-cracks created during plug preparation. The CT scan includes images divided into two main parts: longitudinal scan (vertical) and axial. Only three axial images were selected to cover the internal features of the plug from the top, middle, and bottom sections.

3.2.2. Triaxial Tests. The rock mechanical properties of shale are traditionally determined from consolidated undrained (CU) triaxial compression tests using different

levels of confining pressure based on a number of different core plugs from a single depth. The test results from several plugs are then combined to provide the unconfined compressive strength, cohesive strength, and internal friction angle for this depth. In the current work, the consolidated undrained (CU) triaxial test procedure was adopted from soil testing (Fjær et al. 2008). The plug was placed in a standard Hoek cell and loaded radially (applied all around the plug) by a servo pump to a predetermined level of confining pressure and pore pressure. Then, the second phase (consolidation phase) of the test was started by applying constant confining pressure and drainage (at both ends of the plug) of the pore fluid, with a constant pore pressure. In this phase, pore pressure equilibrium was reached in about 20–25 hours (permeability-dependent). The third phase was performed by an undrained axial load using a hydraulic load frame with a constant axial displacement rate until failure of the sample occurred. In the last phase, pore pressures rose during loading because of the undrained boundary condition, which is a good indicator that the plug is fully saturated. During the tests, computer control and a data acquisition system were used to control the triaxial test equipment and monitor/record the axial stress, confining pressure, axial/radial deformation, and pore pressure. This procedure was implemented with 5, 15, and 25 MPa constant confining pressure. During each test, radial and axial deformation was monitored by a computerized digital data acquisition system. Radial deformation of the plug was measured by four strain gauges glued directly to the sample, while axial deformation was measured using a linear voltage displacement transducer (LVDT), which was mounted on the top of the piston assembly such that the axial movement of the piston related to the axial deformation of the test plug.

3.2.3. Compressional Wave Velocity. Ultrasonic measurement of compressional acoustic wave velocity (with frequencies 1 MHz) was performed on the plug samples within the triaxial cell following the pulse transmission technique described by Birch (1960). The ultrasonic sources and detectors were placed inside the triaxial cell on either side of the plug sample. The compressional wave velocity was measured normal to the bedding. The sound velocities were measured using the transit times of the pulse wavelets through the core plug, with a known distance between the source and receiver transducers. Although the compressional wave velocity in high-porosity shales does not change significantly with the stress level, there may be substantial variations in the compressional wave velocity of shales with lower porosity (Holt et al. 1997). The compressional wave velocity was recorded for 25 Mpa confining pressure (which presents the estimated stresses experienced in situ by the formation) with zero axial load to reduce the micro-fracture impact on the bulk velocity (Dewhurst et al. 2015).

4. RESULTS AND DISCUSSION

4.1. STRUCTURE AND POROSITY

The results of (CT) scanner for full diameter core section (~1 m) and the plug samples showed that both induced and natural fractures were observed on some of the samples. As shown in Figure 1 and Figure 2, the green arrow refers to induced fractures, and the yellow arrow refers to natural open fractures (fracture porosity). Some beds and lenses of a different type of rock material (possibly calcite) were observed along the core (light gray areas). Moreover, the scanning electron microscope (SEM) shows that the rock

sample has a well-consolidated texture of shale as well as a micro-cracks and micro-pores were noticed inside the shale sample, as illustrated in Figure 3. The width of the micro-cracks ranged from 0.5–3 μm . The free water content measurements indicate that Zubair shale formation has low-to-moderate porosities (Table 2).

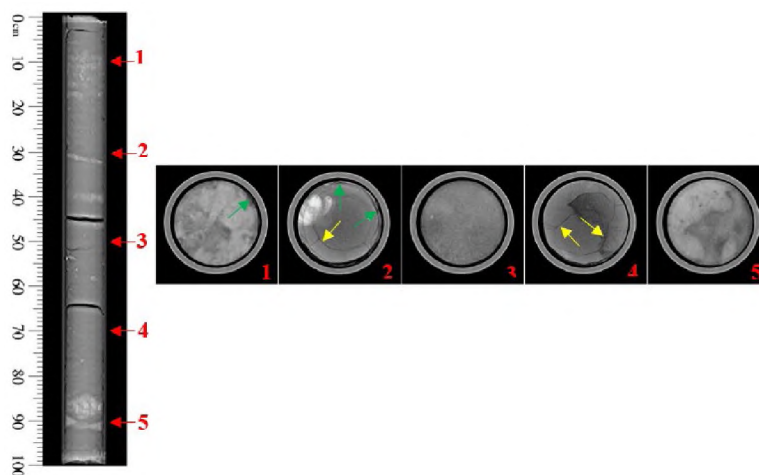


Figure 1. CT scan images for one section of the shale core preserved in a metal casing.

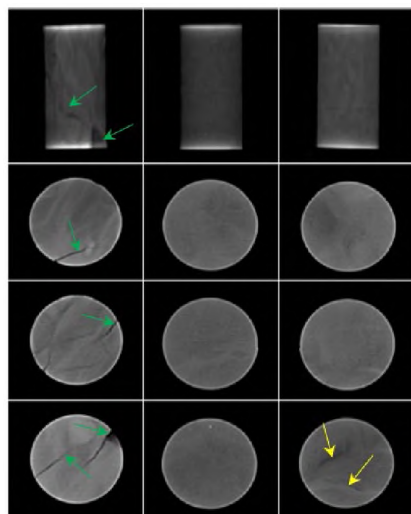


Figure 2. CT scan images showing the three axial scan slices along the longitudinal view of the plug samples.

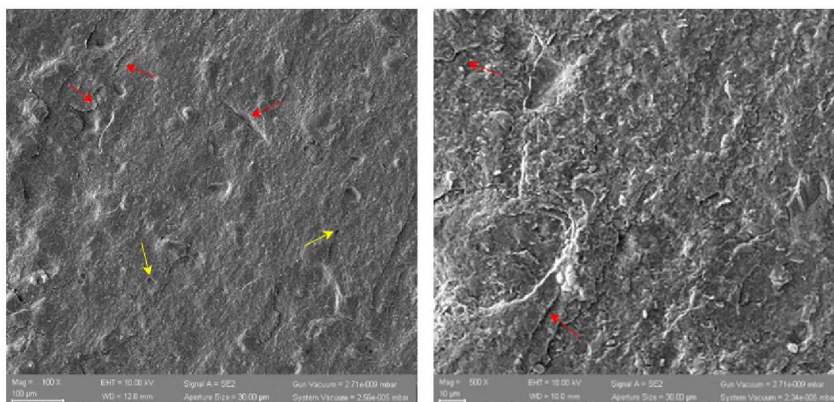


Figure 3. Scanning electron image of Zubair shale specimens. The red arrows refer to micro-cracks, and the yellow arrow refers to micro-pores.

Table 2. Porosity measured by determination of the free water content.

Sample	Porosity (%)
1	4.13
2	8.28
3	2.17
4	5.64
5	9.92

4.2. MINERAL COMPOSITION AND TEXTURE ANALYSIS

The petrographical characteristics of the sample were illustrated by two colored photomicrographs as shown in Figure. 4. It can be seen that the Zubair shale has a moderately laminated structure of well-sorted, silt grade sandy mudstone, poorly cemented and weakly-to-moderately compacted. The sample was composed of abundant amounts of pore-filling detrital clays (Dc), common monocry stalline quartz (Qz), rare pyrite crystals, white grains (calcite minerals or quartz), black assemblies (pyrite or residual hydrocarbons), heavy minerals, kaolinite booklets, illite, and chlorite. The thin section photograph shows that the plug sample has no visual macro-porosity and a few fractures (blue lines mostly 5–15 µm wide) that extend mainly along the bedding plane. These results

are strongly in agreement with the results of the X-ray diffraction test, as summarized in Table 3. It is clear that Zubair shales typically have high clay contents (> 40%).

The tests discussed in this paper characterize the porosity, mineralogy, texture, structure, grain distribution, and consolidation of Zubair shale, which are vital to understanding its fundamental mechanical behavior.

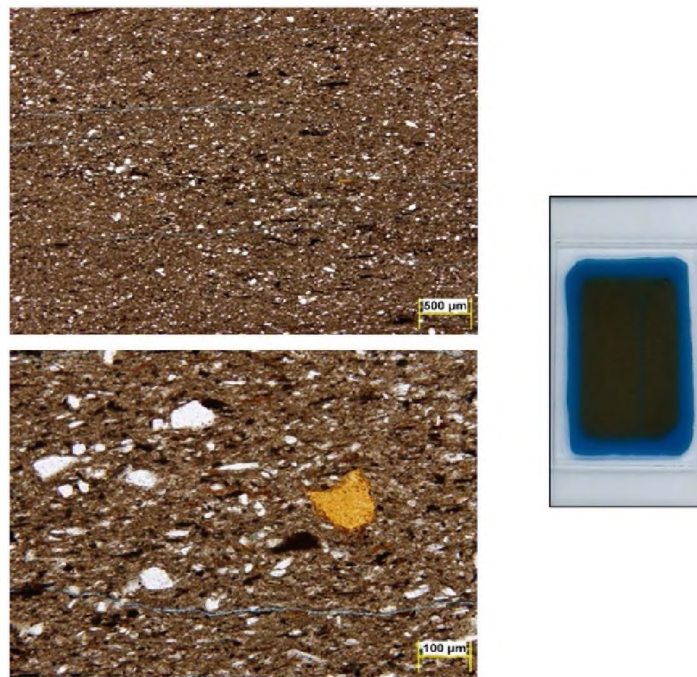


Figure 4. Thin section plate of the Zubair shale formation.

Table 3. X-ray diffraction results for Zubair shale.

Sample	Mineral composition (%)								
	Quartz	Pyrite	Calcite	Dolomite	Illite Smectite	Illite	Kaolinite	Chlorite	
1	41.74	3.41	6.71	1.32	6.7	15.93	22.54	1.65	
2	45.19	5.38	4.62	-	6.06	15.73	21.17	1.85	
3	41.68	4.73	9.26	1.81	3.54	15.62	21.91	1.45	
4	47.36	2.42	7.15	2.04	6.37	13.64	20.44	0.58	
5	42.21	3.87	11.39	-	8.39	14.63	18.53	0.98	

4.3. ROCK STRENGTH PROPERTIES

Mohr circles were plotted for the maximum effective stress (peak axial stress at brittle failure minus pore pressure) and minimum effective stress (confining pressure minus pore pressure) for all tests in a test series (at different effective confining pressures) conducted on plugs taken from the same depth. On a graph with shear stress along the y-axis and effective normal stress along the x-axis, a circle centered on $x = (\sigma_1' + \sigma_3')/2$ of radius $(\sigma_1' - \sigma_3')/2$ was drawn for each test in a test series. An analytical method was applied for calculating the best-fit linear failure envelope by drawing a smooth curve tangent to each Mohr circle (Stafford et al. 1986). The intercept of the failure envelope with the shear stress axis at an effective normal stress equal to zero provides the cohesive strength (C), and $\tan^{-1}m$ is the internal friction angle (ϕ), as shown in Figure 5. The unconfined compressive strength (UCS) was calculated using Eq. 7 (Al-Ajmi and Zimmerman 2005):

$$UCS = \frac{2C \cos \phi}{1 - \sin \phi} \quad (7)$$

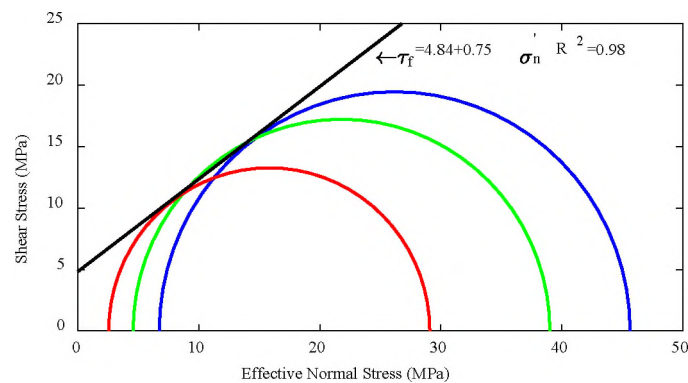


Figure 5. Failure envelope derived from the CU triaxial test on plug samples of Zubair shale taken from the same depth.

4.4. ELASTIC PROPERTIES

Static elastic properties (including Young's modulus and Poisson's ratio) were calculated using the same test (consolidated undrained triaxial test) with confining pressures of 25 MPa. By plotting the axial and radial strain against the axial stress, which was determined by dividing the measured axial load by the initial cross-section area of the plug, the static Young's modulus and static Poisson's ratio were calculated. The static Young's modulus was determined from the slope of the tangent (at 50% of the peak stress) to the axial stress-strain curve in the undrained triaxial phase, while the static Poisson's ratio was determined by calculating the ratio between the slopes of both radial and axial stress-strain curves (Figure 6) in the undrained triaxial phase (Rybacki et al. 2015). The timeline for the response of the consolidated undrained triaxial test of one plug sample with 25 MPa confining pressure is shown in Figure. 7.

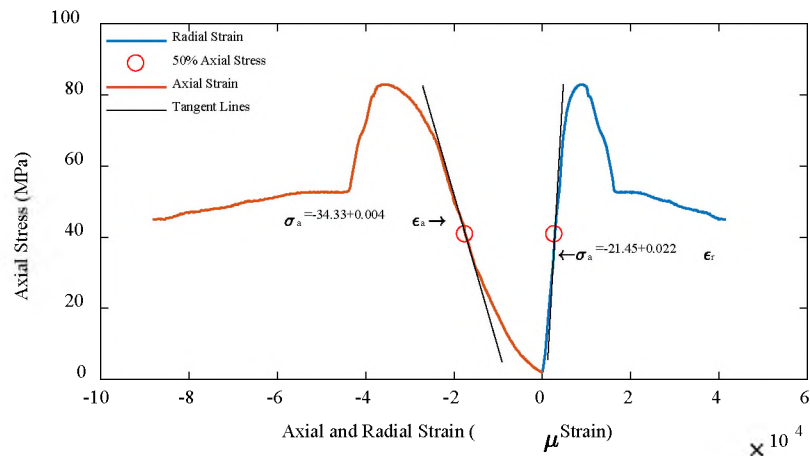


Figure 6. Static elastic parameters derived from plotting the axial stress against the axial and radial strain using the triaxial test conducted on plug samples for Zubair shale.

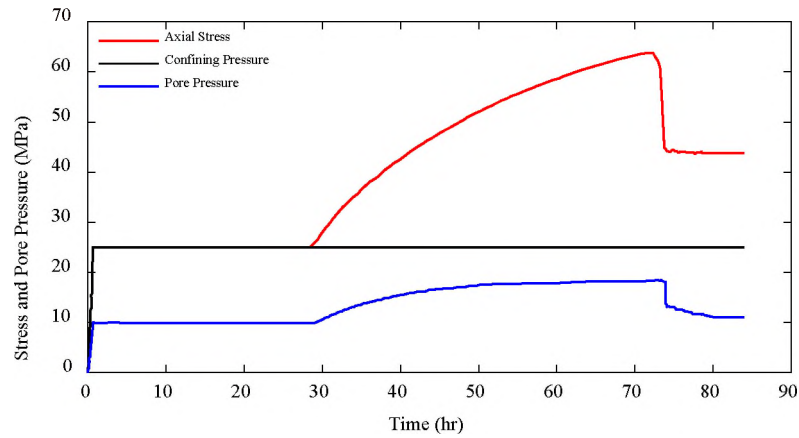


Figure 7. Timeline of the CU triaxial test for Zubair shale.

4.5. CORRELATIONS

All possible correlations between the measured mechanical properties of the Zubair shale and the compressional wave velocities were investigated, and the best-fitting curve with the highest correlation coefficient was selected. An exponential function was found to be the best-fitting curve for all cases. The scatter in the data can be attributed to sample heterogeneities and limited laboratory errors.

4.5.1. Rock Strength Parameters. The correlations between the unconfined compressive strength and the internal friction angle with the compressional wave velocities are shown in Eqs. 8 and 9, respectively. Both the UCS and ϕ increased as the compressional wave velocity increased. The exponential functions are the best-fitting curve, with a correlation coefficient R^2 equal to 0.95 and 0.92, respectively, as shown in Figures. 8a and 8b.

$$UCS = 2.6477e^{0.6006v_p} \quad (8)$$

$$\phi = 17.134e^{0.239v_p} \quad (9)$$

4.5.2. Static Young's Modulus. The static Young's modulus increases with increasing compressional wave velocity, as presented in Figure. 8c. The exponential function is the best-fitting curve for Young's modulus, with a correlation coefficient R^2 of 0.91, where

$$E = 0.2966e^{0.6984v_p} \quad (10)$$

4.5.3. Static Poisson's Ratio. Poisson's ratio was observed to decrease as the compressional wave velocity increased, with the best-fit curve as an exponential function and a correlation coefficient R^2 of 0.87, as illustrated in Figure 8d. Eq 11 is an empirical relationship between Poisson's ratio and the compressional wave velocity for Zubair shale:

$$v_s = 0.7621e^{-0.353v_p} \quad (11)$$

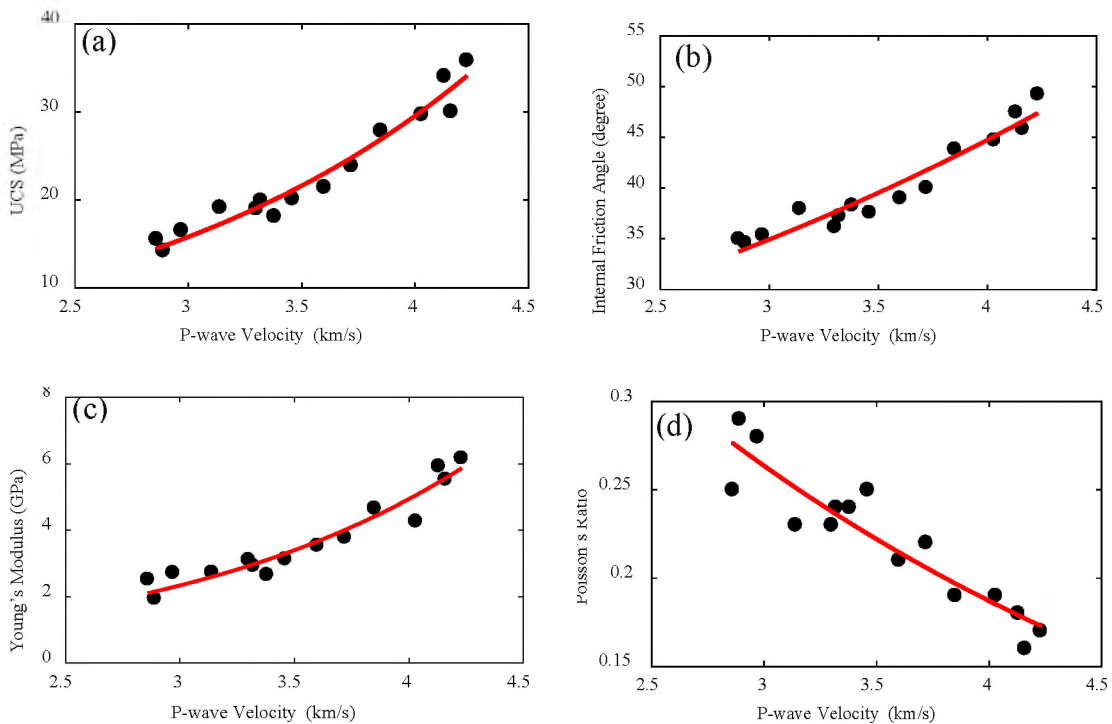


Figure 8. Calibration plots of rock mechanical properties versus lab-measured P-wave velocity.

4.6. STATISTICAL ANALYSIS

The accuracy of the predicted rock mechanical properties based on the abovementioned empirical relationships was examined by statistical analysis. As shown in Table 4, the root mean square error (RMSE) of the compared estimated values (based on Eqs. 8–11) with the corresponding measured data is reasonable and within acceptable values.

Table 4. RMSE of Eqs. 8–11 in estimating rock mechanical parameters.

Empirical Relationship	RMSE
UCS predicted from v_p	1.42 MPa
φ predicted from v_p	1.22 degree
E_s predicted from v_p	0.35 GPa
ν_s predicted from v_p	0.01

Furthermore, the newly suggested empirical correlations were compared with correlations in the literature (Table 1) using a histogram of misfits between the estimated rock mechanical properties and the core-measured values. The results are summarized in Figures 9a–9d for the aforementioned correlations (Eqs. 8–11), respectively. The histogram of misfits (Figure 9a) shows that Eq. 8 predicted the unconfined compressive strength extremely well, fitting 100% of the data within ± 4 MPa. However, Eqs. 1, 3, and 5 fit 65%, 27%, and 39% of the data, respectively, within ± 4 MPa. Eqs 1 and 3 tended to considerably overestimate the unconfined compressive strength. Figure 9b shows that Eq. 9 determined the internal friction angle extremely well, fitting 100% of the data within ± 2 degrees, whereas Eq. 2 fit 7% of the data within ± 2 degrees. Eq 2 tended to underestimate the internal friction angle. Figure 9c shows that Eq. 10 calculated the Young's modulus

extremely well, fitting 100% of the data within ± 2 GPa, while Eqs. 4 and 6 fit 85% and 13% of the data, respectively, within ± 2 GPa. Eqs 4 and 6 seemed to generally overestimate the Young's modulus. Figure 9d illustrates that Eq. 11 predicted Poisson's ratio very well, fitting 100% of the given data within ± 0.03 .

An interesting observation revealed by this analysis is that empirical correlations in the literature did not adequately cover the Zubair shale data, and the rock mechanical properties that were predicted based on the newly suggested empirical correlations have a higher accuracy and reliability.

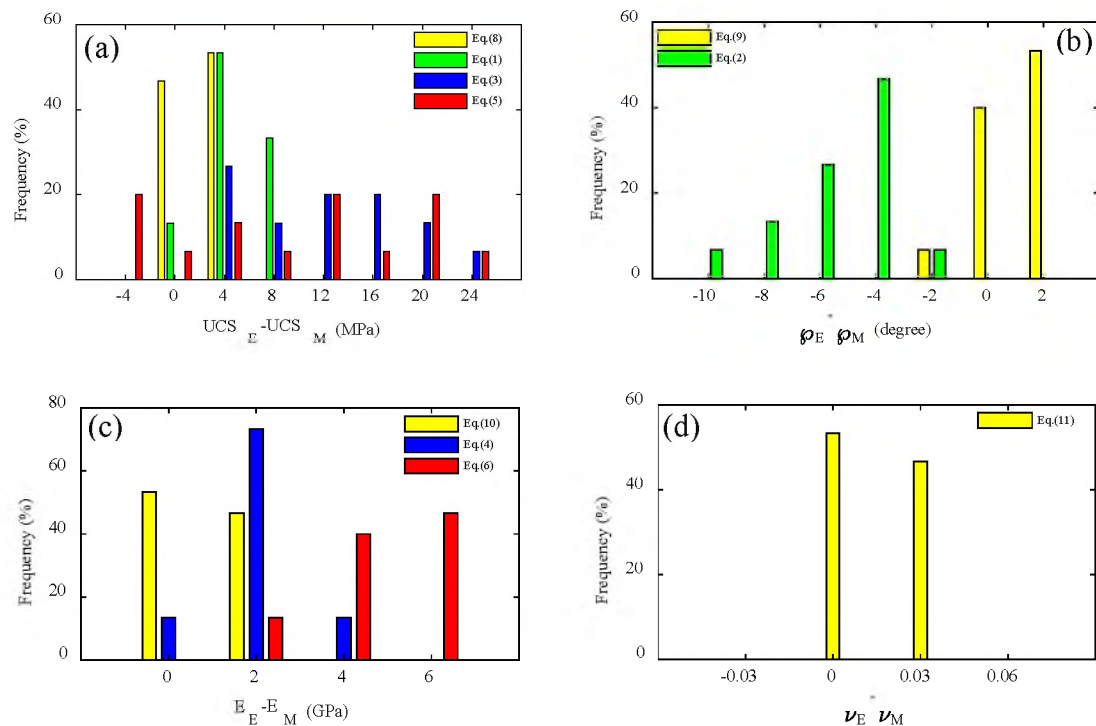


Figure 9. Histograms showing the frequency versus the difference in the estimated (E) and measured (M) of the rock mechanical properties for Zubair shale using the empirical equations shown in Table 1 and the suggested empirical relationships (Eqs. 8–11).

4.7. DERIVATION OF ROCK MECHANICAL PROPERTIES

The suggested empirical correlations (Eqs. 8–11) were implemented to derive a continuous profile of the rock mechanical properties from wireline sonic log. This is done in two steps:

4.7.1. Calibration of Wireline Sonic Log (P-Wave Velocity) with the Laboratory-Measured P-Wave Velocity. Sonic travel time logging is routinely used in exploration boreholes (Oyler et al. 2010). The compressional wave velocity can be directly estimated from the sonic log. Laboratory-measured compressional wave velocities are consistently higher than the compressional wave velocities from the sonic log, with a 6.04% absolute relative average difference (ARAD) (Figure. 11). The difference between logged and lab-measured velocities is attributed due to the temperature effect and the difference in frequency used in the laboratory and during downhole logging (Horsrud, 2001). Acoustic laboratory measurements were performed at room temperature, while the sonic log measurements were performed at downhole temperature. These measurements are temperature-dependent because the P-wave velocity decreases with increasing temperature (Horsrud et al. 1994). P-wave velocity prior to the derivation of the rock mechanical properties from the sonic log. An empirical correction was implemented between the wireline sonic log and the core-measured P-wave velocity at corresponding depths for one of the cored wells. The results show that the best-fit curves were simple linear least square regressions, with a correlation coefficient of $R^2 = 0.99$, as shown in Figure 10. Eq. 12 expresses the best-fit line that was applied to derive the calibrated sonic log:

$$P_{vc} = 1.0839P_v - 0.0698 \quad (12)$$

The laboratory-measured P-wave velocity was added to the plot of the calibrated sonic log. As shown in Figure 11, there is good agreement between the calibrated sonic log and the individual laboratory-measured P-wave velocities, with 0.54% ARAD.

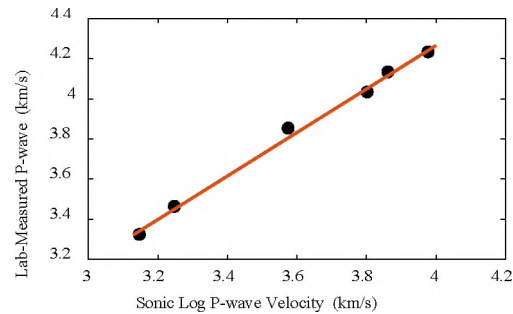


Figure 10. Empirical correlation between the sonic log P-wave velocity and lab-measured P-wave velocity.

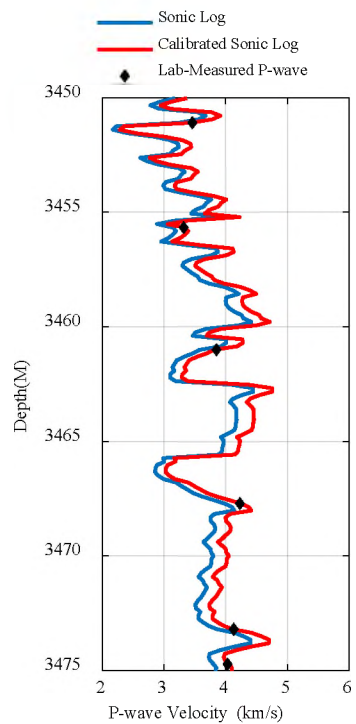


Figure 11. Wireline sonic log and lab-measured P-wave velocity.

4.7.2. Implementation of the Correlations to Derive Rock Mechanical Properties. The empirical correlations described previously were used to derive rock mechanical properties from the calibrated sonic log. The derived rock mechanical logs were plotted against depth. The laboratory-measured rock mechanical properties were added to the plot to assess the level of agreement between the experimentally measured rock mechanical properties and the derived rock mechanical logs. Figures 12 and 13 present examples of the rock mechanical property logs for one of the cored wells in the Zubair shale formation. As can be seen, there is a good degree of correlation between the calculated rock mechanical property logs (i.e., UCS, internal friction angle, Young's modulus, and Poisson's ratio) and those derived from the laboratory, with ARADs of 4.5%, 3.94%, 8.21%, and 3.72%, respectively.

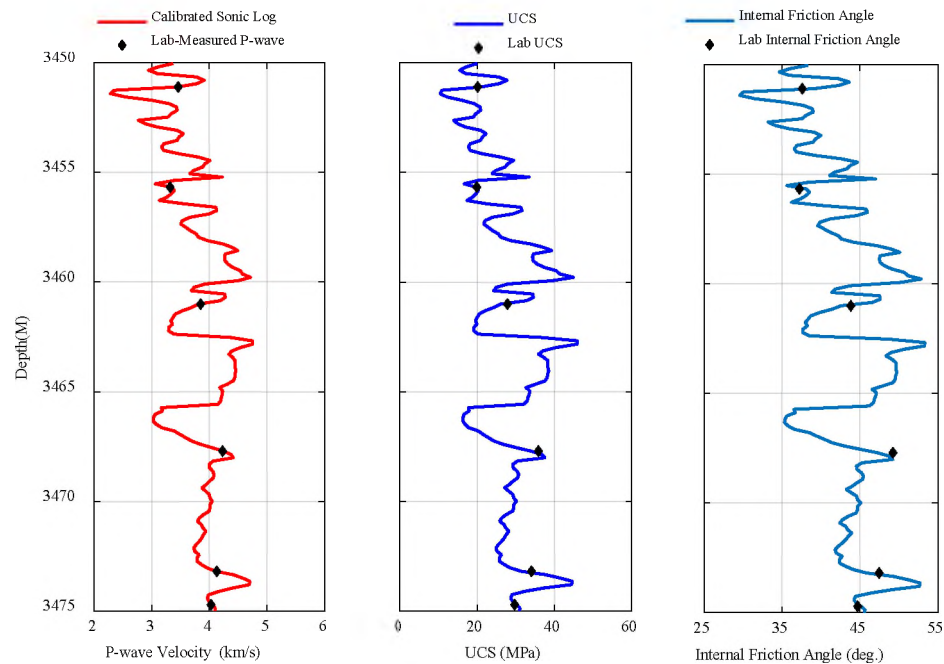


Figure 12. Predicted unconfined compressive strength and internal friction angle logs using Eqs. 8 and 9, respectively.

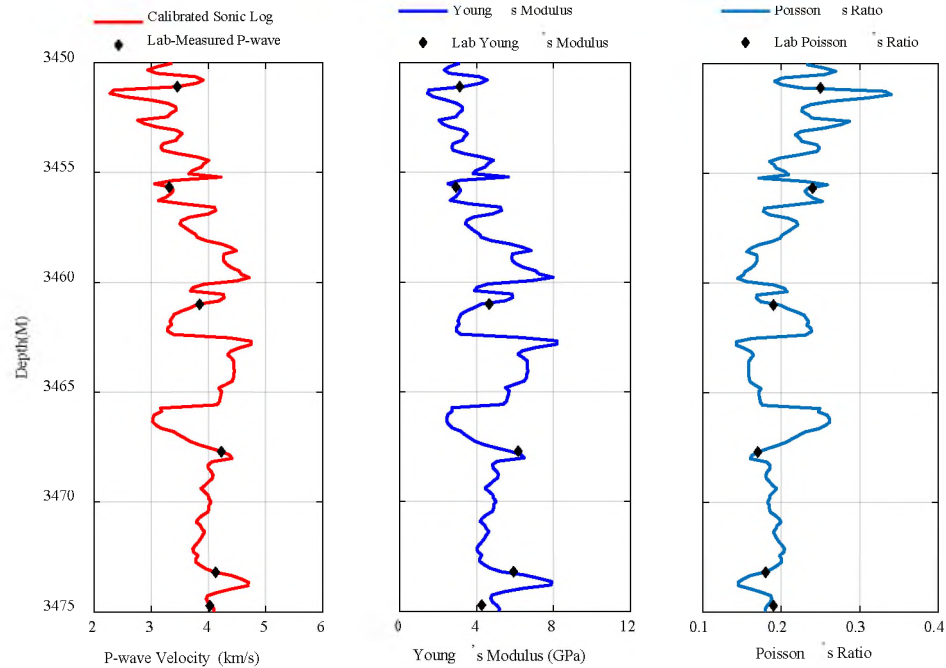


Figure 13. Predicted Young's modulus and Poisson's ratio logs using Eqs. 10 and 11, respectively.

5. SUMMARY AND CONCLUSIONS

Zubair shale was comprehensively characterized in terms of porosity, mineralogy, texture, structure, grain distribution, and consolidation. Triaxial tests were performed on Zubair shale core specimens, and the values of the rock mechanical properties were measured. The results illustrate that the rock mechanical properties correlate closely with the compressional wave velocity. Rock strength and the elastic modulus increased when the compressional wave velocity increased. This was reflected in the anticipated trend: as compressional wave velocity increased, the magnitude of the open pore space decreased, while both the rock strength and the elastic modulus increased. In contrast, Poisson's ratio rose with decreasing compressional wave velocity. These findings agree with those in

previous studies in other geographical regions. The empirical expressions described herein were formulated to relate the rock mechanical properties with the laboratory-measured compressional wave velocity. Throughout the Zubair shale formation, the exponential function correlations were more reliable than the linear expression and power functions for the rock mechanical properties. The compressional wave velocity is a primary input parameter in all the correlations. There are various sources for determining the compressional wave velocity, such as the sonic wireline log, MWD sonic, and acoustic measurements on cuttings. Therefore, these correlations can be used to obtain continuous estimates of the Zubair shale mechanical properties at various stages in the process of drilling a borehole. The accuracy of the predicted rock mechanical properties based on the compressional wave velocity was tested using statistical analysis, finding that the root mean square error (RMSE) was reasonable. In addition, the newly suggested empirical correlations were compared with the existing commonly used correlations reported in the literature on real field data from Zubair shale. The performance of the suggested empirical correlations was better and more accurate than the correlations reported in the literature. The obtained results provide further evidence that empirically based correlations are not universally applicable. The correlations are based on one type of lithology for the specific geographical area. These correlations may not be applicable to other geographical regions. Consequently, it is recommended to check the validity of the correlations before using them in rock mechanical prediction for other geological and geographical areas. It can therefore be concluded that the specific empirical correlations for a specific formation are more reliable than general ones.

The newly suggested correlations are based on data from the Zubair shale formation, where they appear to apply with reasonable confidence to other geographical areas. It is highly recommended to compare some standard types of characterizations (i.e., porosity, mineralogy, texture, structure, etc.) for the specific zones of interest with Zubair shale characterizations. It should be realized that there are systematic errors attached to these corrections, such as temperature effects and the difference in frequency between laboratory and downhole logging measurements. The correlations have to include a temperature-correction term to account for downhole temperatures, which will be the focus of future work.

ACKNOWLEDGMENTS

The author would like to thank the Higher Committee for Education Development (HCED) in Iraq for awarding him a fully funded Ph.D. scholarship. The authors would like to thank Basrah Oil Company in Iraq for support related to core samples and for their permission to publish the results. We also want to thank Missouri University of Science and Technology for providing the facilities to do this work.

REFERENCES

- Abbas, A. K., Al-Asadi, Y. M., Alsaba, M., Flori, R. E., and Alhussainy, S., 2018. Development of a Geomechanical Model for Drilling Deviated Wells through the Zubair Formation in Southern Iraq. SPE/IADC Middle East Drilling Technology Conference and Exhibition, 29-31 January, Abu Dhabi, UAE. <https://doi.org/10.2118/189306-ms>.

- Al-Ajmi, A. M. and Zimmerman, R. W. (2005). Relation between the Mogi and the Coulomb Failure Criteria. *Int J Rock Mech Min Sci* 42 (3): 431–439. <http://dx.doi.org/10.1016/j.ijrmms.2004.11.004>.
- Ameen, M. S., Smart, B. G., Somerville, J., Hammilton, S. and Naji, N. A. 2009. Predicting Rock Mechanical Properties of Carbonates from Wireline Logs (A Case Study: Arab-D Reservoir, Ghawar Field, Saudi Arabia). *Mar Pet Geol* 26 (4): 430–444. <http://dx.doi.org/10.1016/j.marpetgeo.2009.01.017>.
- Birch, F. 1960. The Velocity of Compressional Waves in Rocks to 10 Kilobars. *J. Geophys Res* 65: 1083–1102.
- Chang, C., Zoback, M. D. and Khaksar, A. 2006. Empirical Relations between Rock Strength and Physical Properties in Sedimentary Rocks. *J Pet Sci Eng* 51 (3–4): 223–237. <http://dx.doi.org/10.1016/j.petrol.2006.01.003>.
- Chenevert, M. and Sharma, A. 1993. Permeability and Effective Pore Pressure of Shales. *SPE Drill & Compl* 8 (01): 28–34. <http://dx.doi.org/10.2118/21918-pa>.
- Choo, C., Takahashi, M., & Jeong, G., 2014. Identification and Three-Dimensional Characterization of Micropore Networks Developed in Granite using Micro-Focus X-ray CT. *Journal of Engineering Geology*, 24(2), 179–189. <https://doi.org/10.9720/kseg.2014.2.179>.
- Dewhurst, D. N., Sarout, J., Delle Piane, C., Siggins, A. F., Raven, M. D. and Kuila, U. 2010. Prediction of Shale Mechanical Properties from Global and Local Empirical Correlations. *SEG Technical Program Expanded Abstracts* 2010. <http://dx.doi.org/10.1190/1.3513380>.
- Dewhurst, D. N., Sarout, J., Piane, C. D., Siggins, A. F. and Raven, M. D. 2015. Empirical Strength Prediction for Preserved Shales. *Mar. Pet. Geol.* 67, 512–525. <http://dx.doi.org/10.1016/j.marpetgeo.2015.06.004>.
- Edlmann, K., Somerville, J., Smart, B., Hamilton, S. and Crawford, B. 1998. Predicting Rock Mechanical Properties from Wireline Porosities. Presented at the SPE/ISRM Rock Mechanics in Petroleum Engineering, Trondheim, Norway. 8–10 July. SPE-47344-MS. <http://dx.doi.org/10.2118/47344-ms>.
- Fang, C., Amro, M., Jiang, G. and Lu, H. 2016. Laboratory Studies of Non-Marine Shale Porosity Characterization. *J Nat Gas Sci Eng* 33: 1181–1189. <http://dx.doi.org/10.1016/j.jngse.2016.04.006>.
- Fjær, E., Holt, R. M., Horsrud, P., Raaen, A. M. and Risnes, R. 2008. *Petroleum Related Rock Mechanics*, second edition. Amsterdam: Elsevier Science.

- Guo, T., Zhang, S., Zou, Y. and Xiao, B. 2015. Numerical Simulation of Hydraulic Fracture Propagation in Shale Gas Reservoir. *J Nat Gas Sci Eng* 26: 847–856. <http://dx.doi.org/10.1016/j.jngse.2015.07.024>.
- Holt, R., Furre, A. and Horsrud, P. 1997. Stress Dependent Wave Velocities in Sedimentary Rock Cores: Why and Why Not? *Int J Rock Mech Mining Sci Geomech Abstr* 34 (3–4): 399–399. [http://dx.doi.org/10.1016/s0148-9062\(97\)00167-8](http://dx.doi.org/10.1016/s0148-9062(97)00167-8).
- Horsrud, P. 2001. Estimating Mechanical Properties of Shale from Empirical Correlations. *SPE Drill & Compl* 16 (02): 68–73. <http://dx.doi.org/10.2118/56017-pa>.
- Horsrud, P., Holt, R., Sonstebo, E., Svano, G. and Bostrom, B. 1994. Time Dependent Borehole Stability: Laboratory Studies and Numerical Simulation of Different Mechanisms in Shale. *Proceedings of Rock Mechanics in Petroleum Engineering*, Delft, The Netherlands, 12–15 August. <http://dx.doi.org/10.2523/28060-ms>.
- Horsrud, P., Sønstebø, E. and Bøe, R. 1998. Mechanical and Petrophysical Properties of North Sea Shales. *Int J Rock Mech Min Sci* 35 (8): 1009–1020. [http://dx.doi.org/10.1016/s0148-9062\(98\)00162-4](http://dx.doi.org/10.1016/s0148-9062(98)00162-4).
- Josh, M., Esteban, L., Piane, C. D., Sarout, J., Dewhurst, D. and Clennell, M. 2012. Laboratory Characterisation of Shale Properties. *J Pet Sci Eng* 88–89: 107–124. <http://dx.doi.org/10.1016/j.petrol.2012.01.023>.
- Kassab, M. A., Teama, M. A., Cheadle, B. A., El-Din, E. S., Mohamed, I. F., and Mesbah, M. A., 2015. Reservoir characterization of the Lower Abu Madi Formation using core analysis data: El-Wastani gas field, Egypt. *Journal of African Earth Sciences*, 110, 116-130. <https://doi.org/10.1016/j.jafrearsci.2015.06.008>.
- Kovari, K., Tisa, A., Einstein, H. H. and Franklin, J. A. 1983. Suggested Methods for Determining the Strength of Rock Materials in Triaxial Compression: Revised Version. *Int. J. Rock Mech. Min. Sci. Geomech Abstr* 20: 283–290.
- Labani, M. M. and Rezaee, R. 2014. The Importance of Geochemical Parameters and Shale Composition on Rock Mechanical Properties of Gas Shale Reservoirs: A Case Study from the Kockatea Shale and Carynginia Formation from the Perth Basin, Western Australia. *Rock Mech Rock Eng* 48 (3): 1249–1257. <http://dx.doi.org/10.1007/s00603-014-0617-6>.
- Lal, M. 1999. Shale Stability: Drilling Fluid Interaction and Shale Strength. *Proceedings of SPE Asia Pacific Oil and Gas Conference and Exhibition, Jakarta, Indonesia*, 20–22 April. <http://dx.doi.org/10.2523/54356-ms>.

- Lashkaripour, G. R. and Dusseault, M. D. 1993. A Statistical Study of Shale Properties: Relationships among Principal Shale Properties. In *Probabilistic Methods in Geotechnical Engineering*, ed. K. S. Li and S.-C.R. Lo, 195–200. Leiden, the Netherlands: Balkema.
- Li, Q. and Tang, Z. 2016. Optimization of Wellbore Trajectory Using the Initial Collapse Volume. *J Nat Gas Sci Eng* 29: 80–88. <http://dx.doi.org/10.1016/j.jngse.2015.12.038>.
- Lyu, Q., Ranjith, P., Long, X., Kang, Y. and Huang, M. 2015. A Review of Shale Swelling by Water Adsorption. *J Nat Gas Sci Eng* 27: 1421–1431. <http://dx.doi.org/10.1016/j.jngse.2015.10.004>.
- Mike, S., Sandra, G., and Marc, C., 2009. Laboratory Methods to Assess Shale Reactivity with Drilling Fluids. AADE National Technical Conference & Exhibition, New Orleans, Louisiana, USA.
- Mokhtari, M., Wood, D., Ghanizadeh, A., Kulkarni, P., Rasouli, V., Fathi, E., Saidian, M., and Barati, R. 2017. Virtual special issue: Advances in the petrophysical and geomechanical characterization of organic-rich shales. *J Nat Gas Sci Eng* 38: 638–641. <http://dx.doi.org/10.1016/j.jngse.2016.12.043>.
- Onyia, E. 1988. Relationships between Formation Strength, Drilling Strength, and Electric Log Properties. Presented at the SPE Annual Technical Conference and Exhibition, Houston, Texas, 2–5 October. <http://dx.doi.org/10.2118/18166-ms>.
- Oyler, D. C., Mark, C. and Molinda, G. M. 2010. In Situ Estimation of Roof Rock Strength Using Sonic Logging. *Int J Coal Geol* 83 (4): 484–490. <http://dx.doi.org/10.1016/j.coal.2010.07.002>.
- Ranjbar-Karami, R., Kadkhodaie-Ilkhchi, A. and Shiri, M. 2014. A Modified Fuzzy Inference System for Estimation of the Static Rock Elastic Properties: A Case Study from the Kangan and Dalan Gas Reservoirs, South Pars Gas Field, the Persian Gulf. *J Nat Gas Sci Eng* 21: 962–976. <http://dx.doi.org/10.1016/j.jngse.2014.10.034>.
- Rasouli, V. and Sutherland, A. 2013. Geomechanical Characteristics of Gas Shales: A Case Study in the North Perth Basin. *Rock Mech Rock Eng* 47 (6): 2031–2046. <http://dx.doi.org/10.1007/s00603-013-0531-3>.
- Rybacki, E., Reinicke, A., Meier, T., Makasi, M. and Dresen, G. 2015. What Controls the Mechanical Properties of Shale Rocks? – Part I: Strength and Young's Modulus. *J Pet Sci Eng* 135: 702–722. <http://dx.doi.org/10.1016/j.petrol.2015.10.028>.

- Santarelli, F. and Carminati, S. 1995. Do Shales Swell? A Critical Review of Available Evidence. Proceedings of SPE/IADC Drilling Conference, Amsterdam, Netherlands, 28 February–2 March. <http://dx.doi.org/10.2523/29421-ms>.
- Stafford, J., Audsley, E. and Sharp, J. 1986. The Determination of Best Fit Linear Failure Envelopes to Mohr Circles. *J Agri Eng Res* 33 (1): 33–38. [http://dx.doi.org/10.1016/s0021-8634\(86\)80027-0](http://dx.doi.org/10.1016/s0021-8634(86)80027-0).
- Steiger, R. P. and Leung, P. K. 1992. Quantitative Determination of the Mechanical Properties of Shales. *SPE Drill Eng* 7 (03): 181–185. <http://dx.doi.org/10.2118/18024-pa>.
- Stjern, G., Agle, A. and Horsrud, P. 2003. Local Rock Mechanical Knowledge Improves Drilling Performance in Fractured Formations at the Heidrun Field. *J Pet Sci Eng* 38 (3–4): 83–96, [http://dx.doi.org/10.1016/S0920-4105\(03\)00023-8](http://dx.doi.org/10.1016/S0920-4105(03)00023-8).
- Van Oort, E., Hoxha, B., Hale, A.H., Aldin, M, and Patterson, R. 2016. How to test fluids for shale compatibility? AADE-16-FTCE-77, Fluids Technical Conference and Exhibition, April 12-13, Houston, Texas, USA.
- Wang, L., Yang, D., Yang, R. and Chanchole, S. 2016. Investigating the Mechanical Behavior of Shale: A Micro-scale Approach. *J Nat Gas Sci Eng* 36: 1295–1302. <http://dx.doi.org/10.1016/j.jngse.2016.03.051>.
- Yuan, J., Deng, J., Tan, Q., Yu, B. and Jin, X. 2012. Borehole Stability Analysis of Horizontal Drilling in Shale Gas Reservoirs. *Rock Mech Rock Eng* 46 (5): 1157 – 1164. <http://dx.doi.org/10.1007/s00603-012-0341-z>.
- Zhang, R., Ning, Z., Yang, F., Wang, X., Zhao, H. and Wang, Q. 2015. Impacts of Nanopore Structure and Elastic Properties on Stress-dependent Permeability of Gas Shales. *J Nat Gas Sci Eng* 26: 1663–1672. <http://dx.doi.org/10.1016/j.jngse.2015.02.001>.

III. STABILITY ANALYSIS OF HIGHLY DEVIATED BOREHOLES TO MINIMIZE DRILLING RISKS AND NONPRODUCTIVE TIME

Ahmed K. Abbas, Ralph Flori, and Mortadha Alsaba

Department of Petroleum Engineering Engineering, Missouri University of Science and Technology, Rolla, MO 65409

ABSTRACT

The Lower Cretaceous Zubair Formation is a regionally extended gas and oil producing sandstone sequence in Southern Iraq. Due to the weak nature of the Zubair Formation, the lack of wellbore stability is one of the most critical challenges that continuously appears during the drilling development operations. Problems associated with lack of wellbore stability, such as the tight hole, shale caving, stuck pipe, and sidetracking, are both time-consuming and expensive. The present study aims to construct a geotechnical model based on offset well data, including rock mechanical properties, in-situ stresses, and formation pore pressure, coupled with suitable rock failure criteria. Mohr-Coulomb and Mogi-Coulomb failure criteria were used to predict the potential rock failure around the wellbore. The effect of the inclination and azimuth of the deviated wells on the shear failure and tensile failure mud weights was investigated to optimize the wellbore trajectory. The results show that the best orientation to drill highly deviated wells (i.e., inclinations higher than 60°) is along to the minimum horizontal stress (140°). The recommended mud weight for this selected well trajectory ranges from 1.45 to 1.5 g/cc. The present study emphasizes that a wellbore stability analysis can be applied as a cost-effective tool to guide future

highly deviated boreholes for better drilling performance by reducing the non-productive time.

1. INTRODUCTION

Well trajectory and mud weight are important factors in the analysis of wellbore stability (Zhang et al., 2018). Wellbore instabilities during drilling are caused by two major types of wellbore failure (i.e., shear failure and tensile failure) (Chen et al., 2018). Generally, these problems associated with lack of wellbore stability result in billions of dollars of the additional costs for drilling companies annually (Wang et al., 2018; Jingbin et al., 2018). Therefore, the precise study of wellbore stability is a key step in improving the efficiency of drilling operations (Abbas et al., 2018a). As soon as drilling starts through solid rock and the drilling fluid replaces the removed rock, the equilibrium of in-situ stresses around the borehole will be disturbed, which causes a stress concentration at the wall of the borehole (Al Dushaishi et al., 2017; Kamel et al., 207). Hence, borehole failure is anticipated to begin there. In the case that the utilized mud pressure (mud weight) does not counterbalance (less than) the pore pressure in the permeable formation, formation fluids entry into the well, and even well blowout can be expected. Thus, the pore pressure limit defines the minimum mud weight required to maintain hydraulic safety. In addition, if the pressure force from an overbalanced drilling mud column is less than the formation breakout pressure, borehole breakouts may occur due to the fact that the mud pressure is not high enough to support the rock on the borehole wall. On the contrary, if the hydrostatic pressure of the drilling mud column exceeds the minimum horizontal principal stress

magnitude, the tensile condition is dominant and the tensile failure may lead to reopening the natural fractures or any other conductive fissures existing around the borehole, which leads to loss of drilling fluid. Furthermore, if the hydrostatic pressure of the drilling fluid exceeds the breakdown pressure of the formation, tensile failure will occur in the intact rock and drilling-induced tensile fracture (DITF) will begin in the borehole wall.

Wellbore stability analysis is very necessary for drilling new wells because without analysis, high costs may result (Nes et al., 2012; Kiran, and Salehi, 2016; Zhang et al., 2014; Chen et al., 2003). Maintaining a stable borehole during drilling operations results from the interplay of both uncontrollable and controllable factors (Aslannezhad et al., 2015). Uncontrollable factors are rock mechanical properties, in-situ stresses, and formation pore pressure (Chuanliang et al., 2015). Controllable factors include mud weight and wellbore trajectory (Mohiuddin et al., 2007). Therefore, the wellbore can be stabilized during drilling operations by adjusting the engineering practices to select suitable mud weights and appropriate wellbore trajectories. This is typically carried out using wellbore stability analysis to determine an appropriate mud weight required for the stability of the wellbore. The fundamental approach for any geomechanical studies is to integrate all available data, including rock strength and elastic properties, in-situ and induced stresses, pore pressure, etc., into a one-dimensional mechanical earth model (1D-MEM). All of these parameters are then coupled with an appropriate rock strength criterion to predict the minimum limit of the mud weight required to have safe drilling operation (Gholami et al., 2015). In this regard, many rock failure criteria have been developed to calculate the breakout pressure under different stress regimes (Bradley, 1979). However, most of these criteria are mathematically unstable and neglect the effect of the intermediate principal

stress (Mansourizadeh et al., 2016). Therefore, Al-Ajmi and Zimmerman (2005) presented a new polyaxial rock failure criterion known as Mogi-Coulomb criterion. This criterion is proposed to be a linear failure envelope in Mogi's domain and works by two parameters, which can be related to cohesion and the internal friction angle of Coulomb strength parameters (Maleki et al., 2014). To avoid predicting unrealistic results, the Mogi-Coulomb criterion considers the effect of the intermediate principal component stress in rock failure response.

In the present work, a geomechanical model was built based on numerous field and laboratory data for the Zubair Formation. Open-hole wireline logging measurements, including density logs, gamma-ray (GR) logs, sonic logs, formation micro-imager (FMI) logs, neutron logs, and resistivity logs from the offset wells, were used to estimate the in-situ principal stress magnitudes and its orientations, pore pressure, and rock mechanical properties. The 1D-MEM parameters were further calibrated and verified using all the available data such that the model robustly and accurately predicts borehole failure problems around given wellbores. Two common rock failure criteria (i.e., Mohr-Coulomb and Mogi-Coulomb) were then applied to analyze the wellbore stability problems for wells with highly deviated profiles and to define the optimum mud weight and safe wellbore trajectory for future successful drilling operations.

2. MECHANICAL EARTH MODEL

An integrated workflow was applied to build a geomechanical model to drill through the Zubair Formation, as described in Figure 1. The first step in building the

geomechanical model was to collect a proper set of data for the Zubair Formation. The needed data were gathered from various sources from the offset wells, mainly from those with major lack of stability problems and high non-productive time values. The second step was to assess the logging input data. A data audit was performed to make sure that all data, which were acquired from the laboratory and field, were complete, accurate, and reasonable. In general, the data gathered for this study was almost complete and of good quality. Moreover, the necessary data, including gamma-ray logs, density logs, porosity logs, sonic logs (compression and shear wave velocities), resistivity logs, formation micro-imager (FMI) logs, caliper logs, mud logs (master logs), mini-frac tests, and laboratory measurements, were available for most of the selected wells. After that, the data were used to build a basic 1D mechanical earth model (MEM) (Gholami et al., 2017). The development of a 1D-MEM is essential in making the best use of field geomechanics related information. The 1D-MEM is fundamentally comprised of elastic properties, rock strength, and pore pressure as well as the in-situ stress magnitudes and direction. This 1D-MEM includes some time-dependent components such as a formation pressure changes with production and injection operations (Rahman et al, 2003). Such components reflect geomechanical changes taking place over the life of a field. Therefore, the robustness of geomechanical analysis heavily relies on revising and updating the 1D-MEM as more data field becomes available from different sources (i.e., after new field measurements and laboratory tests) (Khan et al., 2015). Then, the mud weight window was predicted using Mohr-Coulomb and Mogi-Coulomb failure criteria. The reliability of the suggested model was evaluated by comparing the predicted wellbore instability with actual borehole failures derived from the caliper logs.

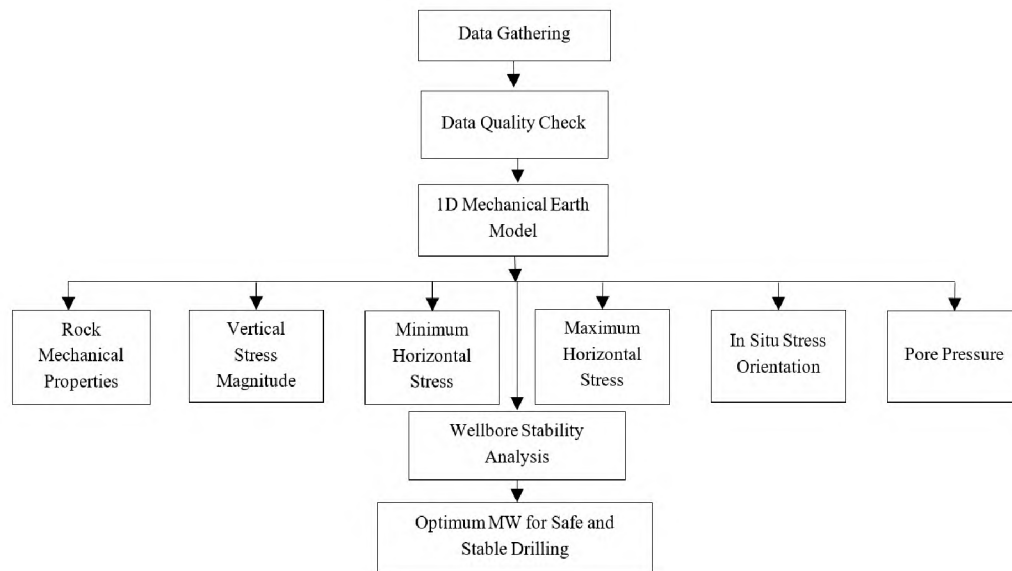


Figure 1. General workflow for the geomechanical model.

2.1. MECHANICAL STRATIGRAPHY

The mechanical responses as well as the properties of both the sandstone and shale formations were significantly different. Therefore, by classifying rocks according to their mechanical stratigraphy, it became possible to use different correlations for different formations to best estimate their rock mechanical properties and geomechanical parameters. The differentiation of non-shale from shale was realized by applying a threshold of 75 gAPI to the gamma-ray logs in the studied wells (Ahmed et al., 2016).

2.2. ROCK MECHANICAL PARAMETERS

Rock mechanical properties consist mainly of strength parameters, tensile strength, and elastic parameters (Abbas et al., 2018b). These properties are mainly used in wellbore stability analysis and the determination of the optimum mud pressure for safe drilling. The continuous profile of rock mechanical properties provides a good indication of the natural

variation in the formation strength and stability around the wellbore in different layers within the interval of interest. Empirical correlations were established between laboratory-derived rock mechanical properties and geophysical well logs, such as porosity and compressional acoustic wave velocity (v_p). Further details about estimating the rock mechanical properties of Zubair sandstone and shale formations using wireline measurements are comprehensively discussed in the studies conducted by Abbas et al. (2018c and 2018d).

2.2.1. Rock Strength Parameters. Rock strength parameters such as unconfined compressive strength (UCS), cohesive strength (C), and internal friction angle (ϕ), indicates to the ability of the rock formation to withstand the in-situ stress environment around the wellbore. The UCS and ϕ are the most commonly used rock strength properties for reservoir geomechanical modeling. These parameters are used primarily to determine wellbore failure during drilling and sanding due to formation pressure drawdown. The UCS and ϕ were determined using consolidated drained (CD) multistage triaxial tests for sandstone and consolidated undrained (CU) triaxial tests for shale. Eqs 1 and 2 were developed to estimate the UCS and ϕ of the sandstone formation as a function of porosity (ϕ), while Eqs. 3 and 4 were developed to estimate these parameters for the shale formation as a function of the compressional wave velocity (v_p) (Abbas et al 2018c; Abbas et al., 2018d).

$$UCS_{sand} = 133.2 - 370.82\phi \quad (1)$$

$$\phi_{sand} = 64.369 - 99.238\phi \quad (2)$$

$$UCS_{shale} = 2.6477e^{0.6006v_p} \quad (3)$$

$$\phi_{shale} = 17.134e^{0.239v_p} \quad (4)$$

2.2.2. Tensile Strength. Tensile strength (T_o) corresponds to the ability of the rock to support tensile failure. The rock materials fail in a sudden and brittle manner at stress magnitudes of only 1/12 to 1/8 of their unconfined compressive strength (UCS). Therefore, the continuous profile of tensile strength was computed as a function of the UCS (Rasouli et al., 2011). The predicted tensile strength was then calibrated to the laboratory measurements, where Brazilian tests were conducted on plug samples retrieved from the Zubair Formation.

2.2.3. Rock Elastic Parameters. Rock elastic properties represent the basic inputs for estimating in-situ stresses. The static elastic parameters (such as Young's modulus (E) and Poisson's ratio (ν)) demonstrate the deformation behavior for isotropic elastic materials. These static elastic parameters were measured using consolidated drained (CD) triaxial tests for sandstone and consolidated undrained (CU) triaxial tests for shale. Eqs. 5 and 6 were developed to estimate the static Young's modulus (E) and Poisson's ratio (ν) of a sandstone formation as a function of the porosity (ϕ), respectively, while Eqs. 7 and 8 were developed to estimate these parameters for a shale formation as a function of the compressional wave velocity (v_p), respectively (Abbas et al 2018c; Abbas et al., 2018d).

$$E_{sand} = 40.476 - 136.79\phi \quad (5)$$

$$\nu_{sand} = 0.1203 - 0.766\phi \quad (6)$$

$$E_{shale} = 0.2966e^{0.6984v_p} \quad (7)$$

$$\nu_{shale} = 0.7621e^{-0.353v_p} \quad (8)$$

2.3. FORMATION PORE PRESSURE

Formation pore pressure is a key constituent in reservoir geomechanical modeling. It is one critical mechanical parameters widely utilized for estimation of in-situ horizontal principal stress magnitudes and operating mud weight window for both safe and stable drilling (Zhang et al., 2014). The pore pressure limit defines the minimum mud weight required to maintain hydraulic safety. Therefore, inaccurate prediction of the pore pressure may lead to well control issues (i.e., kicks and well blowouts). Two methods (i.e., direct and indirect) are often used in the petroleum industry to determine pore pressure. Direct measurement methods use well test techniques, such as the drill stem test (DST) and repeated formation test (RFT) to measure formation pore pressure for specific depths, whereas indirect (empirical and theoretical) methods are based on petrophysical data that are developed to predict pore pressure along the well length (Zhang, 2011). For more confidence, the estimated formation pore pressure from indirect methods is usually validated with the available measured formation pressure points of the DST or RFT. Eaton equation is conventionally used to estimate the pore pressure based on the sonic wireline measurements (Eaton, 1969). This equation formulated as:

$$P_{pg} = OBG - (OBG - P_{hg}) \left(\frac{NCT}{DT} \right)^3 \quad (9)$$

where P_{pg} is the pore pressure gradient, OBG indicated as overburden gradient, P_{hg} is hydrostatic pressure gradient (also known as the normal pore pressure), NCT is the normal compacted trend line that fitting compressional wave log measurements, and DT is the P-wave transit time.

2.4. IN-SITU STRESS MAGNITUDE

The regional stress field at any depth comprises of three principal stress magnitudes: overburden stress (σ_v), and minimum (σ_h) and maximum horizontal stresses (σ_H). This methodology is based on the assumption of an Andersonian in-situ stress state, which is a safe assumption for areas with little tectonic activity and is valid in most areas of petroleum production (Anderson et al., 1973). The overburden stress in the vertical direction is one of the principal in-situ stresses, whereas the other two are the minimum and maximum horizontal principal stresses orthogonal to the overburden stress.

2.4.1. Vertical Stress. Vertical stress is assumed to be a principal stress, and is usually considered to be solely due to the weight of the overburden (Jaeger et al., 2007). The vertical stress at the Zubair Formation was calculated by integrating the bulk density log over the vertical depth, using Eq. 10.

$$\sigma_v = \int_0^z \rho(z)gdz \quad (10)$$

where g represents the acceleration constant due to gravity (m/s^2), z is vertical depth (m), and ρ is the rock bulk density (g/cm^3).

2.4.2. Horizontal Stresses (Minimum and Maximum). The horizontal principal stresses are fundamental inputs to geomechanical analysis. In isotropically and tectonically relaxed areas, the minimum and maximum horizontal stresses are the same. However, the horizontal stresses are not equal where major faults or active tectonics exists. The determination of these principal stresses magnitude is the most difficult component of the stress tensor. Therefore, several laboratory and field methods are used to estimate the minimum and maximum horizontal stress magnitudes such as hydraulic, relief, jacking,

strain recovery, and focal mechanism (Najibi et al., 2017). The poro-elastic horizontal strain is perhaps the most commonly used method for horizontal principal stress estimation (Dokhani et al., 2015; Cao et al., 2018; Gholami et al., 2017). Assuming flat-layered, poro-elasticity deformation in the formation rock, a pair of particular constant strains, ε_y and ε_x , is applied to the formation in the direction of the maximum and minimum stress, respectively. For a fluid-saturated porous material that is assumed to be linear, elastic, and isotropic, considering anisotropic tectonic strain, the horizontal stresses (minimum and maximum) are expressed in Eqs. 11 and 12, respectively (Thiercelin and Plumb, 1994). This approach estimates the magnitudes of horizontal principal stresses along the well length using static Young's modulus, static Poisson's ratio, regional pore pressure, rock deformation, and overburden stress.

$$\sigma_h = \frac{\nu}{1-\nu} \sigma_v + \frac{1-2\nu}{1-\nu} \alpha p_p + \frac{E}{1-\nu^2} \varepsilon_x + \frac{\nu E}{1-\nu^2} \varepsilon_y \quad (11)$$

$$\sigma_H = \frac{\nu}{1-\nu} \sigma_v + \frac{1-2\nu}{1-\nu} \alpha p_p + \frac{E}{1-\nu^2} \varepsilon_y + \frac{\nu E}{1-\nu^2} \varepsilon_x \quad (12)$$

In the above equations, α is the Biot's coefficient, which is maintained at unity to account for the brittle failure of rocks (conventionally $\alpha = 1$), E is static Young's modulus (GPa), ε_x is strain in minimum horizontal stress direction, and ε_y is strain in maximum horizontal stress direction. The two horizontal strains (ε_y and ε_x) can be measured by Eqs. 13 and 14, respectively (Kidambi and Kumar, 2016).

$$\varepsilon_y = \frac{\sigma_v \nu}{E} \left(1 - \frac{\nu^2}{1-\nu}\right) \quad (13)$$

$$\varepsilon_x = \frac{\sigma_v \nu}{E} \left(\frac{1}{1-\nu} - 1\right) \quad (14)$$

The magnitude of the minimum horizontal principal stress acquired from the Eq. 11 can be calibrated against the direct field measurements such as mini-frac test, standard leak-off test (LOT), and extended leak-off test (XLOT) (Zoback et al., 2003).

2.5. ORIENTATION OF IN-SITU STRESSES

Knowledge of in-situ stress orientation is an important aspect in any comprehensive geomechanical model. Borehole failure analysis (e.g., borehole breakouts and drilling-induced tensile fractures) is one of the chief methods for determining the horizontal principal stress orientation (Kingdon et al., 2016). The common use of borehole micro-imager logs and caliper logs in the petroleum industry has yet to yield detailed information about the failure around the borehole (Zoback et al., 1985). In vertical wells, shear failure occurs in the direction of the minimum horizontal principal stress, while tensile failure occurs along the orientation of the maximum horizontal principal stress (Wiprut and Zoback, 2000).

3. STRESS DISTRIBUTION AROUND THE DEVIATED BOREHOLE

The orientation of the wellbore with respect to the in-situ principal stresses has a significant influence on the stresses around a wellbore. This is represented by the deviation of the borehole from the vertical (i) and the drilling direction with respect to σ_H (α) (Al-Ajmi and Zimmerman, 2006). Because the wellbore is drilled in any orientation and the drilling fluid is replacing the removed rock, the formation's in-situ stresses should be transformed into a new Cartesian coordinate system (x, y, z) associated with the wellbore

orientation to conveniently evaluate the stress distribution around the borehole, as shown in Figure 2. The in-situ stresses in (x, y, z) space are defined by the following (Aadnoy and Looyeh, 2011):

$$\begin{aligned}
 \sigma_x &= (\sigma_H \cos^2 \alpha + \sigma_h \sin^2 \alpha) \cos^2 i + \sigma_v \sin^2 i, \\
 \sigma_y &= \sigma_H \sin^2 \alpha + \sigma_h \cos^2 \alpha, \\
 \sigma_{zz} &= (\sigma_H \cos^2 \alpha + \sigma_h \sin^2 \alpha) \sin^2 i + \sigma_v \cos^2 i, \\
 \tau_{xy} &= 0.5(\sigma_h - \sigma_H) \sin 2\alpha \cos i, \\
 \tau_{xz} &= 0.5(\sigma_H \cos^2 \alpha + \sigma_h \sin^2 \alpha - \sigma_v) \sin 2i, \\
 \tau_{yz} &= 0.5(\sigma_h - \sigma_H) \sin 2\alpha \sin i.
 \end{aligned} \tag{15}$$

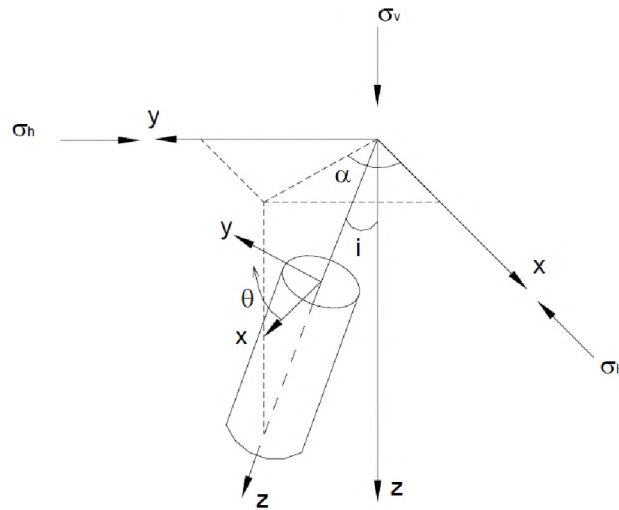


Figure 2. Stress transformation in polar systems for a deviated borehole.

The calculation of stresses around borehole strongly depends on the in-situ principal stresses, the behavior of the rock, formation pore pressure, and the internal wellbore pressure. The stress distribution around the borehole is given in a cylindrical coordinate system (r, z, θ) , taking into account the effect of the wellbore deviation (Chabook et al., 2015) For a rock obeying linear elasticity, the stresses at any point around

the borehole are represented in terms of σ_r , σ_θ , and σ_z , as given by Kirsch's equations (16)

(Aadnoy, 1989):

$$\begin{aligned}
 \sigma_r &= 0.5(\sigma_x + \sigma_y)\left(1 - \frac{R^2}{r^2}\right) + 0.5(\sigma_x - \sigma_y)\left(1 + 3\frac{R^4}{r^4} - 4\frac{R^2}{r^2}\right)\cos 2\theta + \tau_{xy}\left(1 + 3\frac{R^4}{r^4} - 4\frac{R^2}{r^2}\right)\sin 2\theta + \frac{R^2}{r^2}P_w, \\
 \sigma_\theta &= 0.5(\sigma_x + \sigma_y)\left(1 + \frac{R^2}{r^2}\right) - 0.5(\sigma_x - \sigma_y)\left(1 + 3\frac{R^4}{r^4}\right)\cos 2\theta - \tau_{xy}\left(1 + 3\frac{R^4}{r^4}\right)\sin 2\theta - \frac{R^2}{r^2}P_w, \\
 \sigma_z &= \sigma_{zz} - 2\nu(\sigma_x - \sigma_y)\frac{R^2}{r^2}\cos 2\theta - 4\nu\tau_{xy}\frac{R^2}{r^2}\sin 2\theta, \\
 \tau_{r\theta} &= \left[0.5(\sigma_x - \sigma_y)\sin 2\theta + \tau_{xy}\cos 2\theta\right]\left(1 - 3\frac{R^4}{r^4} + 2\frac{R^2}{r^2}\right), \\
 \tau_{rz} &= (\tau_{xy}\cos \theta + \tau_{yz}\sin \theta)\left(1 - \frac{R^2}{r^2}\right), \\
 \tau_{\theta z} &= (-\tau_{xz}\sin \theta + \tau_{yz}\cos \theta)\left(1 + \frac{R^2}{r^2}\right).
 \end{aligned} \tag{16}$$

where σ_r , σ_θ , and σ_z are the radial, tangential and axial stresses, respectively, induced around the borehole at a distance (r) away from a borehole with a radius of (R); P_w is the mud pressure; and the angle θ is measured clockwise from the σ_H direction (varies from 0° to 360°). At the borehole wall (i.e., when $r = R$), Kirsch's equations will be reduced to the following:

$$\begin{aligned}
 \sigma_r &= P_w, \\
 \sigma_\theta &= \sigma_x + \sigma_y - 2(\sigma_x - \sigma_y)\cos 2\theta - 4\tau_{xy}\sin 2\theta - P_w, \\
 \sigma_z &= \sigma_{zz} - 2\nu(\sigma_x - \sigma_y)\cos 2\theta - 4\nu\tau_{xy}\sin 2\theta, \\
 \tau_{r\theta} &= 0, \\
 \tau_{rz} &= 0, \\
 \tau_{\theta z} &= 2(-\tau_{xz}\sin \theta - \tau_{yz}\cos \theta).
 \end{aligned} \tag{17}$$

According to the previous equations, the σ_θ and σ_r stresses are functions of the P_w , but the σ_z stress is not. Consequently, any change in the P_w will only effect σ_r and σ_θ . The σ_θ and σ_z stresses vary in a sinusoidal way around the wellbore circumference because they are a function of the angle θ .

As mentioned previously, there are two main lack of stability problems that could occur at the borehole wall: borehole collapse and drilling-induced tensile fractures. The borehole collapse is expected to occur at the point of maximum tangential stress where the rock is under maximum compression strength, while drilling-induced tensile fractures are anticipated to happen at the point where the tangential stress has the smallest value. A reduction in mud weight is associated with an increased potential for shear failure, whereas a rise in mud pressure is associated with an increased potential for tensile failure (Taleghani and Klimenko, 2015). Therefore, the lower limit for mud pressure corresponds with borehole collapse, and the upper limit of the mud weight is associated with tensile failure (Salehi and Nygaard, 2014; Mahmoud et al., 2017). The effective principal stresses in the cylindrical borehole coordinate system in which shear stress is zero are given by Eqs. 18 and 19 (Zoback, 2007).

$$\sigma_{tmax} = 0.5(\sigma_z + \sigma_\theta + \sqrt{(\sigma_z - \sigma_\theta)^2 + 4\tau_{\theta z}^2}) \quad (18)$$

$$\sigma_{tmin} = 0.5(\sigma_z + \sigma_\theta - \sqrt{(\sigma_z - \sigma_\theta)^2 + 4\tau_{\theta z}^2}) \quad (19)$$

where σ_{tmax} is the highest stress, σ_{tmin} is the lowest stress. Both of these principal stresses can be used in rock failure criteria for wellbore stability analysis (Al-Ajmi and Zimmerman, 2009).

4. ROCK FAILURE CRITERIA

Failure criteria take into account the stress condition around the wellbore to determine the stress magnitudes at which borehole failure may occur. Stress analysis using a suitable failure criterion is the first step in predicting rock failure and in wellbore stability

analysis. Two failure criteria were considered in this study (i.e., Mohr-Coulomb and Mogi-Coulomb) to predict wellbore breakout and maximum tensile stress.

4.1. MOHR-COULOMB FAILURE CRITERION

Mohr-Coulomb is the most common widely used failure criterion in engineering applications. This criterion is considered to be a 2D linear approach because it assumes that the intermediate stress does not influence rock strength. The shear failure would occur in this criterion when shear stress (τ) on a specific plane reaches a value that is sufficient to overcome the frictional force, which is a function of the normal stress components (σ_n), internal cohesion (C_o), and the coefficient of internal friction of the material (μ):

$$\tau = c_o + \mu\sigma_n \quad (20)$$

$$\mu = \tan \varphi \quad (21)$$

The failure equation can be written in terms of principal stresses, as follows:

$$\sigma_1 = UCS + q\sigma_3 \quad (22)$$

where q is a parameter related to the coefficient of internal friction (μ) and the angle of internal friction (φ) by

$$q = \left[(\mu^2 + 1)^{1/2} + \mu \right]^2 = \tan^2(\pi/4 + \varphi/2) \quad (23)$$

$$UCS = 2c_o \cos \varphi / (1 - \sin \varphi) \quad (24)$$

4.2. MOGI-COULOMB FAILURE CRITERION

The Mogi-Coulomb criterion takes into consideration the impact of intermediate stress on rock deformation. This failure criterion can be formulated as follows:

$$\tau_{oct} = f(\sigma_{m,2}) \quad (25)$$

where f is taken to be a nonlinear, power-law function. The octahedral shear stress (τ_{oct}) and the effective mean stress ($\sigma_{m,2}$) are given by

$$\tau_{oct} = 1/3\sqrt{(\sigma_1 - \sigma_2)^2 + (\sigma_2 - \sigma_3)^2 + (\sigma_3 - \sigma_1)^2} \quad (26)$$

$$\sigma_{m,2} = \frac{\sigma_1 + \sigma_2}{2} \quad (27)$$

The failure function Mogi-Coulomb criterion has been criticized because its parameters cannot be easily related to the Coulomb strength parameters, UCS and ϕ (Colmenares and Zoback, 2002). To avoid this issue, Al-Ajmi and Zimmerman (2006) introduced a linear relation that fits well with the polyaxial test results in a similar format to the Mohr-Coulomb criterion, as follows:

$$\tau_{oct} = a + b\sigma_{m,2} \quad (28)$$

where the linear Mogi-Coulomb criterion parameters (a and b) can be calculated by

$$a = \frac{2\sqrt{2}}{3} c_o \cos \phi \quad (29)$$

$$b = \frac{2\sqrt{2}}{3} \sin \phi \quad (30)$$

The strengthening effect of the intermediate stress can be considered in terms of the primary and secondary stress invariants, I_1 and I_2 , which are given by

$$I_1 = \sigma_1 + \sigma_2 + \sigma_3 \quad (31)$$

$$I_2 = \sigma_1\sigma_2 + \sigma_2\sigma_3 + \sigma_3\sigma_1 \quad (32)$$

Using the Mogi-Coulomb criterion, the following is true:

$$\sqrt{I_1^2 - 3I_2^2} = a' + b'(I_1 - \sigma_2) \quad (33)$$

where a' and b' are defined by

$$a' = 2c_o \cos \varphi, \quad b' = \sin \varphi \quad (34)$$

5. FIELD CASE STUDY

This study uses the data from the Zubair Formation in Southern Iraq, which is recorded as being gas and oil-bearing in 30 structures that contain about 30% of Iraq's hydrocarbon reserves (Jassim and Goff, 2006). It is composed mainly of alternating shale and sandstone, with minor streaks of limestone and siltstone. Shale contributes more than 55% of the Zubair Formation. Several wells in the Zubair Formation have had significant geomechanical problems for in these fields, based on the issues experienced during the drilling stages, including lost circulation, wellbore collapse, shale caving, stuck logging tools, and stuck pipe. Many times, due to severe stuck pipe problem and unsuccessful fishing operations, the well has to be drilled with more than one sidetrack or, in the worst case scenario, the wellbore has to be abandoned. Unfortunately, all of the above problems have placed constraints on the field development plans.

5.1. MEM CONSTRUCTED FOR THE ZUBAIR FORMATION

The drilling-related data (e.g., daily drilling reports, daily drilling fluid reports, and mud logs [master logs]) and open hole wireline logging measurements (e.g., density logs, gamma-ray [GR] logs, sonic logs, formation micro-imager [FMI] logs, and neutron logs) are fundamental input parameters for any reservoir geomechanics studies. The open hole

wireline logs of the caliper, gamma-ray (GR), compressional wave transit times (DTCO), shear wave transit times (DTSM), density (RHOZ), and total porosity (PHIT) for the Zubair Formation at a 3205- 3557 m interval. The compressional wave velocity (v_p) and shear wave velocity (v_s) were derived from the compressional and shear wave transit times in the sonic log measurements. Moreover, the total porosity (\emptyset) was determined directly from the neutron log. The lithology of the Zubair Formation includes mainly shale and sandstone. The mechanical responses and properties of grain-supported and clay-supported formations usually differ significantly.

In the current study, the classification of mechanical stratigraphy was used to calculate the rock mechanical properties by employing a variety of correlations. This differentiation of non-shales from shale formations was achieved by applying a threshold to the clay volume log in the analyzed wells. The suggested mechanical stratigraphy was also validated with the data provided in the available master mud logs and pore pressure points, which usually were measured in the non-shale formations (depleted sandstone).

The aforementioned empirical correlations (Eqs. 1-8) were used to derive the rock mechanical properties from the neutron and sonic logs. The previously suggested mechanical stratigraphy was used to apply correlations of shale to the shale formation and correlations of sandstone to the sandstone formation. Then, each derived mechanical property was combined to build a single log from the top to the bottom of the Zubair Formation. The laboratory-measured rock mechanical properties were added to the plot to assess the level of agreement between the experimentally measured rock mechanical properties and the derived rock mechanical logs (Abbas et al., 2018e; Abbas et al, 2018f). Figure 3 presents examples of the rock mechanical property logs for one of the cored wells

in the Zubair Formation. As can be seen, there is a high degree of positive correlation between the calculated rock mechanical property logs (i.e., Poisson's ratio, Young's modulus, UCS, internal friction angle, and tensile strength) and those derived from the laboratory.

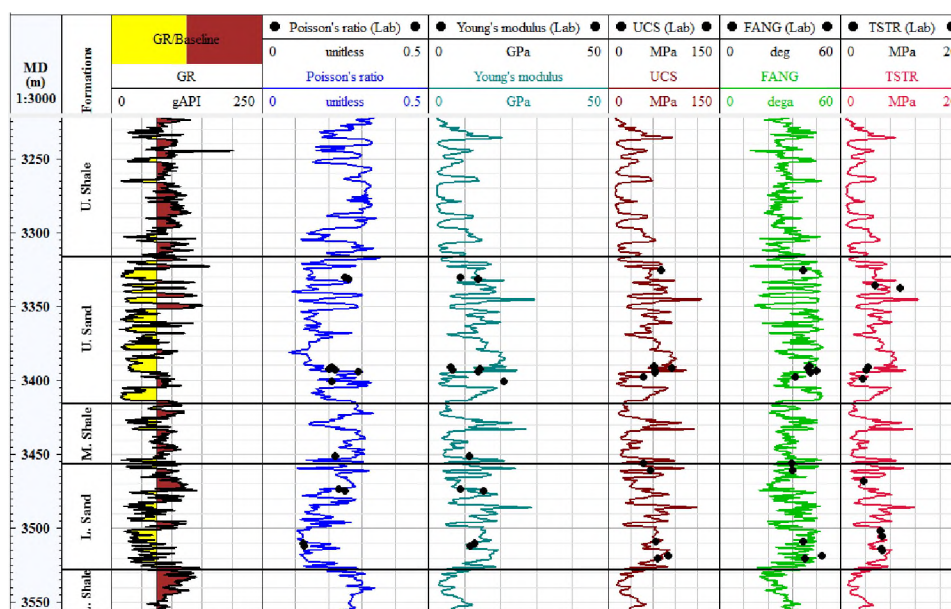


Figure 3. Predicted rock mechanical properties logs and laboratory measurements.

In the current study, the pore pressure of the depleted sandstone formations was computed using constant pressure gradients that were determined from repeated formation test (RFT) measurements. Due to the discontinuity of the RFT data for the shale formations, the pore pressure was estimated using the modified Eaton technique of Eq. (9). The resultant formation pore pressure profile was calibrated against actual pore pressure measurements and the real mud weight that had been used to drill the well, which always should be higher than the pore pressure. As shown in Figure 4, there is good agreement

between the pore pressure profile and the individually measured data from the RFT. The estimated average pore pressure gradient ranged from 0.01~0.011 MPa/m.

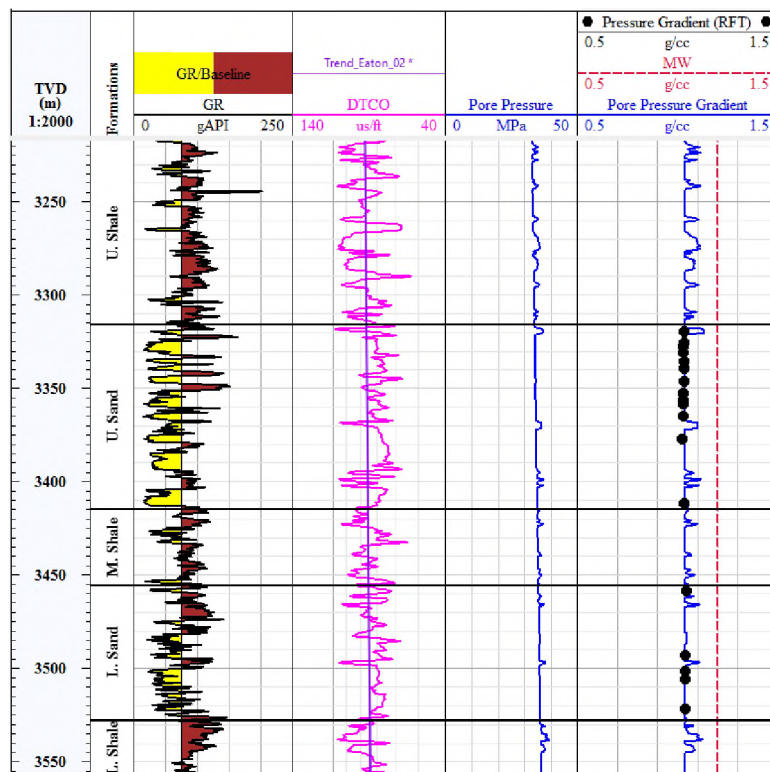


Figure 4. Pore pressure profile calibrated against the available measured pressure points.

The vertical stress magnitude on the Zubair Formation was calculated using the density log, according to Eq. (10). For shallow zones, where the density log was not recorded because it was not of geologic interest, a compaction relationship based on the regional density data was used to create a synthetic density curve to fill the gaps where the direct measurement was not available. The vertical stress gradient estimated in the studied wells was close to 0.0221 MPa/m. Moreover, the continuous estimation of the minimum and maximum horizontal stress magnitudes along the well length was obtained from poro-

elastic formulations using Eqs. (11) and (12), respectively. The result of the minimum horizontal stress was calibrated against direct measurements of closure pressures that were available from the mini-frac test. The predicted minimum horizontal stress from the poro-elastic formulation showed reasonably good agreement with the closure pressures. Figure 5 illustrates the estimate of the vertical stress, maximum horizontal stress, minimum horizontal stress, and pore pressure magnitudes. The results indicate that the tectonic stress regime in the Zubair Formation appears to be a normal faulting regime (i.e., $\sigma_v > \sigma_H > \sigma_h$).

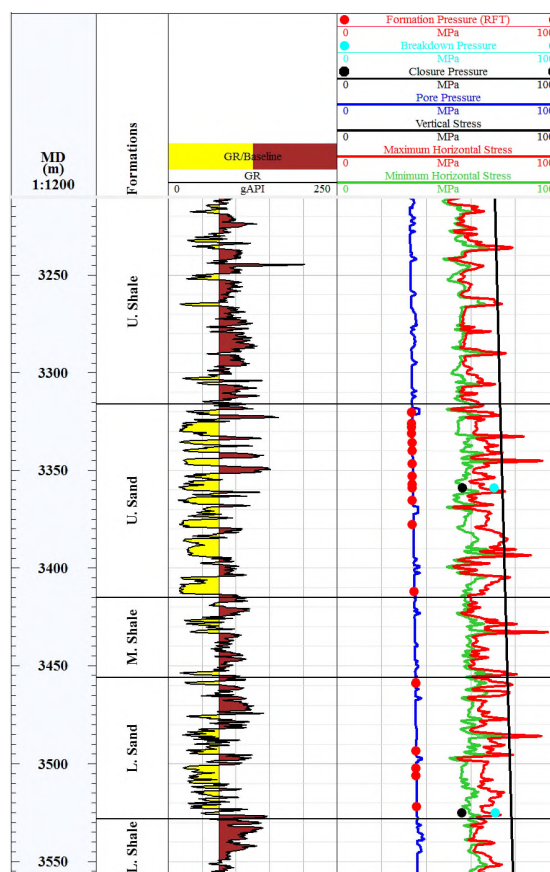


Figure 5. Estimation of the in-situ principal stress magnitudes at a single well location.

In this paper, formation micro-imager (FMI) log data acquired from a vertical well was processed and interpreted to determine the direction of horizontal in-situ stresses using the borehole breakout technique. The results of the interpretation show a combined length of 92 m from 13 distinct breakout zones in a 140° direction, with a standard deviation of 10° (Figure 6). The breakouts in a vertical wellbore develop parallel to the minimum horizontal stress. Therefore, the direction of the minimum horizontal stress is 140° , and the direction of the maximum horizontal stress is 50° , which is perpendicular to the minimum horizontal stress. According to the World Stress Map (WSM) database quality ranking, quality B was assigned based on borehole breakout observations (Tingay et al., 2008). This is in close agreement with nearby stress measurements from a field in Southern Iraq (Mohammed et al., 2018).

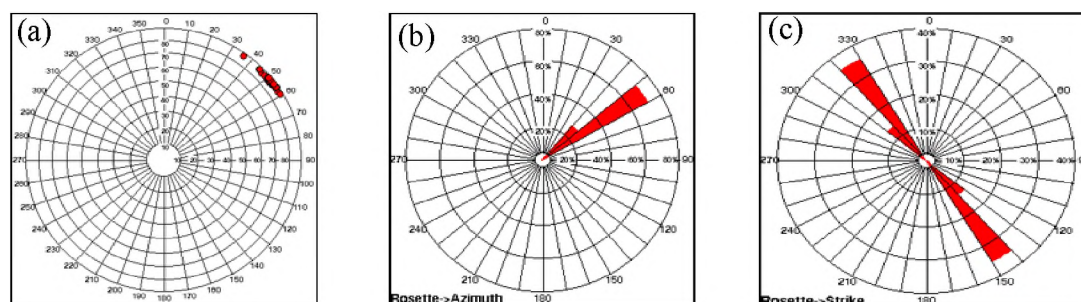


Figure 6. Orientation of the identified borehole breakouts (direction of minimum horizontal stress): (a) Schmidt plot-upper hemisphere, (b) rosette plot of the dip azimuth, and (c) rosette plot of the strike azimuth.

5.2. TRAJECTORY SENSITIVITY ANALYSIS

Mud weight sensitivity analysis to the wellbore orientation provides the relationship between the required shear failure (breakout) and tensile failure (fracture initiation) mud weights with the wellbore inclination and azimuth at a given depth. The

results of such an analysis allow the drilling engineer to identify the most stable inclination and azimuth choice compatible with other well design constraints. This sensitivity analysis was conducted on critical depths across the problematic parts of the Zubair Formation using as inputs the 1D MEM that was built earlier. For stereographic plots of the breakout mud weight versus the inclination and azimuth, the coloration indicates the minimum mud weight required to maintain a stable wellbore; the coloration on the tensile failure plots indicates the maximum allowable mud weight to avoid tensile-induced fracture.

The results show that the mud weight window narrows gradually with an increase in the wellbore inclination. To illustrate the relationship between the mud weight window and well inclination, the breakout and tensile-induced fracture mud weights predicted by the Mohr-Coulomb criterion at an inclination of 0° are about 1.31 and 2.41 g/cc, respectively; however, at an inclination of 90° (in the direction of the minimum horizontal stress), they are about 1.71 and 2.05 g/cc, respectively (Figure. 7). In contrast, the breakout and tensile-induced fracture mud weights calculated by the Mogi-Coulomb criterion at an inclination of 0° are 1.27 and 2.45 g/cc, respectively, whereas at an inclination of 90° (in the direction of the minimum horizontal stress), they are about 1.62 and 2.09 g/cc, respectively (Figure 8). These results indicate that a vertical well requires the lowest mud weight to prevent breakout and, conversely, that horizontal wells require the highest mud weight to maintain wellbore stability. Furthermore, it can be observed that the safe mud weight window determined by the Mogi-Coulomb criterion is a little wider than that obtained by the Mohr-Coulomb criterion. That is because the rock strength predicted by the Mogi-Coulomb is higher than that predicted by the Mohr-Coulomb criterion. This was related to the fact that Mogi-Coulomb criterion considers the effect of intermediate

principal stress on failure prediction and this is a better representation of failure occurring in real situation.

As illustrated in Figures 7b and 8b, higher breakdown mud weights are anticipated in the direction of the minimum horizontal stress with inclinations less than 60° compared to a wellbore drilled parallel to the maximum horizontal stress direction. It can be concluded that the preferred wellbore orientation to drill highly deviated wells (i.e., inclinations higher than 60°) is along the minimum horizontal stress (140°).

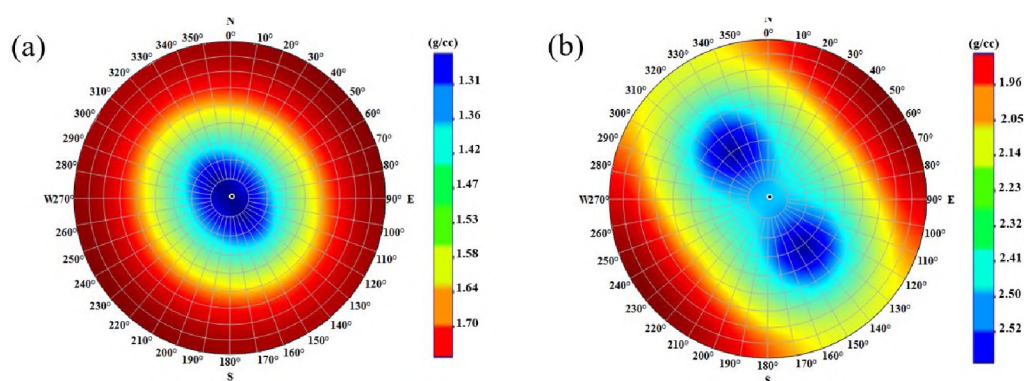


Figure 7. Minimum mud weight plots using the Mohr-Coulomb failure criterion: (a) borehole breakout mud weight vs. well orientation, and (b) formation breakdown mud weight vs. well orientation.

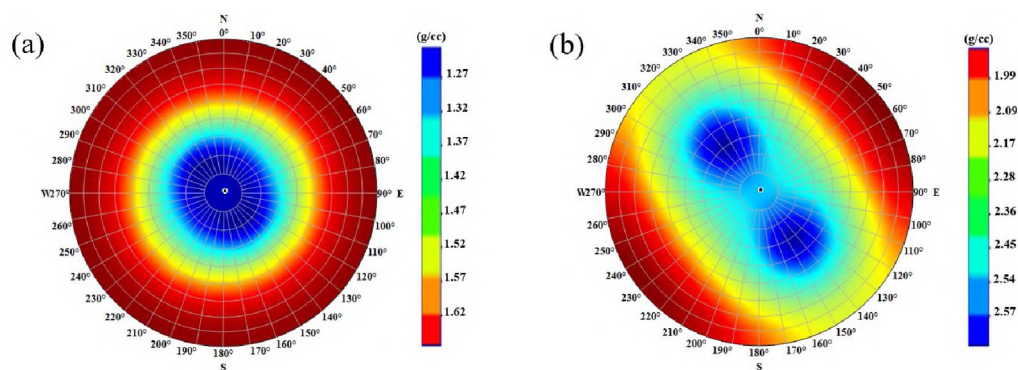


Figure 8. Minimum mud weight plots using the Mogi-Coulomb failure criterion: (a) borehole breakout mud weight vs. well orientation, and (b) formation breakdown mud weight vs. well orientation.

5.3. MUD WEIGHT VERSUS WELLBORE INCLINATION AND AZIMUTH

The mud weight (mud pressure) window for safe drilling should be designed to prevent borehole washouts, collapse, stuck pipe, and mud loss. There are four limits defining the mud weight window: pore pressure, breakout pressure (shear failure pressure), mud loss (minimum horizontal stress), and breakdown pressure. Therefore, the optimum mud pressure should be high enough to ensure borehole stability and low enough not to fracture the formation (i.e., mud losses do not occur). The breakout and breakdown pressures are trajectory-dependent, meaning that they will change with a variation in the inclination and/or azimuth of the wellbore.

In this study, two failure criteria (i.e., Mohr-Coulomb and Mogi-Coulomb) were applied to optimize the well trajectory based on the analysis of the effects of well inclination and azimuth on the mud weight window. Figures 9 and 10 show the mud weight window versus the well inclination and azimuth for single depths obtained by the Mohr-Coulomb and the Mogi-Coulomb criteria, respectively. In this mud weight window, the gray profile shows the mud weight corresponding to kick, while the yellow profile is the mud weight below which breakouts or shear failure will occur. On the right-hand side, if the mud weight exceeds the dark blue or blue profiles, the model predicts mud loss and induced fracture in the formation, respectively. Thus, the white area in the middle is the safe operating mud weight window for drilling through the Zubair Formation. As illustrated in Figures 9a and 10a, the safe mud weight window becomes narrow in wells with an inclination above 40°. In addition, no effect of the wellbore azimuth on the breakout mud weight was observed due to low-stress contrast (Figures 9b and 10b). From the mud weight window shown in Figures 9 and 10, the Mohr-Coulomb criterion underestimates the rock

strength and results in a higher value for the lower bound of the safe mud weight window compared to Mogi-Coulomb failure criteria (Rahimi and Nygaard, 2015). Based on this analysis of the Zubair section, the well trajectory should be designed to avoid a high deviation, or the mud weights should be high enough to prevent the collapse failure and to tolerate limited mud loss.

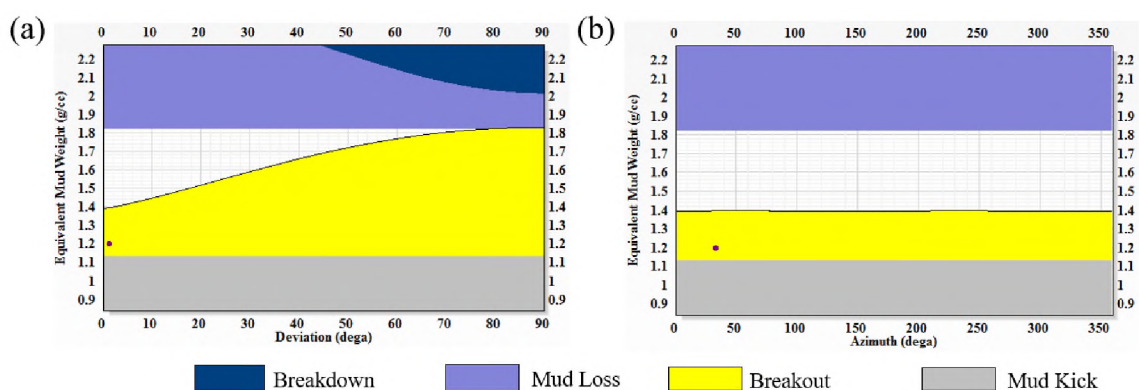


Figure 9. Minimum mud weight plots using the Mohr-Coulomb failure criterion: (a) mud weight window vs. deviation, and (b) mud weight window vs. azimuth.

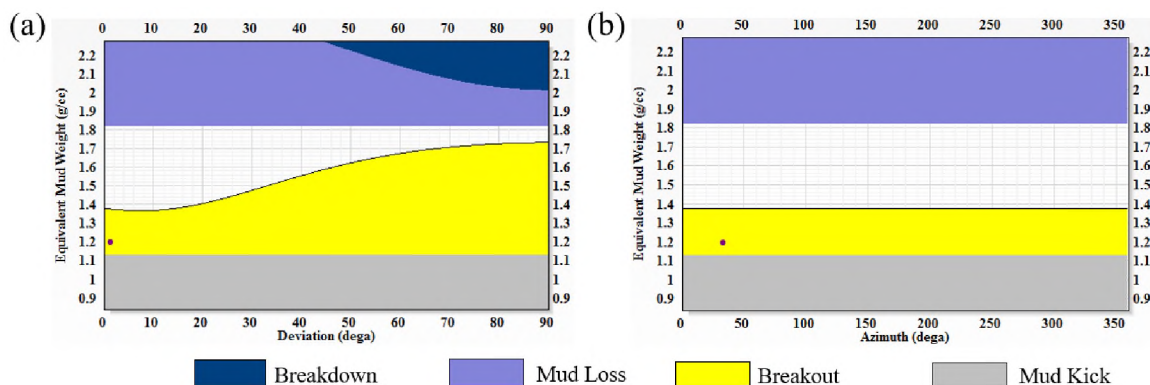


Figure 10. Minimum mud weight plots using the Mogi-Coulomb failure criterion: (a) mud weight window vs. deviation, and (b) mud weight window vs. azimuth.

5.4. MODEL VALIDATION

The validity of a geomechanical model should be verified prior to its application. After the mud weight window of an offset well has been calculated, the predicted occurrences of borehole failure (e.g., losses, breakouts, tensile-induced fractures, etc.) can be predicted by using the actual mud weight that had been used to drill the well. A failure match can then be performed by comparing the predicted lack of wellbore stability with the actual rock failure shown on the image and/or the caliper logs. The calibrated results ensure that all geomechanical model parameters are well constrained with reasonable accuracy. In addition, the calibrated results can also provide a better understanding of any geomechanics-related reasons behind the instability-related events (i.e., mud loss, shale caving, tight holes, stuck pipe incidents, etc.) encountered while drilling. The failure criterion model with the higher degree of matching was considered to be the most reliable model for this particular formation.

In this study, the most commonly applied failure criteria (i.e., Mohr-Coulomb and Mogi-Coulomb) were used to predict the borehole failure regions in the wellbore (Figures 11 and 12), respectively. The caliper log values displayed in this Figure show that severe breakouts were observed with the intervals from 3210-3321 m, 3372-3444 m, and 3528-3557 m. The predicted occurrences of the breakout regions using the Mogi-Coulomb criteria showed a good agreement with the observed breakouts in the caliper log compared to Mohr-Coulomb failure criteria (Figure 12). Therefore, the Mogi-Coulomb criterion was selected as the most appropriate failure criterion for the Zubair Formation because it yields a more reliable and realistic estimate of the safe operating mud weight window.

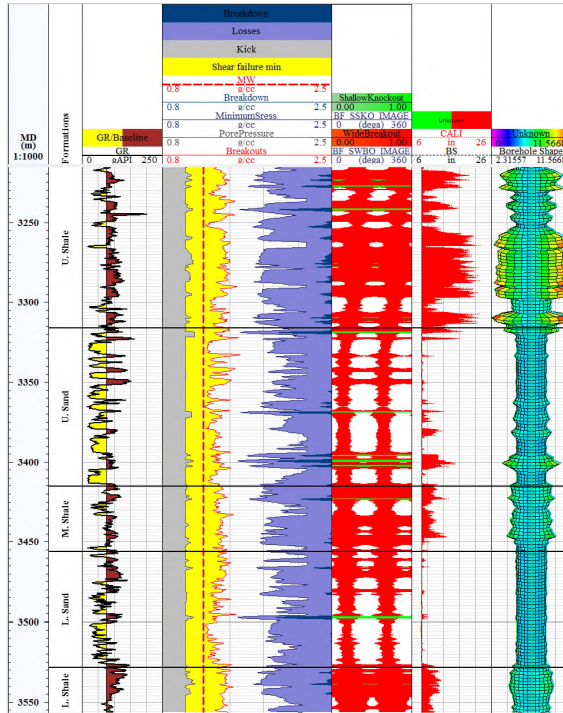


Figure 11. Evaluation of the accuracy of 1D-MEM using Mohr-Coulomb criteria.

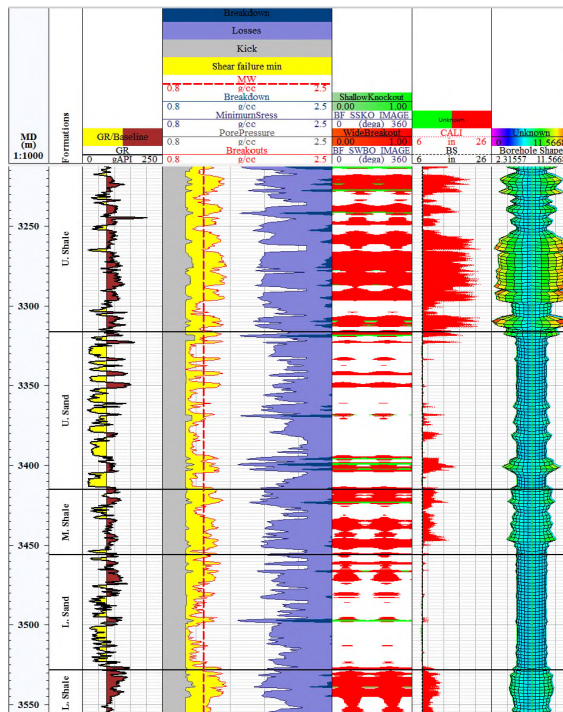


Figure 12. Evaluation of the accuracy of 1D-MEM using Mogi-Coulomb criteria.

5.5. WELLBORE STABILITY FORECAST

A single point analysis of the mud weight sensitivity to the wellbore trajectory allows for the selection of the most stable inclination and azimuth. However, due to the natural variability of the rock properties within a formation, this analysis does not serve to predict the degree of the breakout and tensile failures for a given trajectory. To predict the degree and type of wellbore failure, a wellbore stability forecast is required for the selected well path, based on the trajectory sensitivity analysis.

In this study, a wellbore stability prediction was conducted for the planned highly deviated well to evaluate potential drilling risks and investigate the possible mud weight window to minimize borehole instability-related problems based on the developed geomechanical model from the surrounding wells. Wellbore deformation and potential breakout risks were evaluated for both the weak shale sections and depleted sandstone sections along the proposed trajectory (60° inclination and 140° azimuth), using the Mogi-Coulomb criterion. Based on the mud weight window and lack of wellbore stability forecast shown in Figure 13, a mud weight of 1.5 g/cc was selected as a safe operating mud weight to drill the planned highly deviated well from a 9 5/8" casing shoe (3205 m) to the final total depth (3557 m).

The results of wellbore stability forecast show some breakout expected over several short intervals of weak shale zones (between 3219-3327 m, 3267-3295 m, 3307-3318 m, and 3534-3544 m) at the selected mud weight. As illustrated in Figure 13, it is likely that the mud window disappears in several zones at the depths of approximately 3212 m, 3241 m, 3318 m, 3399 m, and 3497 m, meaning that there is no safe mud window in these zones. Therefore, drilling team should be aware of these specific intervals where potential

wellbore failure could occur. Good drilling practices, including regular borehole cleaning, monitoring tripping speed, proper mud conditioning, and controlling the ROP while drilling through these zones, will help to manage the lack of stability and avoiding major drilling problems. In addition, equivalent circulation density (ECD) would become crucial with an upper mud weight limit to avoid mud losses. Surging the borehole during tripping can have a similar effect by increasing the instantaneous mud pressure above the breakdown pressure. Therefore, the tripping speed of the drill string and casing in these zones should be monitored carefully.

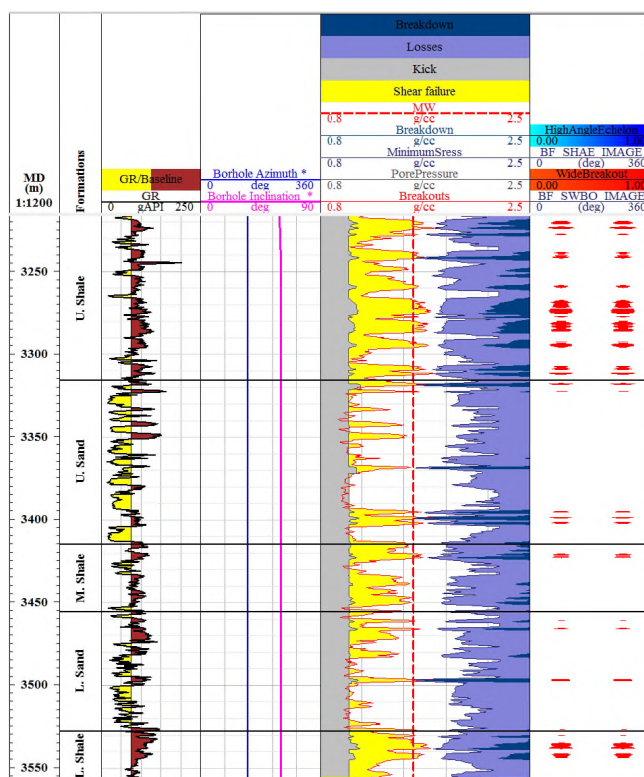


Figure 13. Wellbore stability forecast for the planned highly deviated well.

6. CONCLUSIONS

It was concluded that the heterogeneity of the Zubair Formation should be considered in the mud weight calculation as the mud weight is designed to maintain the stability of weak and non-depleted shale zones. This study found that the results acquired from the Mogi-Coulomb failure criterion are less conservative but more realistic and reliable than that of the Mohr-Coulomb. This was connected to the point that the Mohr-Coulomb criterion neglects the effect of intermediate principal stress on failure prediction. The safe operating mud weight window in the Zubair Formation for inclinations higher than 40° is relatively narrow. When drilling highly deviated wells (i.e., with an inclination above 60°), which is more challenging in terms of hole cleaning and tripping, the preferred orientation is along the minimum horizontal stress (140°). This orientation will provide a comparatively wider mud weight window for stable drilling. In addition, surge and swab should be avoided while drilling these highly deviated wells. Ultimately, good drilling practices, such as good hole cleaning, monitoring tripping speed, proper mud conditioning, and controlling the ROP while increasing the inclination in a shale formation will help to mitigate wellbore instability-related issues while drilling. For designing future complex trajectories and/or multilateral across different zones of the Zubair Formation, it is highly recommended to construct a robust 3D-MEM based on the elements of this study. This will allow a greater integration with the formation's structural geological model; consequently, a 3D-MEM will provide better wellbore stability predictions.

ACKNOWLEDGMENTS

The authors of this article would like to express their gratitude to Basrah Oil Company and Iraqi Drilling Company for their supporting and allowing the publication of this study.

REFERENCES

- Aadnoy, B. S, and Looyeh, R., 2011. *Petroleum Rock Mechanics Drilling Operations and Well Design*. first ed. Oxford: Gulf Professional Pub.
- Aadnoy, B.S., 1989. Stresses Around Horizontal Boreholes Drilled in Sedimentary Rocks. *J. Pet. Sci. Eng.* 2 (4), pp. 349–360. [https://doi.org/10.1016/0920-4105\(89\)90009-0](https://doi.org/10.1016/0920-4105(89)90009-0).
- Abbas, A. K., Al-Hamad, N., and Alsaba, M., 2018b. Enhancing Rock Mechanical Properties Estimation for Thin Beds Using Microresistivity Borehole Imaging Tool. Abu Dhabi International Petroleum Exhibition & Conference, Abu Dhabi, UAE, November 12-15, Paper No. SPE-193143-MS. <http://dx.doi.org/10.2118/193143-ms>.
- Abbas, A. K., Dahm, H. H., Flori, R. E., and Alsaba, M., 2018. Laboratory Measurements of Petrophysical and Geomechanical Properties for Zubair Sandstone Formation in Southern Iraq. 52nd US Rock Mechanics/Geomechanics Symposium (ARMA), Seattle, Washington, USA, June 17–20, Paper No. ARMA 18–243.
- Abbas, A. K., Flori, R. E, and Alsaba, M., 2018c. Estimating Rock Mechanical Properties of the Zubair Shale Formation Using A Sonic Wireline Log and Core Analysis. *J. Nal. Gas Sci. Eng.* 53, pp. 359–369. <https://doi.org/10.1016/j.jngse.2018.03.018>.
- Abbas, A. K., Flori, R. E., AL-Anssari, A., and Alsaba, M., 2018a. Laboratory Analysis to Assess Shale Stability for the Zubair Formation, Southern Iraq. *J. Nal. Gas Sci. Eng.* 56, pp.315–323. <https://doi.org/10.1016/j.jngse.2018.05.041>.
- Abbas, A. K., Flori, R. E., Alsaba M., Dahm, H., and Alkamil, E.H., 2018d. Integrated Approach Using Core Analysis and Wireline Measurement to Estimate Rock Mechanical Properties of the Zubair Reservoir, Southern Iraq. *J. Pet. Sci. Eng.* 166, pp. 406–419. <https://doi.org/10.1016/j.petrol.2018.03.057>.

- Abbas, A. K., Flori, R. E., and Alsaba, M., 2018. Laboratory Geomechanical Characterization of the Zubair Shale Formation. 52nd US Rock Mechanics/Geomechanics Symposium (ARMA), Seattle, Washington, USA, June 17–20, Paper No. ARMA 18– 78.
- Ahmed, M., Al-Shehri, H. A., Haidary, S. A., and Povstyanova, M., 2016. A Comprehensive Geomechanical Study to Understand Drilling Challenges in the Manifa field offshore, Saudi Arabia. Kingdom of Saudi Arabia Annual Technical Symposium and Exhibition, Dammam, Saudi Arabia, April 25–28, Paper No. SPE-182833-MS. <https://doi.org/10.2118/182833-ms>.
- Al Dushaishi, M. F., Nygaard, R., and Stutts, D. S., 2017. An Analysis of Common Drill Stem Vibration Models. *ASME J. Energy Resour. Technol.*, 140(1), p. 012905. <http://dx.doi.org/10.1115/1.4037682>.
- Al-Ajmi, A. M., and Zimmerman, R. W., 2006. Stability Analysis of Vertical Boreholes Using the Mogi-Coulomb Failure Criterion. *Int. J. Rock Mech. Min. Sci.* 43 (8), pp. 1200–1211. <http://dx.doi.org/10.1016/j.ijrmms.2006.04.001>.
- Al-Ajmi, A. M., and Zimmerman, R. W., 2009. A New Well Path Optimization Model for Increased Mechanical Borehole Stability. *J. Pet. Sci. Eng.* 69 (1–2), pp. 53–62. <http://dx.doi.org/10.1016/j.petrol.2009.05.018>.
- Al-Ajmi, A. M., and Zimmerman, R.W., 2006. A New 3D Stability Model for the Design of Non-Vertical Wellbores. 41st U.S. Symposium on Rock Mechanics (USRMS), Golden, Colorado, June 17–21, Paper No. ARMA-06-961.
- Al-Ajmi, A.M., and Zimmerman, R.W., 2005. Relation Between the Mogi and the Coulomb Failure Criteria. *Int. J. Rock Mech. Min. Sci.* 42 (3), pp. 431–439. <http://dx.doi.org/10.1016/j.ijrmms.2004.11.004>.
- Anderson, R., Ingram, D., and Zanier, A., 1973, Determining Fracture Pressure Gradients from Well Logs. *J. Petrol. Tech.* 25 (11), pp. 1259–1268. <http://dx.doi.org/10.2118/4135-pa>.
- Aslannezhad, M., Khaksar, A., and Jalalifar, H., 2015. Determination of A Safe Mud Window and Analysis of Wellbore Stability to Minimize Drilling Challenges and Non-productive Time. *J. Pet. Expl. Prod. Tech.* 6 (3), pp. 493–503. <http://dx.doi.org/10.1007/s13202-015-0198-2>.
- Bradley, W. B., 1979. Failure in Inclined Boreholes. *Trans. ASME J. Energy Resour. Technol.*, 101, pp. 232–239. <http://dx.doi.org/10.1115/1.3446925>.

- Cao, C., Pu, X., Zhao, Z., Wang, G., and Du, H., 2018. Experimental Investigation on Wellbore Strengthening Based on a Hydraulic Fracturing Apparatus. *ASME J. Energy Resour. Technol.*, 140 (5), p. 052902. <http://dx.doi.org/10.1115/1.4038381>.
- Chabook, M., Al-Ajmi, A., and Isaev, V., 2015. The Role of Rock Strength Criteria in Wellbore Stability and Trajectory Optimization. *Int. J. Rock Mech. Min. Sci.* 80, pp. 373–378. <http://dx.doi.org/10.1016/j.ijrmms.2015.10.003>.
- Chen, X., Gao, D., Yang, J., Luo, M., Feng, Y., and Li, X., 2018. A Comprehensive Wellbore Stability Model Considering Poroelastic and Thermal Effects for Inclined Wellbores in Deepwater Drilling. *ASME J. Energy Resour. Technol.* 140 (9), pp. 092903. <https://doi.org/10.1115/1.4039983>.
- Chen, X., Tan, C., and Detournay, C., 2003. A study on Wellbore Stability in Fractured Rock Masses with Impact of Mud Infiltration. *J. Pet. Sci. Eng.* 38 (3–4), pp.145–154. [http://dx.doi.org/10.1016/s0920-4105\(03\)00028-7](http://dx.doi.org/10.1016/s0920-4105(03)00028-7).
- Chuanliang, Y., Jingen, D., Xiangdong, L., Xiaorong, L., and Yongcun, F., 2015. Borehole Stability Analysis in Deepwater Shallow Sediments. *ASME J. Energy Resour. Technol.*, 137(1), p. 012901. <http://dx.doi.org/10.1115/1.4027564>.
- Colmenares, L., and Zoback, M., 2002. A Statistical Evaluation of Intact Rock Failure Criteria Constrained by Polyaxial Test Data for Five Different Rocks. *Inter. J. Rock Mech. Min. Sci.* 39 (6), pp. 695-729. [http://dx.doi.org/10.1016/s1365-1609\(02\)00048-5](http://dx.doi.org/10.1016/s1365-1609(02)00048-5).
- Dokhani, V., Yu, M., Miska, S. Z., and Bloys, J., 2015. The Effects of Anisotropic Transport Coefficients on Pore Pressure in Shale Formations. *ASME J. Energy Resour. Technol.*, 137 (3), p. 032905. <http://dx.doi.org/10.1115/1.4029411>.
- Eaton, B. A., 1969. Fracture Gradient Prediction and Its Application in Oilfield Operations. *J. Petrol. Tech.* 21 (10): pp.1353–1360. <http://dx.doi.org/10.2118/2163-pa>.
- Gholami, R., Aadnoy, B., Foon, L. Y., and Elochukwu, H., 2017. A Methodology for Wellbore Stability Analysis in Anisotropic Formations: A Case Study from the Canning Basin, Western Australia. *J. Nal. Gas Sci. Eng.* 37, pp. 341–360. <http://dx.doi.org/10.1016/j.jngse.2016.11.055>.
- Gholami, R., Rabiei, M., Aadnoy, B., and Rasouli, V., 2017. A Methodology for Wellbore Stability Analysis of Drilling into Presalt formations: A Case Study from Southern Iran. *J. Pet. Sci. Eng.* 167, pp. 249–261. <http://dx.doi.org/10.1016/j.petrol.2017.11.023>.

- Gholami, R., Rabiei, M., Rasouli, V., Aadnoy, B., and Fakhari, N., 2015. Application of Quantitative Risk Assessment in Wellbore Stability Analysis. *J. Pet. Sci. Eng.* 135, pp. 185–200. <http://dx.doi.org/10.1016/j.petrol.2015.09.013>.
- Jaeger, J. C., Cook, N. G., and Zimmerman, R. W., 2007. *Fundamentals of Rock Mechanics*. fourth ed. Hoboken, NJ: Wiley-Blackwell.
- Jassim, S. Z., and Goff, J. C., 2006. *Geology of Iraq*. first ed. Brno and Prague, Czech Republic: Dolin and Moravian Museum.
- Jingbin, L., Guangqing, Z., Gensheng, L., Zhongwei, H., and Weichang, L., 2018. A Method to Double the Extension Ability of Radial Jet Drilling Technology. *ASME J. Energy Resour. Technol.*, 140(9), p. 093102. <http://dx.doi.org/10.1115/1.4039977>.
- Kamel, M. A., Elkatatny, S., Mysorewala, M. F., Al-Majed, A., and Elshafei, M., 2017. Adaptive and Real-Time Optimal Control of Stick–Slip and Bit Wear in Autonomous Rotary Steerable Drilling. *ASME J. Energy Resour. Technol.*, 140(3), p. 032908. <https://doi.org/10.1115/1.4038131>.
- Khan, K., Abdulaziz, A.A., Ahmed, S., and Ahmed, M., 2015. Managing Wellbore Instability in Horizontal Wells through Integrated Geomechanics Solutions: A Case Study from A Carbonate Reservoir. Middle East Oil & Gas Show and Conference, Manama, Bahrain, March 8–11, Paper No. SPE-172550-MS. <http://dx.doi.org/10.2118/172550-ms>.
- Kidambi, T., and Kumar, G. S., 2016. Mechanical Earth Modeling for A Vertical Well Drilled in A Naturally Fractured Tight Carbonate Gas Reservoir in the Persian Gulf. *J. Petrol. Sci. Eng.* 141, pp. 38–51. <http://dx.doi.org/10.1016/j.petrol.2016.01.003>.
- Kingdon, A., Fellgett, M. W., and Williams, J. D., 2016. Use of Borehole Imaging to Improve Understanding of the In-Situ Stress Orientation of Central and Northern England and Its Implications for Unconventional Hydrocarbon Resources. *Mar. Pet. Geol.* 73, pp. 1–20. <http://dx.doi.org/10.1016/j.marpetgeo.2016.02.012>.
- Kiran, R., and Salehi, S., 2016. Thermoporoelastic Modeling of Time-Dependent Wellbore Strengthening and Casing Smear. *ASME J. Energy Resour. Technol.*, 139(2), p. 022903. <https://doi.org/10.1115/1.4033591>.
- Mahmoud, M., Bageri, B. S., Elkatatny, S., and Al-Mutairi, S. H., 2017. Modeling of Filter Cake Composition in Maximum Reservoir Contact and Extended Reach Horizontal Wells in Sandstone Reservoirs. *ASME J. Energy Resour. Technol.*, 139(3), p. 032904. <https://doi.org/10.1115/1.4035022>.

- Maleki, S., Gholami, R., Rasouli, V., Moradzadeh, A., Riabi, R.G., and Sadaghzadeh, F., 2014. Comparison of Different Failure Criteria in Prediction of Safe Mud Weigh Window in Drilling Practice. *Earth Sci. Rev.* 136, pp. 36–58. <http://dx.doi.org/10.1016/j.earscirev.2014.05.010>.
- Mansourizadeh, M., Jamshidian, M., Bazargan, P., and Mohammadzadeh, O., 2016. Wellbore Stability Analysis and Breakout Pressure Prediction in Vertical and Deviated Boreholes Using Failure Criteria – A Case Study. *J. Pet. Sci. Eng.* 145, pp. 482–492. <http://dx.doi.org/10.1016/j.petrol.2016.06.024>.
- Mohammed, H. Q., Abbas, A. K., and Dahm, H. H., 2018. Wellbore Instability Analysis for Nahr Umr Formation in Southern Iraq. 52nd US Rock Mechanics/Geomechanics Symposium (ARMA), Seattle, Washington, June 17-20, Paper No. ARMA 18–916.
- Mohiuddin, M., Khan, K., Abdulraheem, A., Al-Majed, A., and Awal, M., 2007. Analysis of Wellbore Instability in Vertical, Directional, and Horizontal Wells Using Field Data. *J. Pet. Sci. Eng.* 55 (1–2), pp. 83–92. <http://dx.doi.org/10.1016/j.petrol.2006.04.021>.
- Najibi, A. R., Ghafoori, M., Lashkaripour, G. R., and Asef, M. R., 2017. Reservoir Geomechanical Modeling: In-Situ Stress, Pore Pressure, and Mud Design. *J. Pet. Sci. Eng.* 151, pp. 31–39. <http://dx.doi.org/10.1016/j.petrol.2017.01.045>.
- Nes, O., Fjær, E., Tronvoll, J., Kristiansen, T. G., and Horsrud, P., 2012. Drilling Time Reduction Through an Integrated Rock Mechanics Analysis. *ASME J. of Energy Resour. Technol.*, 134(3), p. 032802. <https://doi.org/10.1115/1.4006866>.
- Rahimi, R., and Nygaard, R., 2015. Comparison of Rock Failure Criteria in Predicting Borehole Shear Failure. *Inter. J. Rock Mech. Min. Sci.* 79, pp. 29–40. <http://dx.doi.org/10.1016/j.ijrmms.2015.08.006>.
- Rahman, M. K., Chen, Z., and Rahman, S. S., 2003. Modeling Time-Dependent Pore Pressure Due to Capillary and Chemical Potential Effects and Resulting Wellbore Stability in Shales. *ASME J. Energy Resour. Technol.*, 125(3), pp. 169–176. <http://dx.doi.org/10.1115/1.1595111>.
- Rasouli, V., Pallikathakathil, Z. J., and Mawuli, E., 2011. The Influence of Perturbed Stresses Near Faults on Drilling Strategy: A Case Study in Blacktip field, North Australia. *J. Pet. Sci. Eng.* 76 (1–2), pp. 37–50. <http://dx.doi.org/10.1016/j.petrol.2010.12.003>.

- Salehi, S., and Nygaard, R., 2014. Full Fluid–Solid Cohesive Finite-Element Model to Simulate Near Wellbore Fractures. *ASME J. Energy Resour. Technol.*, 137(1), p. 012903. <https://doi.org/10.1115/1.4028251>.
- Taleghani, A. D., and Klimenko, D., 2015. An Analytical Solution for Microannulus Cracks Developed Around a Wellbore. *ASME J. Energy Resour. Technol.*, 137(6), p. 062901. <https://doi.org/10.1115/1.4030627>.
- Thiercelin, M., and Plumb, R., 1994. A Core-Based Prediction of Lithologic Stress Contrasts in East Texas Formations. *SPE Form. Eval.* 9 (04), pp. 251–258. <http://dx.doi.org/10.2118/21847-pa>.
- Tingay, M., Reinecker, J., and Müller, B., 2008. Borehole Breakout and Drilling-Induced Fracture Analysis from Image Logs. World Stress Map Project. http://dc-app3-14.gfz_potsdam.de/pub/guidelines/WSM_analysis_guideline_breakout_image.pdf (accessed 23 April 2018).
- Wang, X., Ni, H., Wang, R., Zhang, L., and Wang, P., 2018. Drag-Reduction and Resonance Problems of a Jointed Drillstring in the Presence of an Axial Excitation Tool. *ASME J. Energy Resour. Technol.*, 141(3), p. 032904. <http://dx.doi.org/10.1115/1.4041155>.
- Wiprut, D., and Zoback, M., 2000. Constraining the Stress Tensor in the Visund Field, Norwegian North Sea: Application to Wellbore Stability and Sand Production. *Inter. J. Rock Mech. Min. Sci.* 37 (1–2), pp.317–336. [http://dx.doi.org/10.1016/s1365-1609\(99\)00109-4](http://dx.doi.org/10.1016/s1365-1609(99)00109-4).
- Zhang, J., 2011. Pore Pressure Prediction from Well Logs: Methods, Modifications, and New Approaches. *Earth Sci. Rev.* 108 (1–2), pp. 50–63. <http://dx.doi.org/10.1016/j.earscirev.2011.06.001>.
- Zhang, Q., Wang, Z., Wang, X., and Yang, J., 2014. A New Comprehensive Model for Predicting the Pressure Drop of Flow in the Horizontal Wellbore. *ASME J. Energy Resour. Technol.*, 136(4), p. 042903. <http://dx.doi.org/10.1115/1.4027572>.
- Zhang, Q., Wang, Z., Wang, X., and Yang, J., 2014. A New Comprehensive Model for Predicting the Pressure Drop of Flow in the Horizontal Wellbore. *ASME J. Energy Resour. Technol.*, 136 (4), p. 042903. <http://dx.doi.org/10.1115/1.4027572>.
- Zhang, Z., Xiong, Y., and Guo, F., 2018. Analysis of Wellbore Temperature Distribution and Influencing Factors During Drilling Horizontal Wells. *ASME J. Energy Resour. Technol.*, 140(9), p. 092901. <http://dx.doi.org/10.1115/1.4039744>.

Zoback, M. D., 2007. *Reservoir Geomechanics*. first ed. Cambridge: Cambridge University Press.

Zoback, M. D., Barton, C. A., Brudy, M., Castillo, D. A., Finkbeiner, T., Grollimund, B. R., Moos, D. B., Peska, P., Ward, C. D., and Wiprut, D. J., 2003. Determination of Stress Orientation and Magnitude in Deep Wells. *Int. J. Rock Mech. Min. Sci.* 40 (7–8), pp. 1049–1076. <http://dx.doi.org/10.1016/j.ijrmms.2003.07.001>.

Zoback, M. D., Moos, D., Mastin, L., and Anderson, R. N., 1985. Well Bore Breakouts and In Situ Stress *J. Geophys Res: Solid Earth* 90 (B7), pp. 5523–5530. <http://dx.doi.org/10.1029/jb090ib07p05523>.

IV. LABORATORY ANALYSIS TO ASSESS SHALE STABILITY FOR THE ZUBAIR FORMATION, SOUTHERN IRAQ

Ahmed K. Abbas, Ralph Flori, and Mortadha Alsaba

Department of Petroleum Engineering Engineering, Missouri University of Science and Technology, Rolla, MO 65409

ABSTRACT

The Zubair Formation consists of approximately 55% shale, which causes almost 70% of wellbore problems due to incompatibilities between drilling fluids and shale formations. The most common and effective solution to shale instability is through the design and selection of appropriate drilling fluids. Understanding the interaction between drilling fluids and shale has been a challenge due to the complexity of both the physical and chemical variations in shale formations. This paper presents some of the primary laboratory and wellsite testing techniques that are often used by mud engineers to characterize and remediate drilling fluids and shale interactions. Well-preserved core samples retrieved from the Zubair shale formation in Southern Iraq were run through extensive testing to describe the special characterization of the Zubair shale. These characteristics were measured and described, including the structure, texture, mineralogy, and reactivity, using a scanning electron microscope (SEM), a thin-section photograph, X-ray diffraction analysis (XRD) imaging, and cation exchange capacity (CEC) analysis. Moreover, a capillary suction timer (CST), hot rolling dispersion test, bulk hardness test, linear swell meter (LSM), and fracture development test were used to evaluate the stability of shale in the presence of test fluids. The test fluids included fresh water, 20 wt% NaCl

brine, 7 wt% KCl brine, and a combination of 7 wt% KCl and 3 vol% glycol. The results illustrated that the Zubair shale is composed mainly (average content of 51.46%) of brittle minerals (i.e., quartz and calcite), along with 43.54% of clay minerals. The predominant clay minerals were kaolinite and illite, with an average content of 48.06% and 34.71%, respectively. In addition, the cation exchange capacity analysis and capillary suction time test indicated that Zubair shale has a low-to-moderate reactivity with drilling fluids. Furthermore, among the fluid systems tested, the best shale inhibition was achieved when the 7 wt% KCl and 3 vol% glycol solution was used. Shale sample analyses methods were used to understand the geologic features of the Zubair shale formations and to achieve a better perspective on the potential interactions of shale formations with drilling fluids. Understanding the properties and responses of shale formations to fluids is a significant step in achieving the chemical clay stabilization objectives. Proper design of drilling fluids, with appropriate mud weight and suitable additives, can lead to substantial cost reduction in drilling operations.

1. INTRODUCTION

Wellbore instability is frequently reported as one of the most serious obstructions during drilling in the Zubair shale formation in several oil and natural gas fields in Southern Iraq (Abbas et al., 2018a). Wellbore instability problems (e.g., wellbore collapse, tight hole, stuck pipe and logging tools, poor log quality, wellbore enlargement, and poor primary cement jobs) result in excessive operational costs and delays in drilling time (Mohiuddin et al., 2007; Ferreira et al., 2016). These problems are generally caused by the

imbalance created between the wellbore stress and rock strength (Lal, 1999). This usually happens when the wellbore stress exceeds the strength of weaker rocks, such as shale. In addition, drilling fluids can cause shale instability by altering the pore pressure or effective stress state and the shale strength through fluid/shale interactions (Xu et al., 2018). The mud density and chemistry invariably play major roles in solving wellbore instability problems. The minimum required mud weights to drill a stable well are often selected based on geomechanical wellbore stability modeling studies, while the mud type and chemistry are selected based on a laboratory evaluation of the drilling fluids performance (Jain and Mahto, 2017). Addressing the optimum drilling fluids chemistry and formulations requires a set of laboratory tests that evaluate the shale/fluid interaction and shale stability (Temraz and Hassanien, 2016; Li et al., 2017). Nevertheless, the behavior and responses of shale to the drilling and completion fluids are complex and were not well understood for many years because of the various and complex chemical and physical variations present in these type of formations (Van Oort, 2003). A complicating factor that distinguishes shale from other rocks is its sensitivity to fluids, particularly water, because of its large surface area and consequential strong adsorption capacity (Tang et al., 2014). Shale stability is strongly affected by shale characterizations (e.g., wettability, mineralogy, structure, texture, and reactivity with fluids) and the properties of the drilling fluid it contacts (e.g., density, salinity, and ionic concentration) (Shen et al., 2016; Villabona-Estupiñán et al., 2017). For these reasons, the interaction of shale with drilling fluid is not entirely understood, and drilling optimization is often approached on a trial-and-error basis. Therefore, shale characterization can help to understand the different responses of the shale to fluids and

improve the selection of chemical additives to minimize or delay the shale/fluid interaction (Huang and Zhao, 2017).

Obtaining the representative preserved core samples is a critical step in deciding on the proper drilling and completion fluids. Shale formations are not the main target of hydrocarbon exploration; therefore, shale samples from deep boreholes are almost never available for testing due to the extra cost related to coring operations in deep wellbores. Even if core samples are taken from depths of interest, shale cores may be further damaged by the action of the drill bit during coring operations and by subsequent improper preservation and sample preparation. This may affect shale properties significantly and make core samples useless for fluid/shale interaction analysis (Al-Bazali, 2011). It is well known that the use of well-preserved shale core samples will provide highly accurate and reliable laboratory test results, which can help to assess shale reactivity with drilling fluids. In addition, the preserved shale core samples tend to maintain their natural wettability, so that the fracture network is conserved and less likely to be altered by the natural drying process.

Due to the severity of shale instability while drilling in the Zubair shale section, field owners and operator companies were motivated to core and test shale core samples to understand the petrologic and deformation features of the Zubair shale formation. In the present work, well-preserved core samples retrieved from the Zubair shale formation in Southern Iraq were fully characterized in terms of structure, mineralogy, and shale reactivity in relation to the drilling fluids. A thin-section photograph and X-ray diffraction (XRD) analysis were applied to understand the mineralogy, texture, grain distribution, and consolidation of the Zubair shale. Scanning electron microscope (SEM) imaging was used

to observe the substructure morphology of the shale. The cation exchange capacity (CEC) analysis was applied to assess the shale reactivity in relation to various drilling fluids. Moreover, shale interaction tests were performed by exposing core fragments to four conventional types of fluids. The capillary suction time test, hot rolling dispersion test, bulk hardness test, linear swelling test, and fracture development test were then used to evaluate the applicability of these fluids. This holistic approach is very effective not only because the actual shale formation can be used for the experiments but also because it can integrate and cover many geological characteristics of the rock samples, including the type of clay, amount of clay, and reactivity.

2. METHODOLOGY

2.1. SHALE SAMPLES

Shales are fine-grained sedimentary rocks that contain a significant amount of clay minerals. In practice, this means that their clay content needs to be higher than about 40% (Fjær et al., 2008). Shale's extremely low permeability, clay content, and sensitivity to fluids make it a very special rock material to study (Chenevert and Sharma, 1993; Zhang et al., 2015). Shale is very sensitive to wetting fluids, such as water, or to a loss of fluid from its pores (Lyu et al., 2015). Van Oort et al. (2016) further clarified these concerns, describing that the natural pore fluid of a poorly preserved shale evaporates from the pore space, which then fills with air. As the shale sample is no longer 100% saturated when it is exposed to atmospheric conditions, special procedures should be applied to prevent the loss of the natural pore fluid. Otherwise, the laboratory testing will not give an accurate

reflection of the actual behaviors of the shale samples in fluids. Therefore, the shale samples that were used in this study were all well-preserved in a metal casing at the point of recovery, and the two ends were sealed with rubber caps to prevent the native pore fluid from being lost after the coring operations. The preserved cores were obtained from three wells, covering a wide range of the Zubair shale formation interval.

2.2. SHALE CHARACTERIZATIONS METHODS

2.2.1. CT Scanning Technique. X-ray computed tomography (CT) is a technique that allows visualization of the internal structure of a scanned object without cutting it. CT operates by using an X-ray generator that rotates around the central axis of the scanned sample. Each of the specimens was scanned at 1-degree increments about the vertical axis for a full 360 degrees. The X-ray detectors are positioned on the opposite side of the circle from the X-ray source. CT images record differences in the degree of attenuation of the X-rays, which is both material and energy-dependent (Choo et al., 2014). CT produces data that can be manipulated to demonstrate various bodily structures based on their ability to absorb the X-ray beam. The CT images generated were in the axial or transverse planes, perpendicular to the long axis of the body sample. The degree of digital image resolution depends mainly on the distance between the camera positioned within the scanning device and the scanned object. In this study, one recovered full diameter core section (~1 m) was scanned by a 2-D computed tomography (CT) scanner to examine the initial sample conditions and evaluate the presence of any preexisting (i.e., natural) fractures and/or mechanical damage caused by drilling and the coring processes. The CT scan was performed in two main parts: longitudinal (i.e., vertical) and axial. Five axial images

(slices) were selected (at 20-cm intervals) to cover the internal features of the shale core samples.

2.2.2. Scanning Electron Microscope (SEM). A shale sample from the Zubair Formation was imaged using an SEM to determine the integrity of the rock and measure the degree of cementing and compaction, using a clean sample mounted on the specimen stage and placed into the instrument. SEM photographs allow for better 3-D observations of micro-cracks and micro-laminations in the specimen that are not easily seen using transmitted light or transmitted electron microscope techniques. The texture and orientation of the shale, its degree of compaction, and the presence of embedded minerals and pores can be observed (Stephens et al., 2009). SEM images of a specimen were produced by scanning the surface with a focused beam of electrons. These electrons interact with atoms in the specimen, producing various signals that contain data about the specimen's surface topography and composition. For SEM, a specimen needs to be completely dry and large enough to withstand the vacuum conditions and high-energy beam of electrons. Magnification in a scanning electron microscope can be controlled over a range of about six orders of magnitude from about 10 to 1,000,000 times. The magnification ranges that were used for shale analyses ranged from 100 to 500x.

2.2.3. Thin-Section Analysis. A petrographic analysis was carried out to provide a detailed description of the texture (i.e., grain size, sorting, and grain contacts), sedimentary structures (i.e., laminations and bioturbation), framework grain composition, authigenic minerals, and types and distribution of macroporosity seen in a thin section. Thin-sectioning and impregnation procedures are critical to successful petrographic analysis. Thin-section preparation involved vacuum impregnation with a low-viscosity,

blue-dyed resin to facilitate the recognition of porosity as well as staining with a mixed Alizarin Red-S and potassium ferricyanide solution to allow the observation of the carbonate minerals (Kassab et al., 2015). In addition, samples were stained with a sodium cobaltinitrite solution to aid in the identification of alkali feldspars. Thin sections were carefully ground to 30-micron thick sections of rock mounted on a glass slide, to avoid fracturing and plucking. Basic petrographic analysis was performed in transmitted light using a petrographic polarizing microscope. Petrographic analysis of thin sections involves either qualitative description or quantitative estimation of the texture, mineralogy, and porosity.

2.2.4. X-Ray Diffraction (XRD). X-ray diffraction (XRD) analysis was performed on the Zubair shale sample. The shale samples were initially milled in methanol to a particle size of less than 10 microns, then filtered and air-dried. Thereafter, each specimen was placed into the X-ray diffractometer and rotated through a series of angles to help homogenize the intensity of the measured X-ray beam. As the specimen was rotated in the X-ray diffractometer, it was being illuminated with a very intense X-ray beam. The crystalline structures of the individual minerals in the sample diffract the X-ray beam. This results in an X-ray diffraction pattern that is unique for each mineral in the sample (Stephens et al., 2009). The computer automates the data collection and data reduction steps of the analysis. To obtain a semiquantitative measurement of the mineral components of a given sample, the maximum intensity of each identified mineral was measured and compared to the standard intensity obtained from a pure mineral sample.

2.2.5. Cation Exchange Capacity (CEC). The cation exchange capacity (CEC) is a measure of the exchangeable cations present in clay minerals in a shale sample, which is

a crucial method for assessing shale reactivity in relation to drilling fluids. Usually, some cations (i.e., positively charged ions) of clays are easily replaced by other cations present in the suspension, when those clays are part of aqueous suspensions (Garcia et al., 2013). Most of the exchangeable ions in shale samples are from smectite, while the exchange ions are sodium, calcium, magnesium, iron, and potassium. This exchange occurs because these exchangeable cations are not as compatible with the negatively charged clay particles. As more cations are replaced, there will be more interaction between clays and the suspension. Thus, this capacity of exchanging cations is an indicator of the reactivity level, and it is closely related to the content of highly reactive clay minerals. Finely ground dried shale samples were used to perform this test according to the American Petroleum Institute (API)-recommended methylene blue test (MBT) (API 2004). The shale sample was dispersed in distilled water and mixed by a magnetic stirrer for 5 min. After that, the sample was titrated with a methylene blue solution to saturate the active clay particles. The endpoint of the test was reached when a drop of the sample suspension placed on a filter paper resulted in a faint blue halo surrounding the dyed solids.

2.3. FLUIDS AND SHALE INTERACTIONS

2.3.1. Preparation Of Test Fluids. Test fluid selection and preparation are essential steps in the design of fluid and shale interaction laboratory tests. Selecting the shale inhibitors for the testing program is a process that depends on many factors, such as shale characteristics and drilling environments (e.g., high temperature and high pressure) (Villada et al., 2017). Simple inorganic salts, such as sodium chloride (NaCl) and potassium chloride (KCl), are relatively inexpensive and most widely used as shale

inhibitors. Also, they are chemically very stable, so they can be applied in a variety of drilling environments and in a wide range of pH conditions (Gomez and Patel, 2013). However, the presence of these salts in large quantities in the drilling fluids may adversely affect the rheology, filtration control, and the chemical biological ecosystems (Zhong et al., 2011; Akhtarmanesh et al., 2013). The concentrations of salts between 2 and 37wt% are frequently recommended in treating fluids to minimize the swelling of clays (Gomez et al., 2013). In general, increasing the percentages of salt concentrations will lead to reduce the amount of water that can be absorbed by increasing in yield point (YP), plastic viscosity (PV) and mud weight.

A variety of organic additives, such as glycol, in combination with KCl shows a higher performance of shale inhibiting as compared to KCl alone (Abbas et al., 2018b). However, organic shale inhibitors alone offered little success in providing the satisfactory results (Patel et al., 2007). The glycol will also significantly affect the rheology of drilling fluid when the concentration is high (Zhao et al., 2017a).

In this study, three fluid systems and fresh water were used to evaluate the interaction of the Zubair shale core samples with each fluid. Two of these fluid systems were composed of distilled water with KCl (7 wt%) and distilled water with NaCl (20 wt%), while the third system was composed of distilled water with KCl (7 wt%) and glycol (3 vol%). These concentrations of salts and glycol were selected based on the reactivity of Zubair shale formation (Berry et al., 2008).

2.3.2. Capillary Suction Time (CST) Test. This method measures the time required for a slurry filtrate to travel a given distance on thick, porous filter paper (Wilcox et al., 1987). This technique simulates the manner in which free water in water-based fluid

penetrates into the formation under the capillary suction pressure of a porous filter cake. The CST test studies the inhibition performances of additives (by the time of filtration) to characterize the shale inhibitor and thereby minimize its effect on shale formation.

A small amount of dry shale (30 g) was ground and screened using a 100-mesh sieve. The shale samples were mixed with 250 mL of the test fluid in a small commercial blender cup, creating a colloidal suspension. Then, 250 mL of the colloidal suspension was allowed to hydrate for 15 min, and a 1-mL sample was withdrawn to perform the CST test. The rate at which the filtrate spread away from the suspension is controlled predominantly by the filterability of the suspension. The time was measured in seconds, using a stopwatch, as the filtrate advanced between radially separated electrodes when a fixed area of special filter paper was exposed to the suspension. Because the repeatability of this method is poor, the CST test was performed three times, and the CST values were reported as an average of these three readings. A longer time of capillary suction indicates a higher reactivity of the shale sample to the test fluid. The same test procedure was repeated for all the test fluids.

2.3.3. Hot Rolling Dispersion Test. The hot rolling dispersion test is used to simulate the action of shale formation cuttings being circulated up the borehole annulus during the drilling process. The test is implemented to assess the effectiveness of inhibitor additives to maintain the integrity of the cuttings and minimize the interaction of drilling fluids with the shale formation during the drilling and completion operations (Xu et al., 2017). The fluids that provide a higher level of recovery are thought to minimize the uptake of water by the shale samples, which protects against shale dispersion (Zhong et al., 2015).

The dispersion test procedure was adopted by the API as part of its drilling fluid test criteria (API 1997). In the current student, the test was performed by exposing 50 g of the collected dry shale sample seized through 6–10 mesh (using standard sieves) to one laboratory barrel equivalent (350 mL) of the mentioned fluids in a conventional roller oven cell. The fluid and shale samples were rolled together in a roller oven for 16 hours at 150°C. This provided a long-term exposure of the shale to the fluid under mild agitation conditions. Under such conditions, dispersion of the shale pieces into the fluid occurs depending on the tendency of the shale to disperse and the inhibitive properties of the fluid. After being cooled to room temperature, the fluid was poured over a 20-mesh sieve, and the retained shale pieces were recovered and washed gently with distilled water to remove the excess fluid. The recovered shale sample was dried in an oven at 110°C until a constant sample weight was reached. The dry shale sample was weighed to determine the percentage recovery of the shale using the following equation:

$$R(\%) = (W_1 / W_2) \times 100 \quad (1)$$

where R is the percentage recovery of the shale (%), W_1 is the weight of the recovered dry shale (g), and W_2 is the initial weight of the dry shale (50 g). The greater the R , the better the inhibition performance of the tested sample. This procedure was repeated three times for each test fluid, and the average values were reported.

2.3.4. Bulk Hardness Test. This method is designed to evaluate the relative hardness of a shale sample after exposure to drilling fluids. Shale that interacts with the drilling fluids will become softer after absorbing water from the fluids. Therefore, the continued hardness of the shale can be related to the effectiveness of the shale inhibitor in reducing the clay's tendency to absorb water from the aqueous environment of the drilling

fluids (Mehtar et al., 2010). The bulk hardness test typically gives greater information on the relative levels of hydration suppression of the fluid being evaluated (Friedheim et al., 2011).

In this test, a 50-g dry shale sample (screened by a 6-10 mesh sieve) was added to 350 mL of each test fluid in a conventional roller oven cell. Then, the fluid and shale samples were hot rolled and recovered in a manner similar to the one used in the hot roll dispersion test. After that, the recovered shale samples were placed into the bulk hardness tester. By rotating the torque wrench at a steady rate, the shale was extruded through a perforated steel plate that permits measuring the maximum torque value indicated during each revolution. The force required for extrusion was reported as bulk hardness. Highly efficient shale inhibitor additives yield harder shale cuttings, which is indicated by higher torque readings.

2.3.5. Linear Swell Meter (LSM) Tests. The swelling test specifically measures the hydration or dehydration tendency of shale samples when exposed to drilling fluids, and it is certainly the most appropriate technique when the rock samples have a significant amount of swelling clays (Beg et al., 2018). The amount of swelling the shale undergoes after it is in contact with the fluid is a measure of the reactivity of the shale to the fluid (Stephens et al., 2009).

Prior to this test, shale samples were first ground into powder. This shale powder was prepared in a cylindrical shape (pellet) with a diameter of 25.4 mm by hydraulic compressing under 1,500 psi for 30 min. The initial thickness of the pellet was measured using a Vernier caliper and entered in the computer software. The sample was then placed in the shale chamber that confines the pellet between a pair of screens and confines swelling

to the vertical direction. These compacted shale pellets were immersed in the different fluids to be tested. Once the compacted pellets came in contact with the testing fluid, the pellets absorbed water and swelled vertically. This causes the linear variable differential transformer (LVDT) sensor to rise, which sent data to the computer to calculate the percent of linear expansion during the fluid exposure time. The percentage of the swelling rate was calculated using the ratio of the swelled height to the initial height of the shale pellet. A higher swelling rate indicates a higher potential for hydration and swelling.

2.3.6. Fracture Development Test. The fracture development test (immersion) is a relatively simple technique that can be used to directly observe and evaluate the shale/fluid interactions and the development of fractures in shale formations when they are exposed to fluids (Gomez and He, 2012). This method can reflect the effects of the shale structure on the fracture development in drilling fluids, which, as previously mentioned, traditional test methods cannot always achieve. Sample preparation for the traditional methods is one of the main reasons for this inconsistency. As discussed in the previous sections, the sample preparation involves grinding the shale sample into very small pieces; in some cases, the shale sample is ground into powder and reconstituted as a pellet. Consequently, the sample preparation process would largely remove the influence of the rock structure on fracture development and shale stability by completely destroying the natural structure of the rock.

The fracture development test was performed on core shale fragments, which were exposed to four types of fluids to evaluate the stability of Zubair shale in the presence of the test fluids. The shale core samples were sawed into comparable pieces, approximately equal in size, oriented to show a cross-section of the bedding plane in the same direction

for all the rock pieces. A diamond blade for dry cutting application was used to avoid any contact between the rock and the fluid before testing. The test samples were photographically documented before exposure to the fluids (initial-dry). The samples were then fully immersed in the fluids inside containers for 48 hours at room temperature. After that, the samples were removed from the fluids and allowed to dry for 16 hours at room temperature. Final photographs of the shale samples were taken to record the physical changes during the exposure of these samples to fluids. These observations were recorded to compare quantitatively the effects of the test fluids (e.g., maximum fracture width, number of fractures, and typical fracture width).

3. RESULTS AND DISCUSSION

3.1. SHALE CHARACTERIZATIONS METHODS

3.1.1. Structure. The results of the CT scanner for the core section showed that the core had multiple fractures, mainly parallel to the bedding plane, as shown in Figure 1. Additionally, it could be seen that other small fractures extended perpendicularly and diagonally, connecting multiple fractures that covered a major area of the sample. Some beds and lenses of a different type of rock material (light gray areas, possibly calcite) were observed along the core. The SEM showed that the core sample had a well-consolidated texture of shale as well as micro-cracks and micro-pores, as illustrated in Figure 2. The width of the micro-cracks ranged from 0.5 – 3 μm . Moreover, direct observation of the rock indicated that the shale core sample was fragile and broken mainly around the center

of the core. The fragments from the shale core sample exhibited curved shapes, and a laminated structure was also observed in some of the pieces (Figure 3).

The problems that occur while drilling are often related to the presence of the laminated structure, weak bedding planes, and fractures, which can have a significant impact on the failure behavior of shale. The impact of such shale structures on wellbore instability is closely related to the penetration of the drilling fluids along the fractures. Capillary pressure is a key factor for drilling fluid penetration, which is related to the saturation of the wetting and non-wetting phases. The hydraulic overbalance pressure must be greater than the capillary pressure during drilling fluid penetration. The wetting fluid has a smaller capillary pressure than the non-wetting fluid; therefore, it has a strong potential to penetrate into the fissures and bedding planes compared to the non-wetting fluid (Gomez and He, 2012). In this case, a non-wetting drilling fluid is highly recommended to drill shale formations. In contrast, the effect of the capillary pressure decreases in shale formations with large opening fractures or faults, which provide a channel for drilling fluid penetration. Hence, fluid can flow along the large fractures from high pressure to low pressure. Therefore, appropriate bridging particles and drilling fluid properties may help to minimize the fluid flow along large fractures.

In addition to the traditional bridging particles, other kinds of drilling fluid additives can also seal the pores and retard the pore pressure transmission. For example, a combination of polyalcohol and polyetheramine as an excellent shale stabilizer (Zhao et al., 2017b). Polyalcohol can effectively retard pore pressure transmission and filtrate invasion by sealing the wellbore above the cloud point, while polyetheramine can strongly inhibit shale hydration.

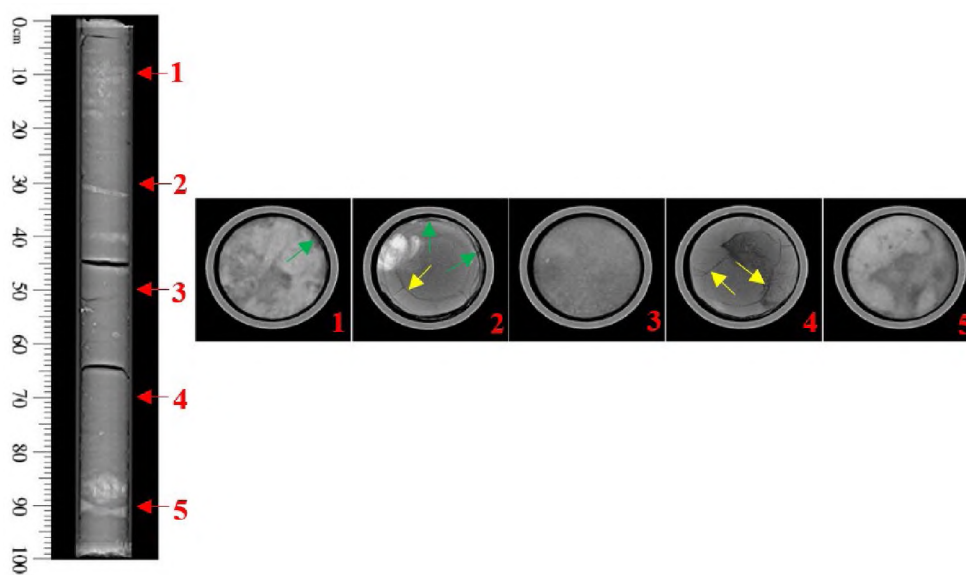


Figure 1. CT scan images for one section of the shale core. The green arrows refer to induced fracture, and the yellow arrows refer to natural open fractures (Abbas et al., 2018c).

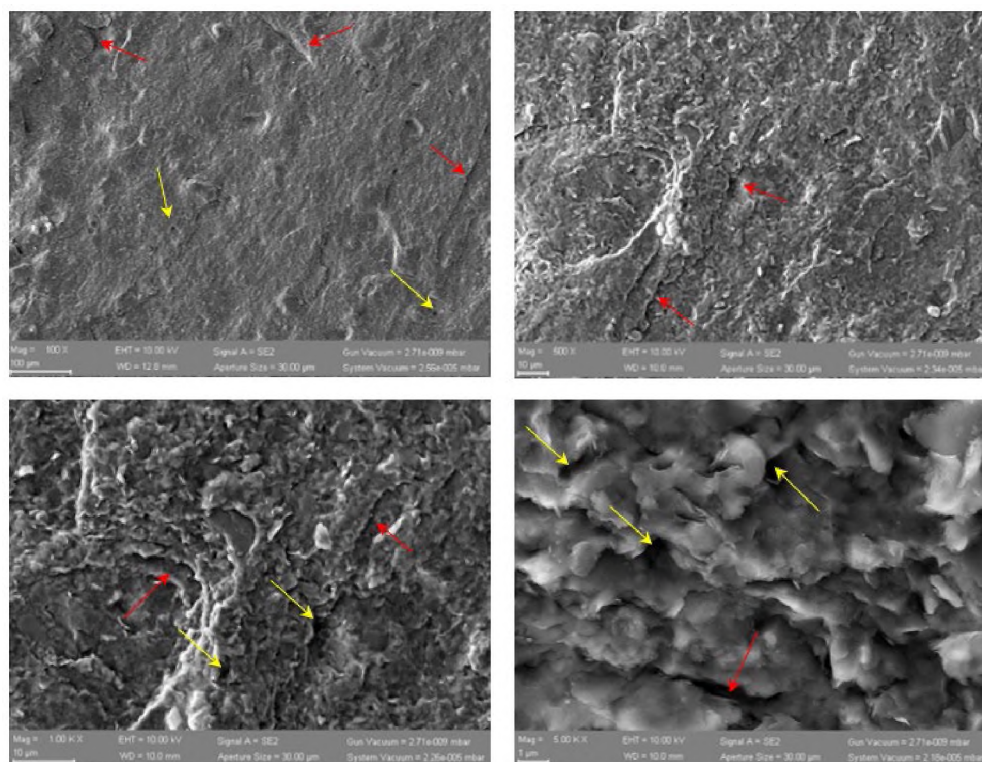


Figure 2. SEM image of Zubair shale specimens. The red arrows refer to micro-cracks, and the yellow arrows refer to micro-pores.



Figure 3. Fragments of the Zubair shale core samples.

3.1.2. Mineralogical Composition and CEC. The Zubair shale samples were subjected to X-ray diffraction (XRD) analysis, and the mineralogical compositions are reported in Table 1. The results of the XRD analysis showed that the shale was composed mainly of brittle minerals (i.e., quartz and calcite) with an average content of 51.46%, and clay minerals with an average content 43.54%. Kaolinite and illite were the predominant clay minerals, with an average content of 48.06% and 34.71%, respectively, as summarized in Table 2. Smectite (including an illite/smectite mixed layer) content was moderate, averaging 14.28%. Smectite has a strong hydration and swelling tendency, while kaolinite and illite do not exhibit significant swelling when they come in contact with water (Aghamelu and Okogbue, 2015). Furthermore, the petrographical characteristics of the Zubair shale sample were illustrated by colored photomicrographs, as shown in Figure 4. It can be seen that the Zubair shale has a moderately laminated structure of well-sorted, silt-grade, sandy mudstone, poorly cemented and weakly-to-moderately compacted. The sample was composed of abundant amounts of pore-filling detrital clays (Dc), common

monocrystalline quartz (Qz), a minor amount of black pyrite crystals (indicated by yellow arrows), white grains (i.e., calcite minerals or quartz), black assemblies (i.e., pyrite or residual hydrocarbons), heavy minerals, kaolinite booklets (K), illite, and chlorite. The thin-section photograph shows that the sample has no visual macroporosity and a few fractures (indicated by blue lines, mostly 5–15 μm wide) that extend mainly along the bedding plane. The cation exchange capacity (CEC) analysis showed that the samples have low-to-moderate reactivity, exhibiting values of 7 to 9 meq/100 g (Table 3).

Based on the results of the mineral composition and CEC analysis, the shale from the Southern Iraq Zubair formation is typically brittle shale and has low-to-moderate hydration. However, the relatively high content of kaolinite and illite could contribute to the structural failure and instability of the rock.

Table 1. X-ray diffraction results for the entire sample analysis.

Sample	Mineral composition (%)				
	Quartz	Pyrite	Calcite	Dolomite	Clay mineral
1	41.74	3.41	6.71	1.32	46.82
2	45.19	5.38	4.62	-	44.81
3	41.68	4.73	9.26	1.81	42.52
4	47.36	2.42	7.15	2.04	41.03
5	42.21	3.87	11.39	-	42.53

Table 2. X-ray diffraction results for the entire sample analysis.

Sample	Clay mineral content (%)			
	Illite/Smectite mixed layer	Illite	Kaolinite	Chlorite
1	14.31	34.03	48.14	3.52
2	13.53	35.11	47.24	4.12
3	8.34	36.73	51.53	3.40
4	15.51	33.26	49.82	1.41
5	19.73	34.41	43.57	2.29

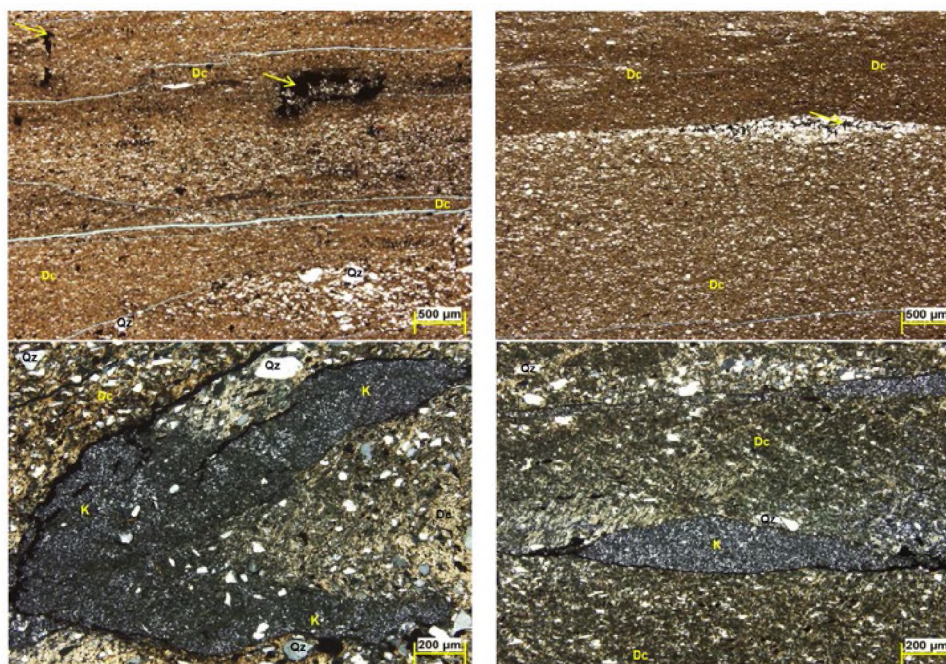


Figure 4. Thin-section plate of the Zubair shale formation.

Table 3. Cation exchange capacity (CEC) results for Zubair shale.

Sample	CEC (meg/100g)
1	8
2	8
3	9
4	7
5	9

3.2. FLUIDS AND SHALE INTERACTION EVALUATION

3.2.1. Capillary Suction Time Test (CST). CST was conducted to measure the effect of additives on the inhibition of shale hydration and dispersion. A less effective shale inhibitor leads to less free water and highly dispersed particles in the dispersion system, giving rise to a relatively impermeable filter cake and a higher CST value. In contrast, a more effective shale inhibitor prevents clay swelling, and in return more free water and

flocculated clay particles occur in the dispersion system, resulting in higher filter cake permeability and a lower CST value (Luo et al., 2017). As can be seen from the results (Figure 5), the CST value of deionized (DI) water without additives (i.e., the reference sample) was 113 seconds, which indicates that Zubair shale particles are low-to-moderately dispersed in deionized water. The CST value of fresh water is only 85 seconds, slightly lower than that of deionized (DI) water, but much higher than that of 7 wt% KCl brine (38 seconds) or 20 wt% NaCl brine (35 seconds). The combination of 7 wt% KCl with 3 vol% glycol gave a slightly better performance (31 seconds) than 7 wt% KCl brine and 20 wt% NaCl brine. These experimental results demonstrate that the Zubair shale sample would fall into a classification of low-to-moderate reactivity. It also indicates that the introduction of cations, either sodium or potassium, greatly reduced the dispersive tendency of the clay. Furthermore, the results show that the combination of 7 wt% KCl and 3 vol% glycol performed as an excellent shale inhibitor.

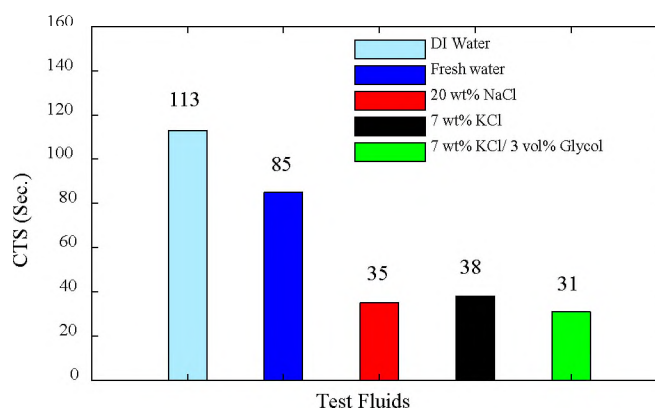


Figure 5. CST test results of the base fluid with and without different inhibitors, using Zubair shale.

3.2.2. Hot Rolling Dispersion Test. This method measures the change in the weight of shale resulting from hydration. When the shale hydrates in water, the weight of the shale decreases. This change in weight was characterized according to the performance of inhibitors. The higher the percentage recovery of the shale cuttings, the better the inhibition capability of the inhibitor (Guancheng et al., 2016). Figure 6 shows the percentage recovery of the shale cuttings for the base fluids formulated with different shale inhibitors through a hot rolling dispersion test at high temperature (150°C). The percentage recovery of the dispersions was enhanced by the addition of inorganic shale inhibitors in comparison to the freshwater fluid (88%). When 7 wt% potassium chloride (KCl) was added, a percentage recovery of 92% was observed. Similarly, the inhibiting capacity of 20 wt% sodium chloride (NaCl) was 93%, which was approximately equal to that of 7 wt% KCl. It was also observed that combining 7 wt% KCl with 3 vol% glycol yielded a better capacity (up to 95%) to inhibit shale dispersion and swelling at a high temperature.

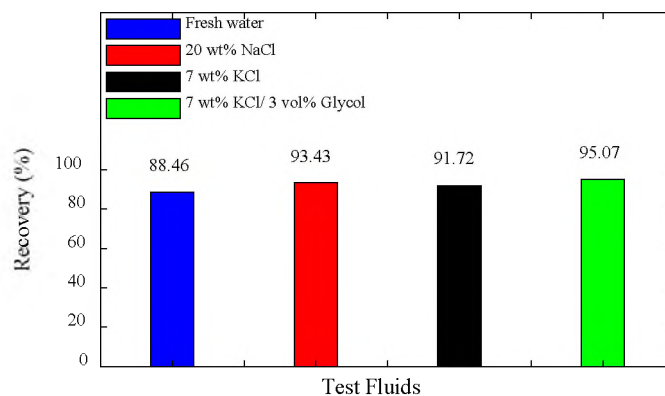


Figure 6. Hot rolling dispersion test of the base fluid with and without different inhibitors, using Zubair shale.

3.2.3. Bulk Hardness Test. Shale hardness can be related to the inhibition capability of the fluid being tested. Depending upon the condition of the shale sample and the efficiency of shale inhibitor, the torque may continue to rise during extrusion and reach a maximum torque of 225 inch lbs. (Gomez and Patel, 2013). Figure 7 illustrates the hardness curves of the Zubair shale samples that were exposed to different fluids. The hardness curves of all inhibited fluids showed no significant differences in tendency with strong increasing to reach the maximum torque. The total number of turns required to reach the maximum torque for 7 wt% KCl, 20 wt% NaCl brine, and the 7 wt% KCl with 3 vol% glycol solution were 11 turns, while for fresh water, 14 turns were required. Although the total number of required turns for all inhibited fluids was similar, the number of turns required to start increasing the torque varied based on the additives. The number of turns required to cause an initial increase in the torque value for fresh water, 7 wt% KCl brine, 20 wt% NaCl brine, and the 7 wt% KCl with 3 vol% glycol solution were 9, 6, 5, and 5, respectively.

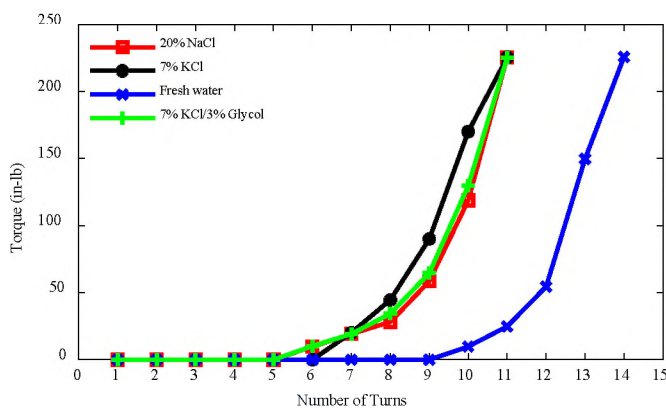


Figure 7. Bulk hardness test results for different test fluids, using Zubair shale.

3.2.4. Swelling Test. Figure 8 shows the linear swell meter data measured for the Zubair shale samples, which were exposed to four test fluids. Fresh water (non-inhibited fluid) was also tested for comparison. After 1,440 min (24 hr) of exposure, the expansion rates of fresh water increased during the testing time, and the ending expansion rate during the test was approximately 11.8%. The ending expansion rates of 7 wt% KCl brine, 20 wt% NaCl brine, and the 7 wt% KCl and 3 vol% glycol solution were 6.9%, 6%, and 4 %, respectively. This means that all the test fluids allowed the water to flow into the shale formation. The expansion rate of 7 wt% KCl brine rapidly increased in the initial 200 min. Then, the expansion rate of the 7 wt% KCl brine was basically stable, indicating that the Zubair shale treated with 7 wt% KCl brine had stopped swelling after 200 min. This differed from the expansion results of 20 wt% NaCl brine and the 7 wt% KCl with 3 vol% glycol solution, which slowly increased during the testing time and were stable for a longer time (about 400 min). The expansion rates of the 7 wt% KCl with 3 vol% glycol solution were basically lower (by approximately 2%) than the 20 wt% NaCl brine.

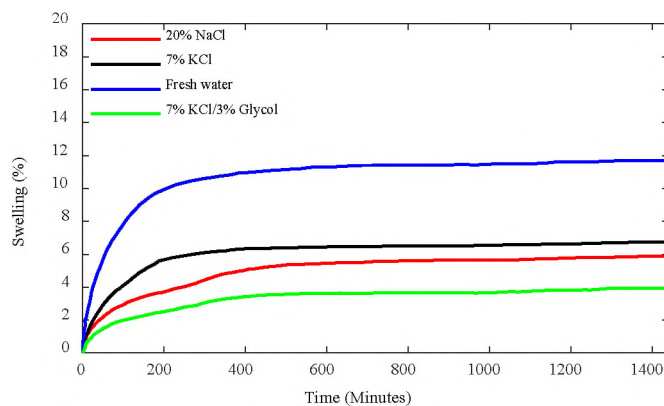
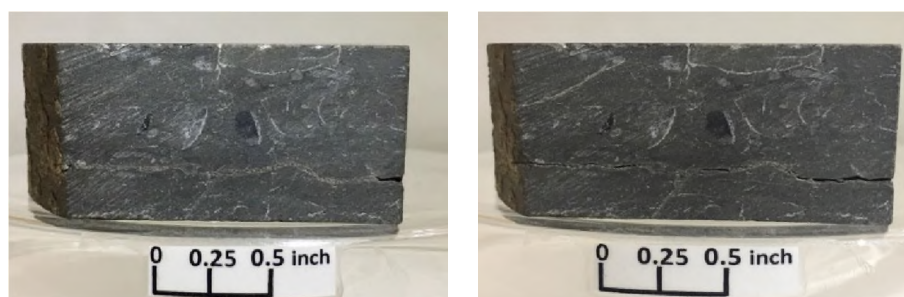


Figure 8. Swelling test results of the Zubair shale samples treated with different additives throughout the testing time.

3.2.5. Fracture Development Test. Figure 9 shows four pieces from the Zubair shale formation that were exposed to test fluids: fresh water, 20 wt% NaCl brine, 7 wt% KCl brine, and a combination of 7 wt% KCl with 3 vol% glycol. The results of the tests also indicate that the existing fractures in the shale samples have a tendency to enlarge with time. In most of the cases, the preexisting natural fractures or new fractures have a tendency to extend parallel to the bedding plane, but in some tests, diagonal and perpendicular fractures to the bedding plane were observed. The shale sample exhibited some fractures after five hours of fresh water exposure. After 48 hours, the enlargement of the fractures and the appearance of new fractures was clearly evident. The shale samples exposed to 7 wt% KCl brine or 20 wt% NaCl brine for 48 hours showed a slight development of small fractures along the bedding plane. It was also observed that the shale sample fractures did not open or enlarge during the test with the 7 wt% KCl and 3 vol% glycol solution. Obviously, inorganic salts such as sodium chloride (NaCl) and potassium chloride (KCl) alone offered little success in providing satisfactory results; instead, these inorganic salts need to be used in combination with glycol.



7 wt% KCl brine

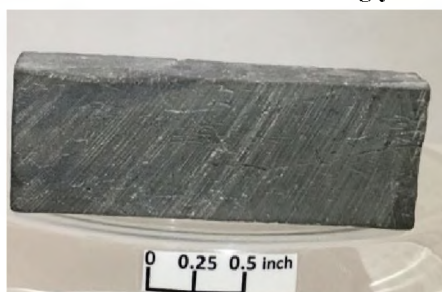
Figure 9. Change in Zubair shale after exposure to different test fluids for 48 hours at ambient conditions. Left: before fluid exposure, right: after 48 hours of fluid exposure.



20 wt% NaCl brine



Combination of 7 wt% KCl and 3 vol% glycol



Fresh water

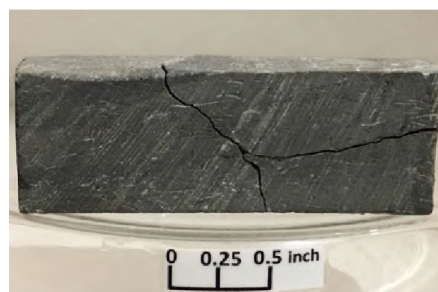


Figure 9. Change in Zubair shale after exposure to different test fluids for 48 hours at ambient conditions. Left: before fluid exposure, right: after 48 hours of fluid exposure (cont.).

4. CONCLUSIONS

The integrated analysis of different shale characterizations revealed the nature of the reactive clay in the shale samples and anticipated the potential instability mechanisms when shale contacted various fluids. Consequently, the proper assessment and treatment of shale formations can be determined during drilling and completion operations. Quantitative

and semiquantitative methods were used in this study to interpret and understand the chemistry of the Zubair shale formation. According to X-ray analysis, the Zubair shale formation is typical a brittle shale, with a weak-to-moderate hydration. Therefore, hydration swelling is not the significant factor in borehole collapse. The thin-section and SEM analyses showed that the Zubair shale had a fractured structure, with preexisting natural fractures propagating both parallel and perpendicular to the bedding plane, covering a significant area of the sample. Such fractures in the rock are open channels for fluids to intrude and react with the clay present in the rock, which weakens the rock structure. Furthermore, the intersection of cross-bedding fractures with other multiple fractures creates a more complex instability scenario. Therefore, the addition of filtration control and appropriate bridging materials are highly recommended to seal micro-fractures and laminations to reduce the fluid invasion into the formation, thereby minimizing instability problems. It is can be concluded from the laboratory test results (i.e., capillary suction timer [CST]; hot rolling dispersion test; bulk hardness test; linear swell meter [LSM]; and fracture development test) that the reactive part of the shale is sensitive to fresh water and that the inorganic shale inhibitors (NaCl and KCl) are good inhibitors as they reduce the dispersive tendency of the clay by inhibiting the water migration into and uptake by the clay mineral. As a result of these laboratory tests, the combination of 7 wt% KCl and 3 vol% glycol was found to be most optimal of all the fluid systems used in this study, which shows a higher performance of shale inhibition compared with using inorganic salts alone. This leads to the recommendation that such monovalent salts plus glycol should be components of the water phase of a drilling mud for the Zubair section. In addition,

reducing the length of the exposure of shale to the drilling fluid will help to mitigate the drilling problems that result from the time-dependent shale instability.

Finally, the Zubair shale sample is fragile and tends to break relatively easily along its irregular planes. The formation appears to be mechanically fragile. This could be the main factor in shale's instability. In general, brittle properties of the shale formations and the presence of natural fractures are important factors to consider for wellbore stability. The formation may fail mechanically along weak planes, creating more fractures and channels for fluid invasion.

ACKNOWLEDGMENTS

The author would like to thank the Higher Committee for Education Development (HCED) in Iraq for awarding him a fully funded Ph.D. scholarship. The authors would like to thank Basrah Oil Company in Iraq for their permission to publish the results. We also want to thank Missouri University of Science and Technology for providing the facilities to do this work.

REFERENCES

- Abbas, A.K., Al-Asadi, Y.M., Alsaba, M., Flori, R. E., Alhussainy, S., 2018a. Development of a Geomechanical Model for Drilling Deviated Wells through the Zubair Formation in Southern Iraq. Presented at the SPE/IADC Middle East Drilling Technology Conference and Exhibition, Abu Dhabi, UAE, 29–31 January. <http://dx.doi.org/10.2118/189306-ms>.

- Abbas, A.K., Flori, R.E., AL-Anssari, A., Alsaba, M., 2018b. Testing and Evaluation of Shale Stability for Zubair Shale Formation. Presented at the SPE Kingdom of Saudi Arabia Annual Technical Symposium and Exhibition, Dammam, Saudi Arabia, 23-26 April.
- Abbas, A.K., Flori, R.E., Alsaba, M., 2018c. Estimating Rock Mechanical Properties of the Zubair Shale Formation Using a Sonic Wireline Log and Core Analysis. *J NaT Gas Sci Eng* 53: 359–369 <http://dx.doi.org/10.1016/j.jngse.2018.03.018>.
- Aghamelu, O., Okogbue, C., 2015. Characterization of Some Clays from Nigeria for Their Use in Drilling Mud. *Appl Clay Sci* 116-117: 158–166. <http://dx.doi.org/10.1016/j.clay.2015.08.025>.
- Akhtarmanesh, S., Shahrabi, M.A., Atashnezhad, A., 2013. Improvement of Wellbore Stability in Shale Using Nanoparticles. *Pet Sci Eng* 112: 290–295. <http://dx.doi.org/10.1016/j.petrol.2013.11.017>.
- Al-Bazali, T.M., 2011. The Consequences of Using Concentrated Salt Solutions for Mitigating Wellbore Instability in Shales. *J Pet Sci Eng* 80 (1): 94–101. <https://dx.doi.org/10.1016/j.petrol.2011.10.005>.
- API. 1997. Recommended Practice for Laboratory Testing of Drilling Fluids, 7th ed. (API 13I Supplement 2-01-jun).
- API. 2004. Methylene Blue Test for Drill Solids and Commercial Bentonites. Section 12 in: API RP 13I: Laboratory Testing of Drilling Fluids, 7th ed. and ISO 10416:2002; American Petroleum Institute, February.
- Beg, M., Sharma, S., Ojha, U., 2018. Effect of Cationic Copolyelectrolyte Additives on Drilling Fluids for Shales. *J Pet Sci Eng* 161: 506–514. <http://dx.doi.org/10.1016/j.petrol.2017.12.009>.
- Berry, S.L., Boles, J.L., Brannon, H.D., Beall, B.B., 2008. Performance Evaluation of Ionic Liquids as a Clay Stabilizer and Shale Inhibitor. Presented at the SPE International Symposium and Exhibition on Formation Damage Control, Lafayette, Louisiana, USA, 13-15 February. <http://dx.doi.org/10.2118/112540-ms>.
- Chenevert, M., Sharma, A., 1993. Permeability and Effective Pore Pressure of Shales. *SPE Drill & Compl* 8 (01): 28–34. <http://dx.doi.org/10.2118/21918-pa>.
- Choo, C., Takahashi, M., Jeong, G., 2014. Identification and Three-Dimensional Characterization of Micropore Networks Developed in Granite using Micro-Focus X-ray CT. *J Eng Geol* 24 (2): 179–189. <https://dx.doi.org/10.9720/kseg.2014.2.179>.

- Ferreira, C.C., Teixeira, G.T., Lachter, E.R., Nascimento, R.S., 2016. Partially Hydrophobized Hyperbranched Polyglycerols as Non-ionic Reactive Shale Inhibitors for Water-based Drilling Fluids. *Appl Clay Sci* 132–133: 122–132. <https://dx.doi.org/10.1016/j.clay.2016.05.025>.
- Fjær, E., Holt, R.M., Horsrud, P., Raaen, A.M., Risnes, R., 2008. *Petroleum Related Rock Mechanics*, second edition. Amsterdam: Elsevier Science.
- Friedheim, J., Guo, Q., Young, S., Gomez, S., 2011. Testing and Evaluation Techniques for Drilling Fluids-Shale Interaction and Shale Stability. Presented at the 45th U.S. Rock Mechanics/Geomechanics Symposium, San Francisco, California, 26–29 June.
- Garcia, M.N., Sorenson, F., Bonapace, J.C., Motta, F., Bajuk, C., Stockman, H., 2013. Vaca Muerta Shale Reservoir Characterization and Description: The Starting Point for Development of a Shale Play with Very Good Possibilities for a Successful Project. Presented at the Unconventional Resources Technology Conference, Denver, Colorado, 12–14 August. <https://dx.doi.org/10.1190/urtec2013-090>.
- Gomez, S.L., He, W., 2012. Fighting Wellbore Instability: Customizing Drilling Fluids Based on Laboratory Studies of Shale-Fluid Interactions. Presented at the IADC/SPE Asia Pacific Drilling Technology Conference and Exhibition, Tianjin, China, 9–11 July. <https://dx.doi.org/10.2118/155536-ms>.
- Gomez, S.L., Patel, A., 2013. Shale Inhibition: What Works? Presented at the SPE International Symposium on Oilfield Chemistry, Woodlands, Texas, 8–10 April. <https://dx.doi.org/10.2118/164108-ms>.
- Guancheng, J., Yourong, Q., Yuxiu, A., Xianbin, H., Yanjun, R., 2016. Polyethyleneimine as Shale Inhibitor in Drilling Fluid. *Appl Clay Sci* 127–128: 70–77. <https://dx.doi.org/10.1016/j.clay.2016.04.013>.
- Huang, X., Zhao, Y., 2017. Characterization of Pore Structure, Gas Adsorption, and Spontaneous Imbibition in Shale Gas Reservoirs. *J Pet Sci Eng* 159: 197–204. <http://dx.doi.org/10.1016/j.petrol.2017.09.010>.
- Jain, R., Mahto, V., 2017. Formulation of a Water based Drilling Fluid System with Synthesized Graft Copolymer for Troublesome Shale Formations. *J NaT Gas Sci Eng* 38: 171–181. <http://dx.doi.org/10.1016/j.jngse.2016.12.018>.
- Kassab, M.A., Teama, M.A., Cheadle, B.A., El-Din, E.S., Mohamed, I.F., Mesbah, M.A., 2015. Reservoir Characterization of the Lower Abu Madi Formation Using Core Analysis Data: El-Wastani Gas Field, Egypt. *J Afr Earth Sci* 110: 116–130. <https://dx.doi.org/10.1016/j.jafrearsci.2015.06.008>.

- Lal, M., 1999. Shale Stability: Drilling Fluid Interaction and Shale Strength. Presented at the SPE Asia Pacific Oil and Gas Conference and Exhibition, Jakarta, Indonesia, 20–22 April. <https://dx.doi.org/10.2118/54356-ms>.
- Li, X., Yan, X., Kang, Y., 2017. Investigation of Drill-in Fluids Damage and Its Impact on Wellbore Stability in Longmaxi Shale Reservoir. *J Pet Sci Eng* 159: 702–709. <http://dx.doi.org/10.1016/j.petrol.2017.10.005>.
- Luo, Z., Wang, L., Yu, P., Chen, Z., 2017. Experimental Study on the Application of an Ionic Liquid as a Shale Inhibitor and Inhibitive Mechanism. *Appl Clay Sci* 150: 267–274. <http://dx.doi.org/10.1016/j.clay.2017.09.038>.
- Lyu, Q., Ranjith, P., Long, X., Kang, Y., Huang, M., 2015. A Review of Shale Swelling by Water Adsorption. *J Nat Gas Sci Eng* 27: 1421–1431. <http://dx.doi.org/10.1016/j.jngse.2015.10.004>.
- Mehtar, M.A., Mielke, S.K., Alfonzo, N.E., Young, S., Brangetto, M., Soliman, A.A., 2010. Effective Implementation of High Performance Water Based Fluid Provides Superior Shale Stability Offshore Abu Dhabi. Presented at the Abu Dhabi International Petroleum Exhibition and Conference, Abu Dhabi, UAE, 1–4 November. <https://dx.doi.org/10.2118/138564-ms>.
- Mohiuddin, M., Khan, K., Abdulraheem, A., Al-Majed, A., Awal, M., 2007. Analysis of Wellbore Instability in Vertical, Directional, and Horizontal Wells Using Field Data. *J Pet Sci Eng* 55 (1-2): 83–92. <http://dx.doi.org/10.1016/j.petrol.2006.04.021>.
- Patel, A., Stamatakis, S., Young, S., Friedheim, J., 2007. Advances in Inhibitive Water-Based Drilling Fluids—Can They Replace Oil-Based Muds? Presented at the International Symposium on Oilfield Chemistry, Houston, Texas, U.S.A, 28 February–2 March. <http://dx.doi.org/10.2118/106476-ms>.
- Shen, Y., Ge, H., Li, C., Yang, X., Ren, K., Yang, Z., Su, S., 2016. Water Imbibition of Shale and Its Potential Influence on Shale Gas Recovery— a Comparative Study of Marine and Continental Shale Formations. *J Nat Gas Sci Eng* 35: 1121–1128. <http://dx.doi.org/10.1016/j.jngse.2016.09.053>.
- Stephens, M., Gomez, S., Churan, M., 2009. Laboratory Methods to Assess Shale Reactivity with Drilling Fluids. Presented at the AADE National Technical Conference and Exhibition, New Orleans, Louisiana, 31 March–2 April.
- Tang, X., Zhang, J., Wang, X., Yu, B., Ding, W., Xiong, J., Yang, Y., Wang, L., Yang, C., 2014. Shale Characteristics in the Southeastern Ordos Basin, China: Implications for Hydrocarbon Accumulation Conditions and the Potential of Continental Shales. *Int J Coal Geol* 128–129: 32–46. <http://dx.doi.org/10.1016/j.coal.2014.03.005>.

- Temraz, M.G., Hassanien, I., 2016. Mineralogy and Rheological Properties of Some Egyptian Bentonite for Drilling Fluids. *J Nat Gas Sci Eng* 31: 791-799. <http://dx.doi.org/10.1016/j.jngse.2016.03.072>.
- Van Oort, E., 2003. On the Physical and Chemical Stability of Shales. *J Pet Sci Eng* 38 (3–4): 213–235. [https://dx.doi.org/10.1016/s0920-4105\(03\)00034-2](https://dx.doi.org/10.1016/s0920-4105(03)00034-2).
- Van Oort, E., Hoxha, B., Hale, A.H., Aldin, M., Patterson, R., 2016. How to Test Fluids for Shale Compatibility? Presented at the AADE-16-FTCE-77, Fluids Technical Conference and Exhibition, Houston, Texas, April 12–13.
- Villabona-Estupiñán, S., De Almeida Rodrigues, J., Nascimento, R.S., 2017. Understanding the Clay-PEG (and Hydrophobic Derivatives) Interactions and Their Effect on Clay Hydration and Dispersion: A Comparative Study. *Appl Clay Sci* 143: 89–100. <https://dx.doi.org/10.1016/j.clay.2017.03.021>.
- Villada, Y., Gallardo, F., Erdmann, E., Casis, N., Olivares, L., Estenoz, D., 2017. Functional Characterization on Colloidal Suspensions Containing Xanthan Gum (XGD) and Polyanionic Cellulose (PAC) Used in Drilling Fluids for a Shale Formation. *Appl Clay Sci* 149, 59–66. <https://dx.doi.org/10.1016/j.clay.2017.08.020>.
- Wilcox, R., Fisk, J., Corbett, G., 1987. Filtration Method Characterizes Dispersive Properties of Shales. *SPE Drill Eng* 2 (02): 149–158. <https://dx.doi.org/10.2118/13162-pa>.
- Xu, J., Qiu, Z., Huang, W., Zhao, X., 2017. Preparation and Performance Properties of Polymer Latex SDNL in Water-Based Drilling Fluids for Drilling Troublesome Shale Formations. *J Nat Gas Sci Eng* 37: 462-470. <http://dx.doi.org/10.1016/j.jngse.2016.11.064>.
- Xu, J., Qiu, Z., Zhao, X., Zhong, H., Li, G., Huang, W., 2018. Synthesis and Characterization of Shale Stabilizer Based on Polyethylene Glycol Grafted Nanosilica Composite in Water-based Drilling Fluids. *J Pet Sci Eng* 163: 371–377. <http://dx.doi.org/10.1016/j.petrol.2018.01.007>.
- Zhang, R., Ning, Z., Yang, F., Wang, X., Zhao, H., Wang, Q., 2015. Impacts of Nanopore Structure and Elastic Properties on Stress-dependent Permeability of Gas Shales. *J Nat Gas Sci Eng* 26: 1663–1672. <http://dx.doi.org/10.1016/j.jngse.2015.02.001>.
- Zhao, X., Qiu, Z., Huang, W., Wang, M., 2017a. Mechanism and Method for Controlling Low-Temperature Rheology of Water-Based Drilling Fluids in Deepwater Drilling. *J Pet Sci Eng* 154, 405-416. <http://dx.doi.org/10.1016/j.petrol.2017.04.036>.

- Zhao, X., Qiu, Z., Wang, M., Huang, W., Zhang, S., 2017b. Performance Evaluation of a Highly Inhibitive Water-Based Drilling Fluid for Ultralow Temperature Wells. *J. Energy Resour Technol* 140 (1), 012906. <http://dx.doi.org/10.1115/1.4037712>.
- Zhong, H., Qiu, Z., Huang, W., Cao, J., 2011. Shale Inhibitive Properties of Polyether Diamine in Water-based Drilling Fluid. *J Pet Sci Eng* 78 (2): 510–515. <http://dx.doi.org/10.1016/j.petrol.2011.06.003>.
- Zhong, H., Qiu, Z., Sun, D., Zhang, D., Huang, W., 2015. Inhibitive Properties Comparison of Different Polyetheramines in Water-Based Drilling Fluid. *J Nat Gas Sci Eng* 26: 99-107. <http://dx.doi.org/10.1016/j.jngse.2015.05.029>.

SECTION

2. CONCLUSIONS AND RECOMMENDATIONS

2.1. CONCLUSIONS

In this dissertation, an integrated wellbore stability study to assess and address existing wellbore stability problems to provide guidance for future well plans. The major findings of this research are summarized below:

- In terms of geomechanics, our results illustrated that the rock strength parameters of sandstone under different confining pressure increase significantly as the confining pressure increases; but the rock elasticity modulus is less impacted by confining pressure and has slight variation under different confining pressures.
- Heterogeneity of Zuair formation as indicated by variations of porosity and permeability has resulted in a wide range of elastic Young's modulus (between 6.07–26.87 GPa) and Poisson's ratio (between 0.20–0.30).
- The mechanical response of shales is sensitive to the state of the test sample (e.g., the degree of saturation, core damage effects) and the shale characterization (e.g., porosity, mineralogy, texture, and structure).
- Based on the triaxial tests results, there are some trends which are of interest and which can be very useful to obtain correlations that can be used to obtain mechanical rock properties from wireline logs.

- The 1-D mechanical earth model (MEM) model and field data were in good agreement, where the majority of the wellbore instability issues in the Zubair Formation were due to inadequate mud support at the borehole wall.
- The heterogeneity of the Zubair Formation should be considered in the mud weight calculation as the mud weight is designed to maintain the stability of weak and non-depleted shale zones. It is also vital to consider how much overbalance this mud will cause in depleted sandstone sections.
- The findings of the study indicate that the results obtained from the Mogi-Coulomb failure criterion were in good agreement with field observations when compared to the Mohr-Coulomb.
- Based on the results of the characterization of the shale analysis, the shale from the Southern Iraq Zubair formation is typically brittle shale and has low-to-moderate hydration. However, the relatively high content of kaolinite and illite could contribute to the structural failure and instability of the rock.
- It indicates that the introduction of cations, either sodium or potassium, greatly reduced the dispersive tendency of the clay. Furthermore, the results show that the combination of 7 wt% KCl and 3 vol% glycol performed as an excellent shale inhibitor.

2.2. RECOMMENDATIONS

The main objective of this study is to reduce the drilling time and cost of wells into Zubair Formation by minimizing wellbore stability problems. The future academic research potentials are outlined to extend the current research in the following points:

- Apply machine learning methods (i.e., ANNs and SVMs) for intelligent prediction of wellbore instability problems.
- Good drilling practices, including regular borehole cleaning, monitoring tripping speed, proper mud conditioning, and controlling the ROP while drilling through the shale intervals, will help to manage the lack of stability and avoiding major drilling problems.
- It is highly recommended to build a robust 3D-MEM based on the elements of this study; This will provide better wellbore stability predictions.
- Mud chemical composition should incorporate sealing polymer to seal-off micro fractures and laminations without reservoir damage.

VITA

Ahmed Abbas was born in Missan, Iraq. He received Bachelor of Science and Master of Science degrees in Petroleum Engineering from University of Baghdad, Baghdad, Iraq in 2007 and 2011. He served as a drilling supervisor for Iraqi Drilling Company for seven years. He was granted a PhD scholarship by the Higher Committee for Education Development in Iraq in 2014. He received a PhD in Petroleum Engineering from Missouri University of Science and Technology, Rolla, MO, August 2020.

Ahmed Abbas was a member of Iraqi Engineers Union and Society of Petroleum Engineering. His research interests included reducing the drilling time and cost for 8 ½” phase of wells in Zubair Formation by minimizing wellbore stability problems. He published some journal and conference papers in these research areas.